U.S.NRC
United States Nuclear Regulatory Commission
Protecting People and the Environment

Technical Letter Report
TLR-RES/DE/REB-2021-13

Summary of Investigations into Addressing the Shallow Surface-Breaking Flaw Issue

Date:

December 2021

Prepared in response to User Need Request NRR-2017-007 and NRR-2020-003:

Marvin Smith
NUMARK Associates, Inc.

Terry Dickson
NUMARK Associates, Inc.

Andrew Dyszel
NUMARK Associates, Inc.

NRC Project Manager:

Patrick Raynaud
Senior Materials Engineer
Component Integrity Branch

Division of Engineering
Office of Nuclear Regulatory Research
U.S. Nuclear Regulatory Commission
Washington, DC 20555–0001

DISCLAIMER

This report does not contain or imply legally binding requirements. Nor does this report establish or modify any regulatory guidance or positions of the U.S. Nuclear Regulatory Commission and is not binding on the Commission.

Summary of Investigations into Addressing the Shallow Surface-Breaking Flaw Issue

Marvin Smith[1], Patrick Raynaud[2], Terry Dickson[1], Andrew Dyszel[1]

[1] NUMARK Associates, Inc., [2] U.S. NRC

Contents

Acronyms

ASME	American Society of Mechanical Engineers
BWR	Boiling Water Reactor
CDR	Cooldown rate (°F/hour)
CPF	Conditional Probability of Failure
CPI	Conditional Probability of Initiation
CTE	Coefficient of Thermal Expansion
EFPY	Effective Full-Power Years
EPFM	Elastic-Plastic Fracture Mechanics
FAVOR	Fracture Analysis of Vessels – Oak Ridge
FCI	Frequency of Crack Initiation
FEM	Finite-Element Method
ID	Inner Diameter
LEFM	Linear-Elastic Fracture Mechanics
NPP	Nuclear Power Plants
NRC	United States Nuclear Regulatory Commission
ORNL	Oak Ridge National Laboratory
PFM	Probabilistic Fracture Mechanics
PNNL	Pacific Northwest National Laboratory
P-T	Pressure and Temperature Limits
PTS	Pressurized Thermal Shock
PWR	Pressurized Water Reactor
RCS	Reactor Coolant System
RPV	Reactor Pressure Vessel
SFT	Stress-Free Temperature
SIFIC	Stress-intensity Factor Influence Coefficients
SSBF	Small Surface Breaking Flaw
TWCF	Through-Wall Cracking Frequency
WPS	Warm Pre-Stress
WRS	Weld Residual Stress

Definitions

K_{IC}

The critical value of stress intensity factor in mode I loading measured under plane strain conditions, also known as the plane strain fracture toughness. It is a measure of the resistance of a material to crack extension under predominantly linear-elastic conditions (i.e. low toughness conditions when there is little to no plastic deformation occurring at the crack tip).

aK_{IC}

The lower bound of K_{IC} fracture toughness, also called arrest toughness, below which a crack is predicted to arrest (i.e. not grow).

Conditional Probability of crack Initiation

The probability is termed conditional because it assumes that the analyzed transient has occurred. To transform CPI into a risk metric it must be multiplied by the probability of the transient occurring.

Frequency of Crack Initiation

The product of the CPI and a matrix defining the sequence (or event) frequency of the loading transients. Calculating a mean FCI for RPVs subjected to pressure and temperature curves requires a statistical representation of the possible overpressurization transients and their frequencies of occurrence.

Conditional Probability of Failure

The probability is termed conditional because it assumes that the analyzed transient has occurred. To transform CPF into a risk metric it must be multiplied by the probability of the transient occurring.

Through-Wall Cracking Frequency

The product of the CPF and a matrix defining the sequence (or event) frequency of the loading transients. Calculating a mean TWCF for RPVs subjected to pressure and temperature curves requires a statistical representation of the possible overpressurization transients and their frequencies of occurrence.

List of Figures

List of Tables

Executive Summary

ORNL/TM-2015/59531/REV-01, "The Effect of Shallow Inside-Surface-Breaking Flaws on the Probability of Brittle Fracture of Reactors Subjected to Postulated and Actual Operational Cool-Down Transients: A Status Report" , February 2016 [1], provided analyses of several reactor pressure vessels (RPVs) subjected to plant cooldown from operating temperature and pressure to cold shutdown. These plant cooldowns were analyzed using the probabilistic fracture mechanics (PFM) code FAVOR [2] [3] to determine the conditional probability of crack initiation (CPI) and conditional probability of vessel failure (CPF) for inner diameter (ID) small surface-breaking flaws (SSBFs) with various depths. This ORNL 2016 analysis showed that the CPI and CPF for shallow, circumferential, ID surface-breaking flaws that extend just into the ferritic steel vessel wall may have calculated CPI and CPF values significantly greater than those for the ¼ thickness reference flaw in the ASME Code, Section XI, Appendix G [4].

To determine whether the higher CPF values calculated for internal SSBFs from the ORNL 2016 study [1] could result in an estimated Through-Wall Cracking Frequency (TWCF) values higher than 1.0E-06 per year, additional sensitivity studies were performed as described in this report for both PWR and BWR plants with assumed internal SSBFs. Plants typically cooldown for refueling outages approximately once every 18-24 months depending on the plant fuel cycle design. Plants may also cooldown to cold shutdown during an operating cycle for required maintenance during a cycle. Therefore, the frequency of a normal plant cooldown is conservatively assumed in this analysis as once per year (which agrees with Table 2 of Enclosure 6 in the BTP 5-3 closure memorandum [5]). Cooldowns that operate along the pressure-temperature (P-T) limit curves were also analyzed in the current report. Because plants administratively maintain margin to the limit curves to avoid exceeding them, the occurrence of these cooldowns is hypothetical, with their frequencies estimated to be 6.0E-06 for PWRs and <1.0E-07 for BWRs per Table 1 of Enclosure 6 in the BTP 5-3 closure memorandum [5].

As discussed in Section 1 of the current report, cooldowns from plant operating temperature to 70°F ambient temperature at a constant cooldown rate (CDR) of 50°F to 100°F per hour along the P-T limit curve may result in a CPF above 1.0E-06. Several potential changes in FAVOR modeling assumptions were investigated to assess the sensitivity of the FAVOR results to these changes. The changes in modeling assumptions evaluated in Sections 2 and 3 of this report include (1) Stress-Free Temperature, (2) Coefficient of Thermal Expansion, (3) Warm Pre-Stress and (4) Shop Hydro Testing. No changes in FAVOR plant modeling assumptions were identified that systematically reduce CPF to less than 1.0E-06 for a constant CDR above 50°F per hour. However, when considering realistic transient frequencies, the TWCF is far below 1E-06 per year.

As discussed in Appendix A, 42 actual normal operation plant cooldown histories were obtained from 17 different PWRs. These cooldown histories were analyzed to determine the pressure and temperature histories corresponding to various percentiles of the pressure and temperature history distributions based on the population considered. The 42 plant cooldowns appeared to represent successfully completed cooldowns, and were treated as a representative sample, but the degree to which they represent fleet-wide cooldowns is unknown. As discussed in Section 4.1, the CPF values for internal SSBFs flaws based on FAVOR analyses of the actual PWR plant cooldowns shown in Appendix A are significantly less than 1.0E-06. Thus, when considering realistic transient frequencies, the TWCF is far below 1E-06 per year.

Section 4.2 provides an evaluation of BWR plant cooldowns and BWR leak tests. BWR plants normally operate at a system pressure close to the saturation pressure for temperature at the core exit. BWR plant cooldowns from full power to cold shutdown must be within P-T limits for reactor coolant system (RCS) pressure and temperature, provided in either Plant Technical Specifications (Section 3.4.9) or the Plant Pressure Temperature Limits Report. Based on cooldowns at plant Technical Specifications P-T limits for two BWRs, BWR plant cooldowns at the maximum allowed cooldown rate and operating pressure result in CPF values significantly below 1.0E-06 for internal SSBFs. Thus, when considering realistic transient frequencies, the TWCF is far below 1E-06 per year.

Section 4.2.3 provides analyses of BWR leak test transients including (1) a hypothetical leak test along the P-T limit with heatup and cooldown rates of 40°F/hour, (2) a hypothetical leak test along the P-T limit with heatup rate of 40°F/hour and cooldown rate of 100°F/hour, and (3) an actual leak test transient at measured pressure and temperature histories. Probabilistic FAVOR analyses were performed for these 3 transients with a 4% internal SSBF of aspect ratio equal to 6 to confirm that the shallow flaw results in CPF values below 1E-06 (and thus TWCF below 1E-06 per year, because leak test transient frequencies are on the order of 1 per year). In all cases, the values of CPF (and thus TWCF) were equal to zero, thus the leak test transients do not appear to be an issue for shallow flaws.

A recent EPRI report, entitled an "*Assessment of the Effect of Small Inner Surface Flaws on ASME Section XI Appendix G Pressure-Temperature Limits (MRP 437 and BWRVIP-328)"* [6], provides an assessment of internal SSBFs. This report assumed a frequency of 1 per year for P-T limit cooldowns from normal operation and for system leak tests, in comparison with 6.0E-06 per year for PWRs and <1.0E-07 per year for BWRs for cooldowns from normal operating pressure and temperature in the BTP 5-3 closure memo [5]. The EPRI report identifies a maximum CDR at temperatures below 250°F for cooldowns along the Appendix G P-T limit curve (from normal operation and related to system leak tests) to maintain CFP less than 1E-06 and TWCF less than 1.0E-06 per year, and a set of relationships to define this limiting CDR as a function of vessel wall thickness and adjusted vessel reference temperature. Both EPRI MRP-437/BWRVIP-328 and this report are consistent in showing that, depending on vessel geometry and embrittlement, the CDR for cooldowns along the Appendix G P-T limit curve needs to be less than the maximum 100°F per hour to keep CPF less than 1.0E-06. Both cooldowns from normal operating pressure and temperature and cooldowns from pressure tests were considered in these studies.

Design considerations (including switch over to the Residual Heat Removal (RHR) system at temperatures below approximately 300°F in PWRs), as well as limitations on plant pressure and temperature in PWR and BWR Technical Specifications, tend to limit CDR as the vessel wall temperature drops below the vessel ART. Based on the FAVOR analyses presented here, realistic plant cooldowns are substantially less limiting in terms of TWCF for internal SSBFs than cooldowns at the maximum CDR and pressure allowed by ASME Section XI, Appendix G.

1 Background and Mechanics of the Shallow Flaw

1.1 Background of Shallow Flaw from ORNL 2016

ORNL/TM-2015/59531/REV-01, "The Effect of Shallow Inside-Surface-Breaking Flaws on the Probability of Brittle Fracture of Reactors Subjected to Postulated and Actual Operational Cool-Down Transients: A Status Report," February 2016 [1] (ORNL 2016), provided analyses of several reactor pressure vessels (RPVs) subjected to plant cool-down from operating temperature and pressure to cold shutdown. These plant cooldowns were analyzed using the probabilistic fracture mechanics (PFM) code FAVOR [2] [3]. In ORNL 2016, the conditional probability of crack initiation (CPI) and conditional probability of vessel failure (CPF) were determined for inner diameter (ID) surface-breaking flaws with various depths. This analysis showed that the CPI and CPF for shallow, circumferential, ID surface-breaking flaws that extend just into the ferritic steel vessel wall have calculated CPI and CPF values significantly greater than the values for the ¼ thickness reference flaw in the ASME Code, Section XI, Appendix G [4]. ORNL found similar results for cooldown transients defined using the EPRI-MRP-250 risk-informed methodology.

The ONRL 2016 study concluded that the higher CPI and CPF for internal SSBFs compared with the ASME Appendix G assumed ¼ vessel wall thickness flaw was the result of two primary factors: (1) the stress discontinuity at the clad interface with the ferritic steel and (2) protection of warm pre-stress (WPS) for the deeper ¼ thickness internal SSBF. There is a stress discontinuity at the clad/base interface resulting from the difference in temperature-dependent thermal elastic material properties of cladding and base materials, most especially the difference in the coefficients of thermal expansion. Figure 1 illustrates the stress discontinuity at the clad to ferritic steel interface.

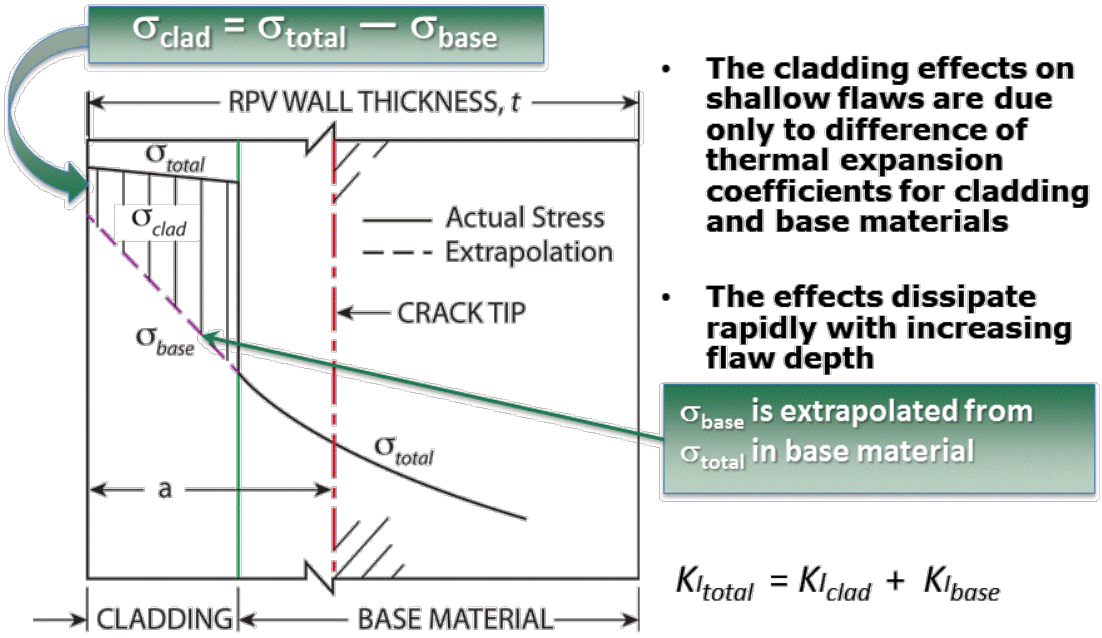

Figure 1: Stress discontinuity between base and clad material is attributable to the difference between the stainless steel and ferritic steel temperature-dependent thermal elastic properties

FAVOR calculates the stress intensity factor for an internal SSBF as the sum of the base metal and clad contributions ($K_{total} = K_{base} + K_{clad}$). FAVOR uses the ASME methodology for the calculation of K_{base}. Because the ASME methodology does not include a calculation for clad, FAVOR uses its own methodology for the calculation of K_{clad} for its contribution to total stress. [2]

FAVOR analyses show that the inclusion of K_{clad} significantly increases the thermal stress at the end of a plant cooldown. Deeper flaws tend to be protected from flaw initiation by warm prestress (WPS) before reaching cold shutdown. The pressure stress for shallow flaws is lower, the thermal stress is higher near the clad base interface, and the total thermal plus pressure stress for shallow flaws may peak at the end of the cooldown. Therefore, WPS may not prevent crack initiation for shallow flaws and the probability of brittle fracture at the end of plant cooldown may be significantly greater for internal SSBFs.

ASME Section XI Nonmandatory Appendix G, presents a procedure for obtaining the allowable loadings for ferritic pressure retaining materials based on the principles of linear elastic fracture mechanics. Appendix G assumes a maximum postulated flaw of ¼ of the thickness of the pressure vessel and calculates the mode I stress intensity factor K_I produced by specified loadings and compares the maximum K_I to a reference critical value K_{Ic} that is defined in G-2110. Figure 2 is an illustration of finite length circumferentially oriented internal SSBFs.

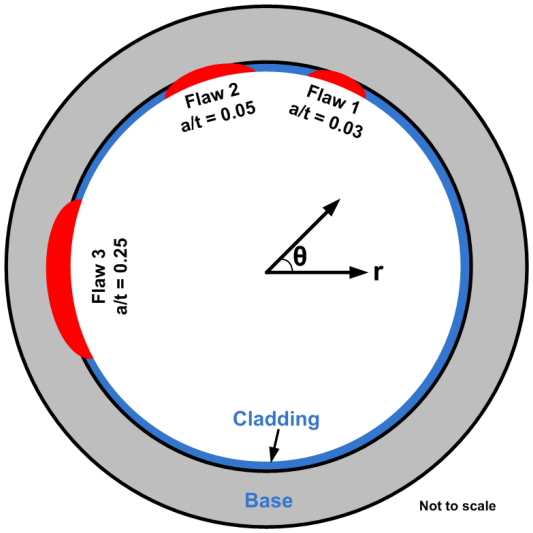

Figure 2: illustration of finite length circumferentially oriented flaws (not to scale)

The standard base case FAVOR code model assumptions and inputs used for the analyses presented in this report are described in Appendix B. Changes to these base case assumptions and inputs are provided with each analysis discussion. As shown in Table B-5, a distribution of shallow flaw aspect ratios from 2 to infinite is assumed for most shallow flaw analyses. To facilitate a comparison between FAVOR and ABAQUS, the analyses discussed in this section assume that all internal SSBFs have an aspect ratio of 6. As shown in Figure 2, the analysis covered flaws with depths from 3% of the wall thickness which just penetrates thru the cladding into the base material up to a flaw with the ¼ (25%) thickness internal SSBF assumed in ASME Section XI, Appendix G.

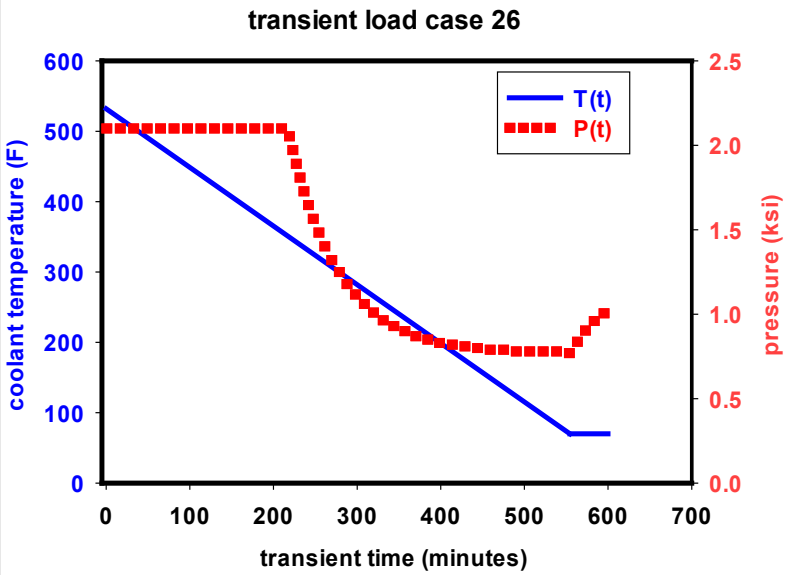

Figure 3: Cooldown at ASME P-T limits

Figure 3 shows the cooldown transient load case 26 from ORNL 2016. The plant cools down at a constant rate of 50°F per hour from normal operating temperature to 70°F. The pressure for this cooldown remains at the normal operating pressure until the pressure must be reduced to remain within the maximum ASME allowed pressure. The pressure shown in Figure 3 was calculated using the ASME Section XI, Appendix G procedure for a plant with an RT_{NDT} of 281°F and a cooldown rate (CDR) of 50°F per hour. This transient and 3% shallow flaw were chosen for this ORNL 2016 analysis because the FAVOR-generated K_I time history had been evaluated for a 3% internal SSBF with an aspect ratio of 6 with both FAVOR and ABAQUS. As shown in Figure 4, the FAVOR calculated total applied K_I for this transient is close to the solution generated by ABAQUS.

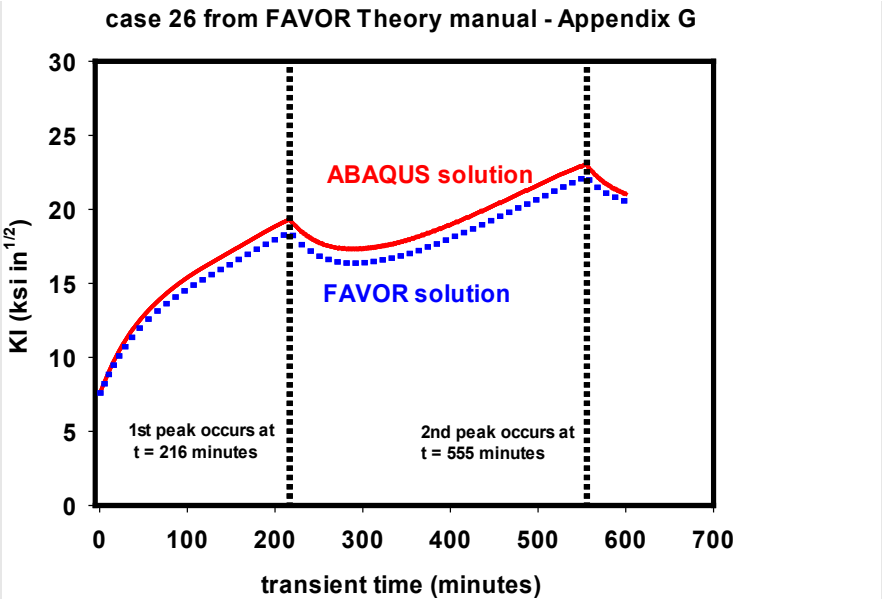

Figure 4: FAVOR and ABAQUS K_I(time) solutions for a 3% circumferentially oriented flaw with an aspect ratio of 6 subjected to the cooldown transient in Figure 3.

This Figure 4 applied total K_I time history exhibits two peaks: the 1st peak is associated with the transient time (216 minutes) corresponding to when the pressure is reduced from steady state operating pressure and the 2nd peak is associated the time (554 minutes) at which the coolant reaches an assumed steady-state temperature of 70°F. This two-peak K_I time history is characteristic of internal SSBFs subjected to a cooldown transient where the pressure is held at full operating pressure until the pressure must be reduced according to ASME Appendix G. When the first peak is greater than the second peak, which is more likely for deeper flaws, crack initiation is prevented at the second peak by WPS. When the 2nd peak is larger, which is more likely for very shallow flaws, crack extension is not prevented by WPS.

The K_I time history solutions in Figure 4 do not include the additional component due to the through-wall weld residual stress (WRS); and therefore, would be applicable to flaws located in plate or forging regions. For this RPV and flaw geometry, the impact of including the through-wall WRS is to increase the FAVOR K_I time history illustrated in Figure 4 by 5.1 ksi $in^{1/2}$ because the overall stress is higher when accounting for the tensile weld residual stress at the crack tip.

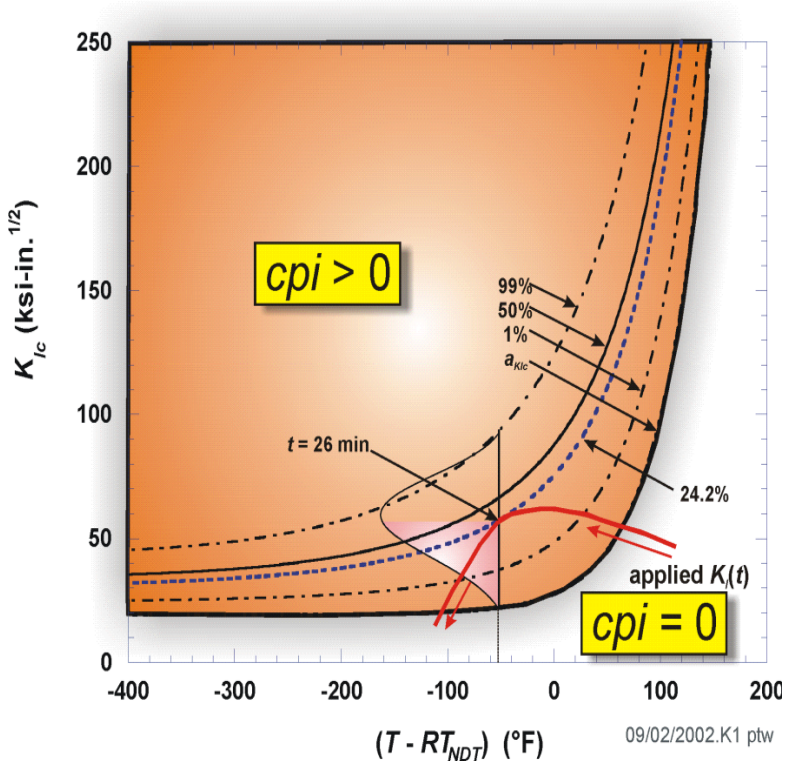

Figure 5: FAVOR model of the Weibull statistical distribution for fracture initiation toughness K_{Ic}.

Figure 5 illustrates the FAVOR model of the statistical distribution for fracture initiation toughness. When WPS is not included in the model, the only condition for an RPV trial to have a CPI > 0 is that the applied $K_I > aK_{Ic}$ at any time during the transient where aK_{Ic} is the lower bound K_{Ic} curve (i.e. the 0th percentile of all data, see Figure 6).

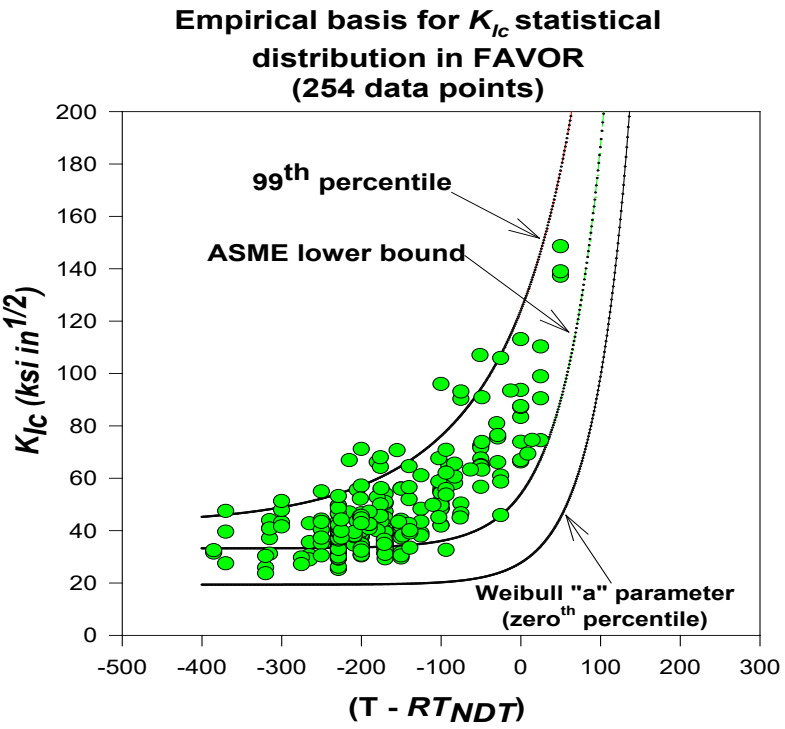

Figure 6 Empirical Basis for the K_{IC} Statistical Distribution in FAVOR

The $_aK_{Ic}$ statistical distribution used in FAVOR was derived from the K_{Ic} database illustrated in Figure 6. The lower bound (0^{th} percentile) for this distribution is defined by the $_aK_{Ic}$ equation:

Figure 6 illustrates that the ASME K_{Ic} curve, which corresponds to the 5^{th} percentile of all data, provides a lower bound in the transition region, and also bounds most (but not all) of the data on the lower shelf. As a result, depending on the RT_{NDT} of the RPV vessel materials, the temperature at the internal SSBF tip may be in the range where some data fall below the ASME K_{IC} curve. This is well understood and widely accepted because the ASME curve constitutes the 5^{th} percentile of the data. It is also well understood that the FAVOR K_{IC} statistical model is conservative compared to the ASME model because the FAVOR model uses the 0^{th} percentile of all data for the determination of $_aK_{IC}$. This difference between the models explains why some FAVOR analyses result in non-zero probabilities of crack growth initiation or failure even for cases where ASME limits are satisfied.

FAVOR was applied to perform probabilistic fracture mechanics (PFM) analyses for a range of 11 internal SSBF depths subjected to the transient illustrated in Figure 3. Each PFM analysis was performed based on the RPV model as described in Appendix B with the assumption that each RPV trial (in the Monte Carlo analysis) contained one circumferential internal SSBF with an aspect ratio of 6. A total of 22 PFM Monte Carlo analyses were performed for 11 flaw depths both with and without WPS. Each PFM analysis was performed for 100,000 RPV trials and was reasonably well converged.

As shown in Table 1-1 (taken from ORNL 2016), WPS prevents brittle fracture for internal SSBFs that extend to a depth more than 4% of the RPV wall thickness. Because of this WPS impact, ORNL 2016 characterized the concern with internal SSBFs as only applying to very internal SSBFs.

Table 1-1: Results of FAVOR PFM Monte Carlo analyses – model includes clad

Flaw Depth		Model with WPS		Model without WPS	
a/t	inches	CPI	CPF	CPI	CPF
0.03	0.263	5.5E-05	**2.5E-05**	5.6E-05	**2.6E-05**
0.04	0.350	2.8E-05	**1.2E-05**	2.8E-05	**1.1E-05**
0.05	0.438	1.5E-08	8.3E-11	1.3E-05	**4.6E-06**
0.06	0.525	4.1E-08	3.6E-10	1.3E-05	**4.7E-06**
0.07	0.613	8.6E-08	5.4E-10	2.5E-05	**8.5E-06**
0.08	0.700	1.5E-07	1.4E-09	4.1E-05	**1.4E-05**
0.09	0.788	2.4E-07	1.5E-09	5.2E-05	**1.8E-05**
0.10	0.875	3.4E-07	3.1E-09	5.9E-05	**2.0E-05**
0.15	1.313	9.6E-07	6.6E-09	8.8E-05	**2.9E-05**
0.20	1.750	1.4E-06	1.2E-08	9.9E-05	**3.7E-05**
0.25	2.188	1.6E-06	1.1E-08	9.5E-05	**5.2E-05**

Note: bold value represent CPF higher than 1E-06, which was the threshold for further investigation

Table 1-1 tabulates the mean CPI and mean CPF results. Both are conditional probabilities, conditional in that the postulated transient is assumed to occur and the postulated flaw is assumed to exist.

Plants typically cooldown for refueling outages that occur approximately every 18 to 24 months depending on the plant fuel cycle design. Plants may also cooldown to cold shutdown during an operating cycle for required maintenance during a cycle, but this is a rare occurrence. Therefore, the probability of a normal plant cooldown is approximately once per 18 to 24 months. However, actual plant cooldown for refueling outages do not normally cooldown at the maximum pressure allowed by ASME, Appendix G. Calculation of the TWCF should be based on the CPF from a typical (actual) cooldown as discussed in Section 4.1.2 and should not be based on the CPF values in Table 1-1.

The PFM analysis results in Table 1-1 show that the CPF for an internal SSBF may be greater than the CPF for deeper flaws, including the ¼ thickness flaw from ASME Appendix G if WPS prevents fracture for the deeper flaw internal SSBFs. Because plant cooldowns are conservatively assumed to occur approximately once per year, the TWCF for these actual cooldowns is approximately equal to the calculated CPF. Therefore, internal SSBFs should be considered in evaluations of TWCF for actual expected cooldowns.

1.2 Summary of Additional Internal SSBF Evaluations after ORNL 2016

As a follow-up to ORNL 2016, additional literature searches and sensitivity studies were performed and discussed in an "Assessment of Reactor Pressure Vessel Inside Diameter Shallow Surface Breaking Flaws," [7]. The objective of this study was to assess the sensitivity of the FAVOR results to changes in assumptions or methods, to determine if these changes could reduce the FAVOR calculated internal SSBF CPF below 1.0E-06 for plant cooldowns along the Appendix G P-T limit curve. The study described in [7] evaluated reduction in Stress-Free Temperature (SFT), cooldown at reduced pressure compared to the

maximum value maximum pressure allowed by ASME Appendix G, and WPS during RPV fabrication shop hydro or other previous transients to determine whether a change in these assumptions would significantly reduce the FAVOR calculated CPF for shallow flaws. Based on the literature reviews and analyses, no well-justified changes in analyses assumptions were identified to significantly reduce the CPI and CPF for internal SSBFs. The literature reviews did identify that the difference in assumed stainless steel and ferritic steel coefficient of thermal expansion (CTE) significantly impacts the FAVOR shallow flaw CPI and CPF. This difference between stainless and ferritic steel CTE creates added thermal stress – especially for internal SSBFs that extend just into the ferritic steel. Based on these analyses, an approximate 10% increase in stainless steel CTE used in ORNL 2016 increases FAVOR calculated CPI and CPF by an order of magnitude.

Because the studies in [7] did not identify well-justified changes in assumptions that would significantly reduce the shallow flaw CPF shown in ORNL 2016, additional evaluations were performed to determine whether actual plant cooldown transients would be less limiting than transients based on the maximum pressure allowed by ASME Appendix G procedures. These evaluations were documented in an "Assessment of Reactor Pressure Vessel Inside Diameter Shallow Surface Breaking Flaws Based on Actual Plant Transients" [8]. The analyses of actual plant transients in reference [8] were performed for 11 actual plant cooldown profiles from normal operating temperature and pressure to cold shutdown. These 11 cooldown profiles were analyzed based embrittlement maps for different PWR plants. When compared to an assumed cooldown at the ASME Section XI, Appendix G maximum allowed CDR of 100°F per hour, the CPF calculations for these 11 actual cooldown profiles were several orders of magnitude lower. As discussed in reference [8] report, cooldowns based on actual plant operational practice may be a way to demonstrate that shallow flaw CPF is less than 1.0E-06 , which was the threshold chosen for further investigation in this study.

1.3 Pressure versus Temperature from Actual Plant Cooldown Data

As discussed in Appendix A, plant operating data from 42 cooldowns at 17 different PWR plants were compiled to describe actual plant cooldowns. Based on this data, PWR plants can cooldown at a rate close to the maximum allowed rate of 100°F per hour before switch-over to the residual heat removal (RHR) system at about 300°F. When the cooldown switches over to RHR, the CDR tends to be limited to less than 100°F per hour by operational constraints and plant specific RCS cooldown limits.

Plant cooldown at the maximum 100°F per hour rate to ambient temperature results in higher thermal stress at the end of the transient. This maximum CDR applies to all plant cooldowns and is a conservative assumption that does not rely on any plant specific limits. This maximum CDR was selected for internal SSBF analyses in Sections 2 and 3 of this report to determine whether any additional CDR limits are needed to demonstrate that the FAVOR calculated CPF is less than 1.0E-06. As noted in Sections 2 and 3, no set of assumptions have been identified that support this maximum 100°F per hour rate for all plants. Therefore, additional analyses are described in Section 4 to define CDR assumptions required to limit FAVOR calculated CPF to below 1.0E-06.

This conclusion that cooldown rates need to be less than 100°F per hour to ensure that CPF is below 1.0E-06 is consistent with internal SSBF evaluations shown in EPRI Report MRP-437 [6]. Figure 4-1 and Table 4-1 from MRP-437 provide maximum cooldown rates as a function of vessel wall thickness and ART required to ensure that CPF remains below 1.0E-06.

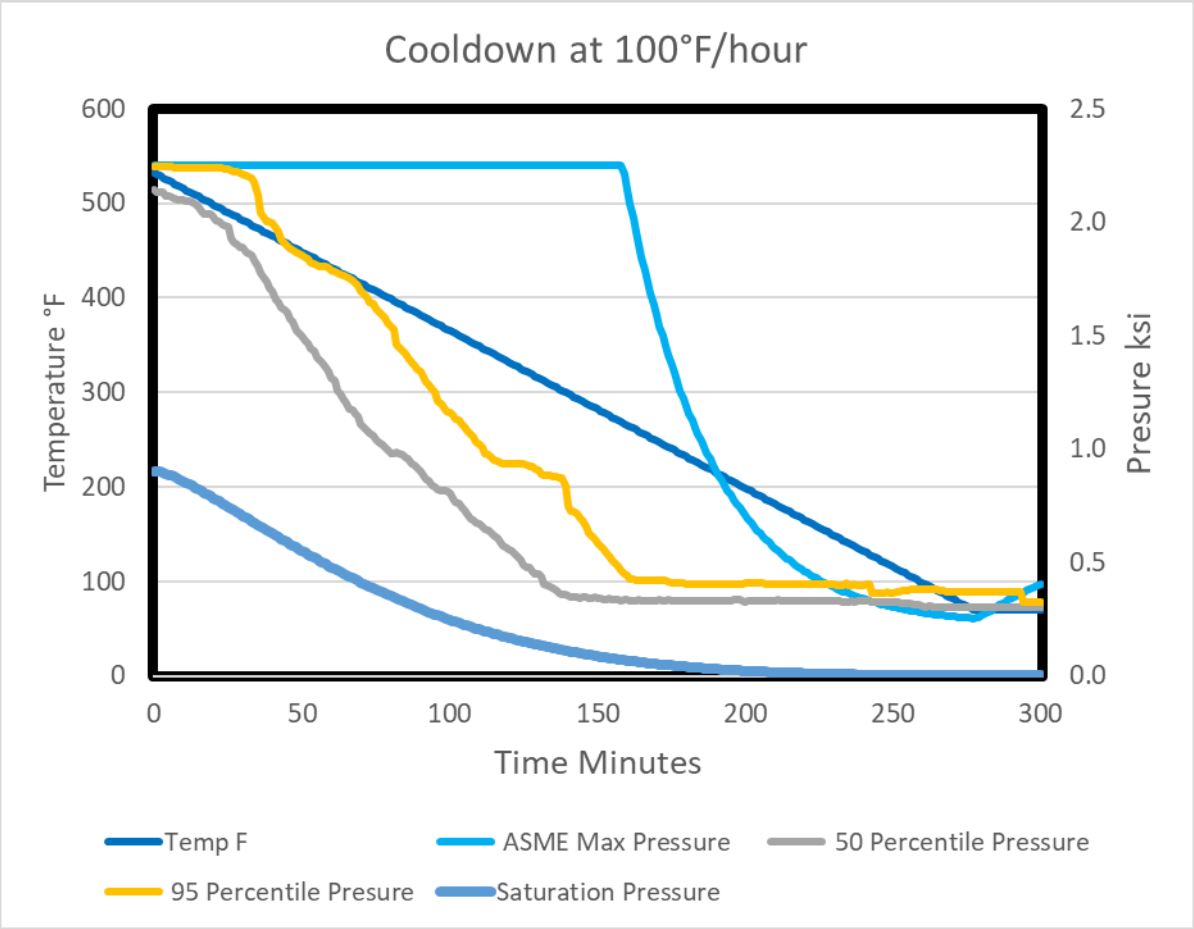

Figure 7 – Pressure/Temperature Curves for 100°F/Hour Cooldown

The internal SSBF analyses in ORNL 2016 all assumed that the pressure during a plant cooldown is at the maximum pressure allowed by ASME Appendix G, which as previously mentioned is only a hypothetical scenario. This assumption produces higher pressure stress early in the transient and an applied K_I(time) that exhibits two peaks (see Figure 4). Figure 7 compares the 50th and 95th percentile data from Appendix A pressure as a function of temperature with ASME Appendix G maximum allowed pressure and saturation pressure.

In the present study, FAVOR analyses at CDR of 100°F per hour were performed for the 50th percentile, 95th percentile, and ASME maximum allowable pressure versus temperature shown in Figure 7. The FAVOR model used for these analyses was based on the RPV with the model inputs and assumptions described in Appendix B

The impact of the pressure versus temperature profile on CPF is shown in Table 1-2. As shown in this table, the CPF is higher than 1.0E-06 for flaws up to 7% of the RPV wall thickness for the 50th percentile pressure versus temperature while the CPF is below 1.0E-06 for all flaw depths above 3% of the RPV wall thickness for the ASME maximum pressure profile.

Table 1-2 Impact of Pressure Temperature Profile on Cooldown at 100°F/hour

Flaw depth	50th Percentile Cooldown * (see Appendix A)	95th Percentile Cooldown * (see Appendix A)	Max ASME Pressure for RT_{NDT} of 281°F *
%	*CPF mean*	*CPF mean*	*CPF mean*
3%	**1.3E-04**	**1.6E-04**	**1.0E-04**
4%	**1.2E-04**	**1.5E-04**	1.0E-10
5%	**8.1E-05**	**1.0E-04**	1.4E-10
6%	**7.5E-05**	1.0E-10	1.7E-10
7%	**9.0E-06**	1.0E-10	9.3E-11
8%	1.0E-10	1.0E-10	1.4E-10
12%	1.0E-10	1.0E-10	1.1E-09
18%	1.0E-10	1.0E-10	9.0E-10
25%	1.0E-10	1.0E-10	3.3E-10

Notes: The higher CPF values for the 50th percentile Cooldown at 6% and 7% flaw depths are due to the loss of WPS protection because of the lower pressure for this hypothetical transient. Bold values represent CPF higher than 1E-06, which was the threshold for further investigation

As demonstrated by the analyses shown in Table 1-2, in the presence of internal SSBFs, the ASME Appendix G maximum pressure versus temperature may underestimate CPF during normal plant cooldowns if WPS is assumed in the FAVOR analysis. As shown in the Table 1-2 analysis, WPS may not prevent brittle fracture for flaw depths up to 7% for the 50th percentile pressure versus temperature cooldown. However, it is important to note that the TWCF that would be associated with the CPF values in Table 1-2 could still be far below 1.0E-6 once the transient frequencies are factored in, especially given that plants typically do not cooldown at 100°F per hour all the way down to room temperature. Furthermore, these results should be understood in the context of the assumptions and conservatisms discussed in the next section.

1.4 Analysis Assumptions and Possible Conservatisms

This section highlights important FAVOR analysis features and assumptions that should be taken into consideration when evaluating the results in the present study, because they represent either definite or potential conservatisms.

1.4.1 Clad Welding

The FAVOR code does not consider the actual welding process by which the cladding is deposited on the vessel inner-surface. This lack of explicit consideration of the cladding deposition process has two consequences on the present analysis.

First, the under-clad heat affected zone (HAZ) that results from tempering during the cladding operation is not explicitly modeled. Consequently, the higher toughness that typically results from the presence of the HAZ, such as that discussed in [9], is not considered in FAVOR's toughness models. Depending on the degree to which the HAZ has a higher toughness than the base metal for a given vessel, the values of CPI and CPF (and thus frequency of crack initiation (FCI) and TWCF) predicted by FAVOR may over-estimate

the actual conditional probabilities of crack growth initiation or vessel failure by an unquantified amount. To date, there have not been systematic studies to evaluate to which degree this potential conservatism may affect FAVOR results.

Second, the number of layers of stainless steel that are deposited to create the cladding is not explicitly modeled. Because of the tempering effect of cladding deposition, vessels that have two-layer cladding are likely to have a higher sub-cladding toughness, which would have an impact on internal SSBFs that extend just beyond the cladding. This potential conservatism may not apply for single-layer clad vessels, but likely has a conservative impact on FAVOR results for two-layer clad vessels. That is, for two-layer clad vessels, the values of CPI and CPF (and thus FCI and TWCF) predicted by FAVOR may over-estimate the actual conditional probabilities of crack growth initiation or vessel failure by an unquantified amount. To date, there have not been systematic studies to evaluate to which degree this potential conservatism may affect FAVOR results.

1.4.2 Flaw Modeling

FAVOR uses LEFM to predict crack growth initiation and failure, because this has widely been accepted as a reasonably accurate way of modeling cracks in reactor pressure vessel base metal, especially after some degree of irradiation embrittlement. By definition, LEFM assumes the presence of infinitely sharp cracks. In reality, any pre-existing cracks could become blunted over time, possibly because of environmental degradation. FAVOR does not consider potential crack blunting that could reduce the stress-intensity factor at the tip of a pre-existing crack, which could potentially result in over-estimation of the stress-intensity factor. If such a phenomenon occurred, it would mean that FAVOR analyses could result in conservative predictions of CPI and CPF. The degree to which such crack blunting may or may not occur is not known, and thus the potential degree of conservatisms associated with assuming infinitely sharp cracks remains unquantified.

The focus of the present study is internal SSBFs. In order to assess these flaws for the transients postulated, these flaws have to be assumed to exist such that a FAVOR analysis may be performed and results obtained. However, the actual existence of such flaws has been questioned. In fact, any significant flaws in the inner surface structural material of a RPV (plate, forging, or weld) would be introduced during fabrication operations, which would have been completed before the application of stainless steel cladding to the inside surface of the RPV. A surface-breaking flaw that existed on the inside surface of the RPV prior to cladding would be converted to a sub-clad flaw by the cladding process, and would have to break through the cladding in order to become a surface flaw again. Furthermore, any potential flaws that might be introduced in the cladding process would likely be detected during pre-service vessel fabrication inspections. In summary, the results presented in this study all assume the presence of an internal SSBF, but the likelihood that such flaws are present in actual vessels, although unquantified, is believed to be very low.

Finally, the crack initiation model in FAVOR assumes that when the applied K_I of a postulated flaw of finite length exceeds K_{IC} of the base metal, an infinitely long flaw is created. An internal SSBF is unlikely to initiate in this manner in a real-life case because the portion of its crack front that can extend in the length direction is in the stainless steel cladding, which has a much higher fracture toughness than the base metal. Instead of becoming an infinitely long flaw, an assumed internal SSBF (when its applied K_I exceeds K_{IC} of the base metal) would more likely propagate via cleavage fracture in the thickness direction and

either continue through the vessel thickness or arrest. Because of its inherent conservatism, the FAVOR crack initiation model could lead to vessel failure when the assumed infinitely long crack propagates through the vessel thickness. However, the impact of a more realistic propagation model for an internal SSBF on the final CPF values calculated by FAVOR cannot be determined at this time because only the infinite flaw propagation is modeled in FAVOR.

1.4.3 Transient Frequencies

In this study, two main types of transients were considered: cooldowns from normal operation (for both PWR and BWR), and leak tests (only for BWR). Table 1-3 shows the corresponding transient frequencies reported in the BTP 5-3 closure memo [5]. This comparison shows that choosing a frequency of 1 per year for P-T limit transients, as was done in the EPRI Study documented in MRP-437 [6], is highly conservative in comparison with the BTP 5-3 closure memo estimated frequencies. However, it represents a conservative assumption for which TWCF = CPF, and eliminates any complexities related to transient frequencies. A commonly accepted limit on TWCF is 1E-06 per year, so setting 1E-06 as a threshold of interest for CPF values is a valid conservative choice for this study. It should be noted here that the exact parameters (including frequency) of an 'actual cooldown' are not well defined and likely are different from reactor to reactor, making it difficult to evaluate the TWCF for such transients, but choosing a frequency of 1 per year for normal cooldowns is in agreement with BTP 5-3. A survey of plant Technical Specifications or Pressure Temperature Limit Reports (PTLRs) could help better define the parameters of 'actual' cooldowns.

Table 1-3: Transient Frequencies from BTP 5-3

Reactor Type	Transient	BTP 5-3 Transient Frequency [events per year]
PWR	100°F/hour P-T limit cooldown	6.0E-06
	Actual cooldown	1.0
BWR	100°F/hour P-T limit cooldown	< 1.0E-07
	40°F/hour P-T limit leak test	1.0E-03
	100°F/hour saturation curve cooldown	1.0
	Plant procedure leak test	1.0

2 Cladding Thermo-Mechanical Modeling

2.1 Cladding Stress-Free Temperature

2.1.1 Summary of ORNL 2016 Stress Free Temperature Evaluation

As discussed in ORNL 2016 Appendix E, FAVOR uses the concept of a SFT to analyze stress resulting from the difference between the CTE values for the RPV stainless-steel cladding and ferritic steel. ORNL 2016 used an SFT of 488°F that was developed from a combination of experimental measurements taken from an RPV shell segment and finite element stress analyses using temperature-dependent thermal-elastic material properties. The SFT of 488°F was determined by analysis to produce a tensile stress of 21.3 ksi at 70°F equal to the average measured circumferential clad residual stress (CRS). The process used in ORNL 2016 is illustrated in Figure 8.

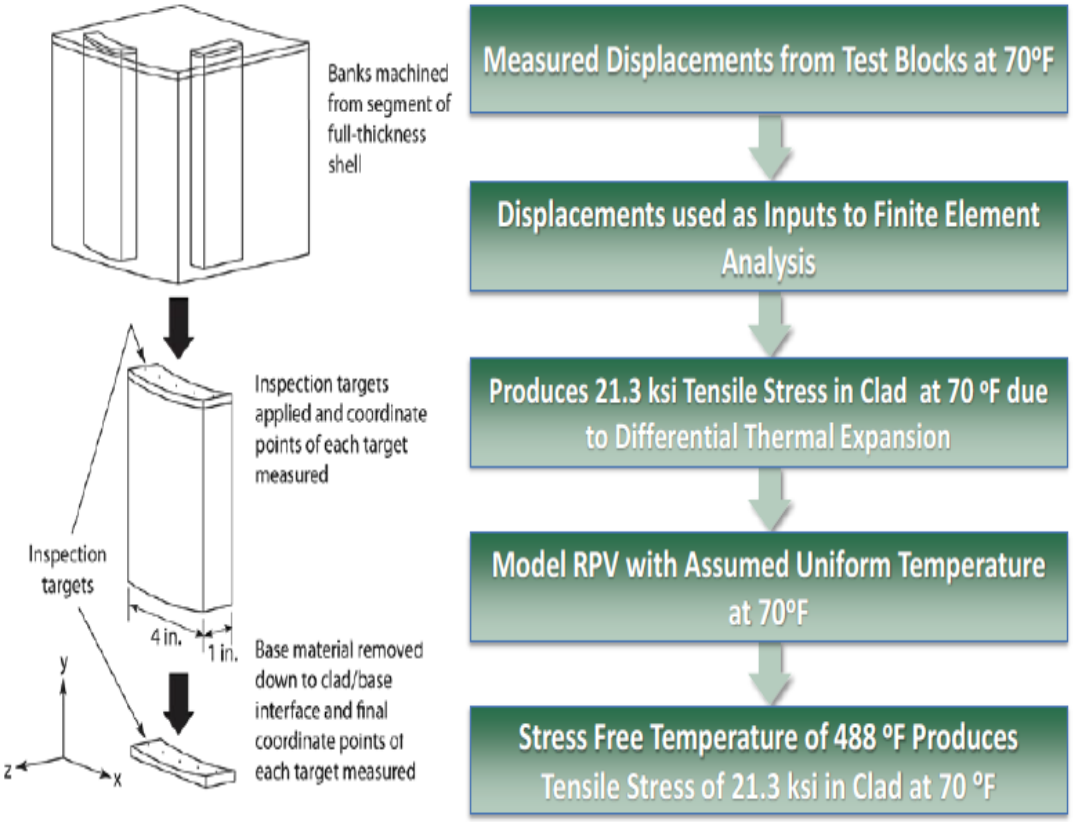

Fig. E-2 Stress-free temperature was determined through combined experimental measurements and finite element analysis.

Figure 8: Process for Determining Stress-Free Temperature

Table 2-1: Stress Components Computed from Strains Measured in Cladding taken from a RPV Shell Segment; stresses are calculated at room temperature (70°F)

Strain Combination	Circumferential Stress (ksi)	Longitudinal Stress (ksi)
Maximum	26.2	17.8
Average	21.3	14.4

As discussed in ORNL 2016, the average measured value of circumferential stress was used to calculate SFT. Because the circumferential and longitudinal stresses do not necessarily go to zero simultaneously, the calculation was based on the larger circumferential component. That application of FAVOR (utilizing temperature-dependent thermal-elastic material properties) determined that a through-clad, average tensile stress of 21.3 ksi at room temperature of 70°F corresponds to a value of SFT of 488°F. This determination of SFT from combined RPV data and analysis allows FAVOR to account for effects of (1) residual stresses produced by weld deposition of the cladding and (2) mismatch in CTE between the cladding and base metal during any loading transient specified by pressure and temperature versus time curves.

As shown Table 2-1, the average measured longitudinal stress was significantly less than the measured circumferential stress. Because longitudinal stress is the most important parameter for the shallow flaws (which are circumferentially oriented due to the cladding welding process), additional ORNL studies were performed to determine the SFT for the average longitudinal stress of 14.4 ksi. This evaluation showed that if the temperature of an unloaded vessel is assumed uniform at 70°F then an SFT of 364°F produces an average thru-clad tensile axial stress of 14.4 ksi that exactly offsets the compressive axial stress.

Because a lower SFT of 364°F suggested by this analysis would reduce the CPF for shallow flaws, literature searches and additional evaluations were performed to determine whether there is a firm technical and experimental basis to support a reduction in SFT to a value significantly below 488°F.

2.1.2 Stress Free Temperature Literature Search

During the search for additional CRS measurements, a report published by the Swedish Nuclear Power Inspectorate (SKI), "Cladding Effects on Structural Integrity of Nuclear Components," Iradj Sattari-Far, Magnus Andersson, June 2006 [10] was identified and reviewed. Section 4 of this report discusses CRS measurements on:

(1) Reactor vessel head of the Ringhals-2 plant

   a. Measured CRS ranged from to 300 MPa (43.5 ksi) 400 MPa (58.0 ksi).

   b. The stress profile reflects the two-layer nature of the manual weld cladding for this plant and showed a larger variation for the tangential stress component.

(2) Reactor nozzles of the Lemonitz plant

   a. The measured CRS peak is between 300 (43.5 ksi) and 350 MPa (50.8 ksi).

   b. The profile of the cladding residual stresses depends on the clad thickness and significant tensile stresses were also found in the base material.

(3) Clad plates (Similar to the Oskarshamn-1 RPV)

a. The hole-drilling techniques and the X-ray diffraction were used to measure CRS.

b. The achieved data from the X-ray technique showed a large scatter with substantially different measured CRS in locations with similar conditions. The measured peak tensile values ranged from about 80 MPa (11.6 ksi) in the center of the cruciform specimen to about 345 MPa (50.0 ksi) in the center of the plate.

c. The hole-drilling technique measured peak CRS was about 200 MPa (29.0 ksi) at 2 mm depth.

(4) Cruciform clad specimens (The NESC-IV project)

a. Framatome ANP GmbH measured CRS of a 100 mm wide strip of a clad beam using the ring core technique.

b. Residual stresses peak at a depth of about 4 mm and range from about 210 MPa (30.5 ksi) to 240 MPa (34.8 ksi).

(5) RPV wall thickness (The ORNL study)

a. Residual stresses from the finite-element analyses for the two cases considered (maximum and average strains) are given to be 148-183 MPa (21.5 to 26.5 ksi) in the circumferential direction and 100-124 (14.5 to 18.0 ksi) in the longitudinal direction.

This report [10] also provided an evaluation of Stress-Free Temperature (SFT) based on a simplified FEM analysis that includes clad welding, post weld heat treatment, pressure test and plant operation. This analysis estimates a clad SFT of 250°C [482°F] as shown in Table 2-2.

Table 2-2 - Clad Residual Stresses at different stages from FEM Analyses [10]

Loading Point	Temperature		Axial stress		Hoop Stress	
	°C	°F	MPa	ksi	MPa	ksi
After Welding	20	68	348	50.5	349	50.6
Post Weld Heat Treatment	600	1112	-2	-0.3	-2	-0.3
After Post Weld Heat Treatment	20	68	35	5.1	136	19.7
Test Pressure	50	122	164	23.8	248	36.0
After Test Pressure	20	68	135	19.6	136	19.7
Operating temperature	300	572	-60	-8.7	-60	-8.7
After operating temperature	20	68	308	44.7	308	44.7
Stress free Temperature	250	482	0	0.0	0	0.0

The measured CRS profile and magnitude depend mainly upon cladding composition, cladding thickness, clad component geometry and temperature. The peak of the cladding residual stresses is about 2-3 mm under the surface of the clad layer, where values in the range of 150 and 500 MPa (21.8 to 72.5 ksi) are reported.

A literature search to identify SFT values used in other RPV stress analyses identified the following values:

1. "3D CFD and FEM Evaluations of RPV Stress Intensity Factor during PTS Loading," used SFT equal to 553°K (536°F). [11]
2. "Probabilistic Fracture Mechanics Round Robin Analysis of Reactor Pressure Vessels during Pressurized Thermal Shock," used SFT equal to 288°C (550°F) as shown in Table 7. [12]
3. "Fracture Mechanical Analysis of a Thermal Shock Scenario for a VVER-440 RPV," indicates an SFT of 267°C (513°F) for the cladded vessel. [13]

Based on this literature review, the 488°F SFT used in ORNL 2016 is within the range of SFT values based on available measurements and analysis. However, the variability and range of CRS measurements do not support a reduction in SFT below 488°F. Because this literature search found several references that indicated that SFT could be higher than 488°F, a sensitivity study of the impact of SFT on CPF was conducted as described in the next section of this report.

2.1.3 Results of SFT Sensitivity Study

A sensitivity study was performed at SFT values of 413°F, 488°F and 563°F with the FAVOR model assumptions and inputs as described in Appendix B. The transient used for these sensitivity studies was a 100°F/hr. cooldown at a reduced pressure (see Figure 12 in [7]). The FAVOR 0.03t flaw calculated K_I(time) is shown in Figure 9. For all three SFTs, the peak K_I(time) occurs near the end of the cooldown. The peak 0.03t flaw K_I increases from 32 to 38 (ksi √in) as SFT increases from 413°F to 563°F. For all three SFT values, the FAVOR calculated 0.03t flaw K_I(time) at low temperature exceeds all previous K_I(time) and the minimum Weibull ${}_aK_{Ic}$ curve. The FAVOR calculated CPF for this SFT sensitivity study varies by about an order of magnitude depending as SFT is increased from 413°F to 563°F as shown in Table 2-3

Table 2-3 – CPF for SFT Values of 413°F, 488°F and 563°F

Stress Free Temp	CPF_{mean}
413°F	1.44E-05
488°F	1.28E-04
563°F	5.33E-04

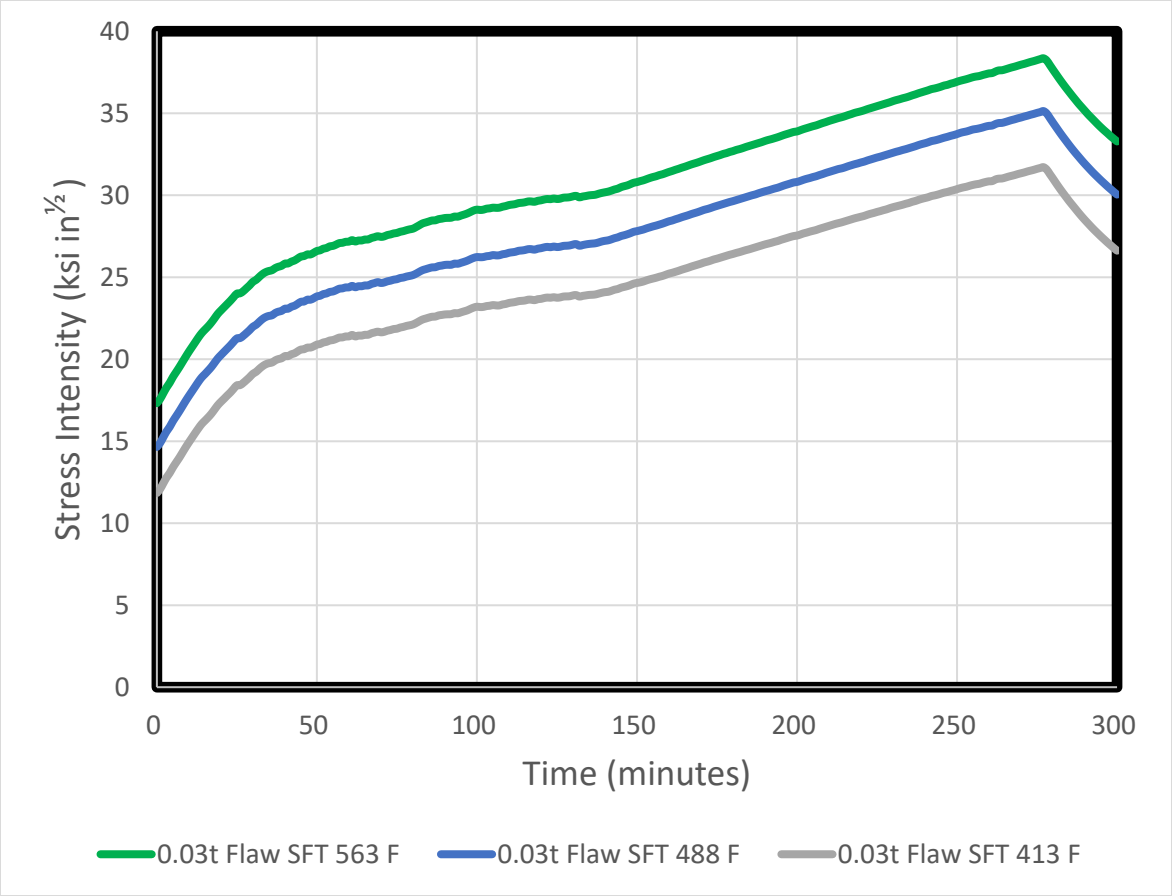

Figure 9 - KI (Time) for 0.03 t Flaw at 413°F, 488°F and 563°F SFT

2.1.4 Summary on SFT for FAVOR Analyses

Based on the literature review discussed in Section 2.1.2, an SFT of 488°F is within the range of SFT values generally used for RPV PFM analyses. FAVOR is a probabilistic analysis that considers a range of values for parameters to determine a mean CPI and CPF. While FAVOR does not specifically consider the variation in SFT values in its probabilistic analysis, the use of an SFT value of 488°F fits within the range of SFT values generally used in PFM analysis and is thus considered to be appropriate for FAVOR shallow flaw analyses. Furthermore, the variability in CRS measurements and calculated SFT does not support a reduction in SFT below 488°F. As a result, SFT changes are not a viable path to decrease the high CPF values resulting from the assumed internal SSBFs in RPVs analyzed in this study.

2.2 Cladding Coefficient of Thermal Expansion

As discussed in Section 1, the differences in physical properties between the stainless-steel clad and ferritic base metal is an important factor in calculating the CPI and CPF for internal SSBFs. The stainless-steel clad CTE used in ORNL 2016 was based on ASME Code, Sect. II, Part D, Material Group D, Table TE-1 (1998) and the CTE of the base metal was based on ASME Code, Sect. II, Part D, Material Group D, Table TE-1 (includes A533B). A literature review and sensitivity study were performed to identify other sources of CTE measured data and to determine whether FAVOR calculated CPI and CPF is sensitive to variations in CTE.

2.2.1 Summary of CTE Literature Review

A report [10] by the Swedish Nuclear Power Inspectorate (SKI) described research into cladding stresses and their significance for RPV structural integrity. This report discusses the welding process for applying RPV cladding, the material data for the stainless-steel cladding and the SKI analysis of RPV structural integrity. The following equation for stainless-steel cladding CTE used in this SKI analysis and was taken from NESC-I 2000:

$$CTE = (15.7 + 0.0096\ T(°C))\ [1.0E\text{-}06/°C]$$

Equation 1

An updated 2015 ASME reference was also identified. This 2015 ASME reference is for austenitic stainless steels (18Cr-8Ni), Material Group 3 and appears on Page 756. As shown in Table 2-4, the ASME 2015 reference CTE values are approximately 1% to 4% higher than the ASME 1998 values and the NESC-I 2000 values are approximately 4% to 9% higher than ASME 1998.

Table 2-4 – Stainless-Steel Clad CTE

Temp (°F)	ASME 1998 (1.0E-06/°F)	ASME 2015 (1.0E-06/°F)	% diff	NESC-I 2000 (1.0E-06/°F)	% diff
100	8.55	8.60	0.6%	8.92	4.3%
200	8.79	8.90	1.3%	9.22	4.9%
300	9.00	9.20	2.2%	9.52	5.8%
400	9.19	9.50	3.4%	9.81	6.7%
500	9.37	9.70	3.5%	10.11	7.9%
600	9.53	9.90	3.9%	10.41	9.2%

2.2.2 Results of Sensitivity Studies

Because differences in CTE between the stainless-steel cladding and the RPV ferritic steel are a potentially important factor in shallow flaw analyses, a sensitivity study was performed to determine the impact of changing clad CTE. The FAVOR model and inputs described in Appendix B were used for these CTE sensitivity studies, except that the CTE was changed to the ASME 2015 and NESC-I 2000 values. Figure 10 shows that the FAVOR calculated 0.03t flaw K_I(Time) is sensitive to the stainless-steel clad CTE as the temperature approaches 70°F.

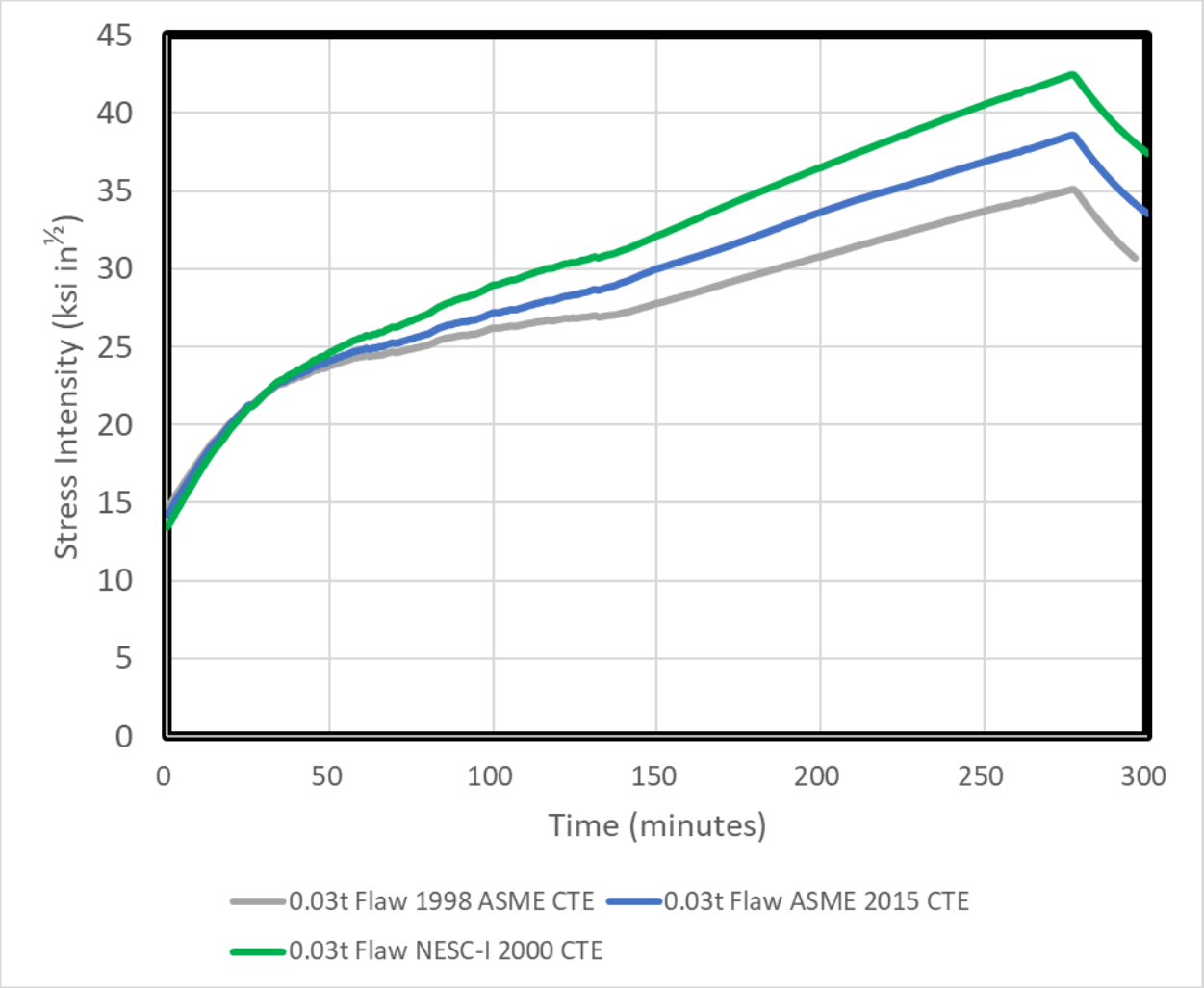

Figure 10 – K_I(Time) for 1998 ASME, 2015 ASME and NESC-I 2000 CTE

FAVOR calculated 0.03t flaw CPI and CPF values are provided in Table 2-5 for the ASME 1998, ASME 2015 and NESC-I 2000 CTE. CPI and CPF are about 3 times higher for the 2015 ASME and about 10 times greater for the NESC-2000 compared with ASME 1998. Based on the sensitivity of CPI and CPF to stainless-steel clad CTE and the variability in CTE shown in the literature for different sources and grades of stainless-steel, CTE is an important factor for shallow flaw analyses. The 1998 ASME CTE correlation results in the lower calculated CPI and CPF, but the overall conservatism built into RPV integrity analysis justifies the continued use of the 1998 ASME CTE.

Table 2-5 - CPF for 0.03 t Flaw for Three Stainless-Steel Clad CTE Data Sources

Clad Coefficient of Thermal Expansion	CPF_{mean}
ASME 1998 CTE	1.28E-04
ASME 2015 CTE	5.83E-04
NESC-I 2000 CTE	1.85E-03

2.2.3 Summary on CTE for FAVOR Analyses

As shown in Table 2-5, changing the CTE data source from the 1998 ASME reference to a NESC-I 2000 data source results in an increase of FAVOR calculated CPI by more than an order of magnitude. The base FAVOR models in Appendix B and Appendix C use the same stainless-steel data source for clad CTE as was used in ORNL 2016 (ASME Code, Sect. II, Part D, Material Group D, Table TE-1 (1998)). The CTE from the 1998 ASME reference results in the lowest calculated CPF, but these values still result in CPF larger than 1.0E-06 (which was the chosen threshold for further investigation), and thus changing the CTE is not a viable path to decrease the high CPF values resulting from the assumed internal SSBFs in RPVs analyzed in this study.

3 Warm Pre-Stress Effects

3.1 Warm Pre-Stress Models

As discussed in Section 4.3.4 of the FAVOR theory manual [2], experimental evidence for the warm prestressing (WPS) effect in ferritic steels was first reported over 40 years ago. Since then, this phenomenon has been the subject of extensive research. The WPS phenomena can be characterized as an increase in the apparent fracture toughness of a ferritic steel after first being "prestressed" at an elevated temperature. Three mechanisms have been identified to produce the WPS phenomena:

1. Preloading at an elevated temperature *work-hardens the material ahead of the crack tip*. The increase in yield strength with decreasing temperature "immobilizes" the dislocations in the plastic zone. Consequently, an increase in applied load is needed for additional plastic flow (a prerequisite for fracture) to occur at the lower temperature.

2. Preloading at an elevated temperature *blunts the crack tip*, reducing the geometric stress concentration, and thus making subsequent fracture more difficult.

3. Unloading after or during cooling from the elevated WPS temperature down to a reduced temperature *produces residual compressive stresses ahead of the crack tip*. The load applied at the reduced temperature must first overcome these compressive stresses before the loading can produce additional material damage and possibly fracture. The residual compressive stresses associated with the unloaded initial plastic zone can be viewed as protecting the crack tip, since higher applied loads are required to achieve a given level of crack driving force compared to the condition before preloading.

Three conditions can be stated for a flaw to not be protected by WPS and, thereby, to be eligible for initiation. These three conditions are:

Condition (1): the applied-K_I is greater than K_{Ic}(min) , where K_{Ic}(min) is defined by the fracture toughness model ($_aK_{Ic}$) for the temperature at the flaw tip.

Condition (2): a rising applied-K_I field – the time-rate-of-change of the applied-K_I is positive.

Condition (3): in a rising applied-K_I field, the driving force at the flaw tip must exceed some portion of the previously-established maximum applied-K_I (designated as K_I(max)) experienced by the flaw during the transient up to the current point in time under consideration:

$$\text{applied KI } (\tau) \geq \alpha \text{ KI(max) } (\tau)$$

Equation 2

FAVOR 16.1 provides four WPS options based on the value of α in the formula in Equation 2 above:

1. **WPS OPTION =** 0 do not include warm prestressing in analysis

2. **WPS OPTION =** 1 crack can only initiate when applied K_I exceeds maximum K_I determined from all previous discrete transient time steps i.e., $\partial K/\partial t > 0$ and $K_I > \alpha K_{I\,max}$ where $\alpha = 1$

3. **WPS OPTION =** 2 crack can only initiate when $\partial K/\partial t > 0$ and $K_I > \alpha K_{I\,max}$ where $\alpha = 0$

4. **WPS OPTION =** 3 crack can only initiate when applied K_I exceeds maximum K_I determined from all previous discrete transient time steps i.e., $\partial K/\partial t > 0$ and $K_I > \alpha K_{I\,max}$ where alpha is sampled from a log-logistic distribution, as discussed in the FAVOR Theory Manual [2], with location parameter = 0, scale parameter = 1.15643, and shape parameter = 20.12346

As discussed in Section 3.1.1, a set of sensitivity studies was performed to evaluate the four WPS models available in FAVOR.

3.1.1 Results of Sensitivity Studies

The FAVOR model described in Appendix B was used to evaluate impact of WPS on FAVOR calculations of CPF from internal SSBFs. In addition to the WPS Option 1 model, analyses were performed with the other three WPS options. The same analyses for a 100°F per hour cooldown with the 50th percentile pressure versus temperature shown in Table 1-2 with WPS option 1 was performed for WPS options 0, 2 and 3. The results of these sensitivity studies is shown in Table 3-1.

Table 3-1 Impact of WPS on FAVOR CPF

Flaw depth	Warm Pre-stress Option 0	Warm Pre-stress Option 1	Warm Pre-stress Option 2	Warm Pre-stress Option 3
%	CPF_{mean}	CPF_{mean}	CPF_{mean}	CPF_{mean}
3%	**1.3E-04**	**1.3E-04**	**1.3E-04**	**1.3E-04**
4%	**1.2E-04**	**1.2E-04**	**1.2E-04**	**1.2E-04**
5%	**8.1E-05**	**8.1E-05**	**8.1E-05**	**8.1E-05**
6%	**7.5E-05**	**7.5E-05**	**7.5E-05**	**7.5E-05**
7%	**9.0E-05**	**9.0E-05**	**9.0E-05**	**9.0E-05**
8%	**1.1E-04**	1.3E-10	**1.1E-04**	**5.6E-06**
12%	**1.6E-04**	1.3E-10	**1.0E-04**	3.2E-07
18%	**2.6E-04**	1.3E-10	**1.2E-04**	5.7E-08
25%	**3.9E-04**	1.3E-10	**1.8E-04**	1.3E-10

Note: bold value represent CPF higher than 1E-06, which was the threshold for further investigation

As discussed in Section 1.3 and shown in Table 3-1, WPS option 1 prevents crack initiation for flaws with a depth more than 7% of the RPV wall thickness. Without any WPS (Option 0), the maximum CPI occurs at the maximum 25% of RPV wall thickness flaw depth analyzed. Using FAVOR WPS Option 2 or 3 provides some reduction in CPF values at flaw depths between 8% and 25%. CPF values for options 2 and 3 are between the CPF for option 0 and 1.

3.1.2 Summary on WPS Models

The existence of WPS has been well established and accepted for FAVOR PFM analysis. In the studies presented in this report, the FAVOR model uses WPS Option 1, which provides the most WPS protection

and thus results in overall lower CPF values. Because this is an accepted WPS model and because WPS Options 0 and 1 bound the results with WPS Options 2 and 3, Option 1 is used for FAVOR internal SSBF evaluations in this report. Even when using WPS Option 1, the calculated CPF values exceed 1.0E-06 (which was the chosen threshold for further investigation), and thus WPS is not a viable path to decrease the high CPF values resulting from the assumed internal SSBFs in RPVs analyzed in this study.

3.2 Shop Hydro Testing

As discussed in Section 3.1, the Appendix B FAVOR model used for internal SSBF analyses in this report assumes WPS (Option 1) based on the transient being evaluated. Shop hydro testing during vessel manufacture may warm pre-stress flaws up to the applied hydro test K_I, for internal SSBFs presumed to exist when the RPV is shop hydro tested. It is important to note that internal SSBFs are generally not expected to exist, however, they are assumed to allow their study in the context of the present assessment of internal SSBFs.

3.2.1 Results from Shop Hydro Test Modeling

Vessel pressure testing requirements are addressed in UG-99 and UG-100 in ASME Code Section VIII Div. 1. Shop hydro tests are performed at a minimum test temperature set by the pressure vessel design minimum metal temperature, with a maximum temperature of 120°F. The maximum hydrostatic test temperature of 120°F results in lower thermal and total pre-stress than testing at a lower temperature. This is because the thermal mismatch stresses are lower as the temperature gets closer to the cladding stress-free temperature of 488°F.

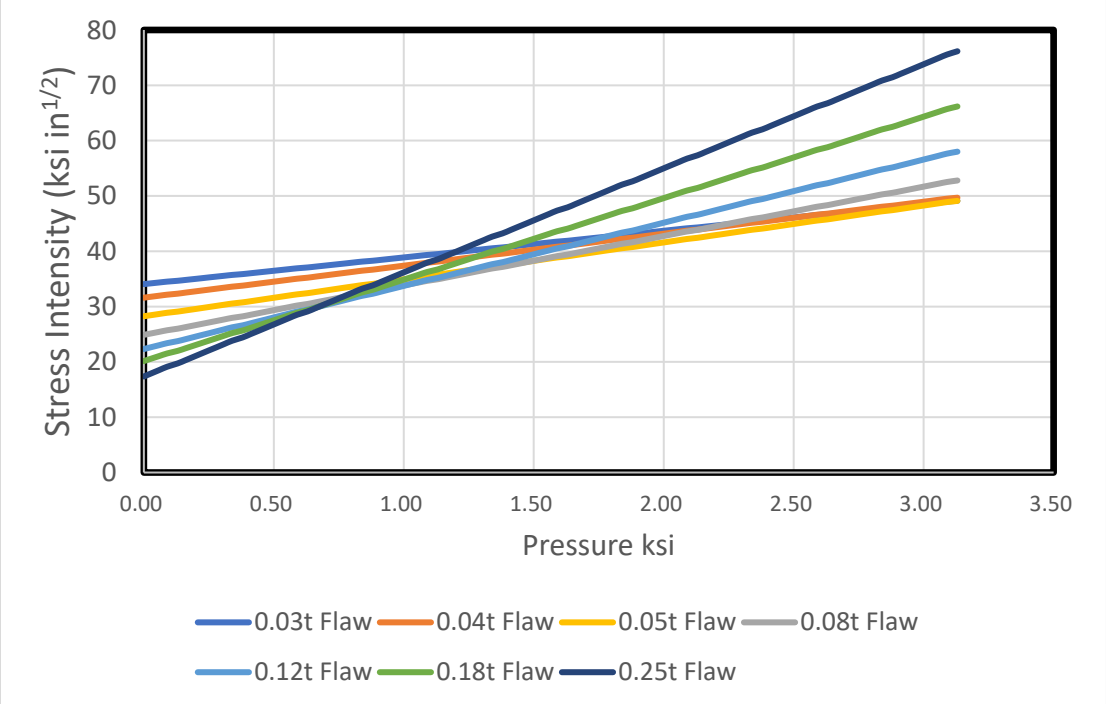

Figure 11- K_I Applied during RPV Hydrostatic Tests

Based on general ASME shop hydro test requirements, a maximum test pressure of 3.125 ksi (1.5 times the design pressure) at 120°F was selected for the analysis of shop hydro WPS. The K_I versus pressure from 0.0 ksi to the assumed 3.125 ksi test pressure is shown in Figure 11 for internal SSBFs from 3% to 25% of the RPV wall thickness. These analyses used the Appendix B model assumptions except that SFT was set to 563°F and the stainless steel CTE is from NESC-I 2000 to maximize calculated stress.

3.2.2 Summary on Shop Hydro Testing

The applied shop hydro K_I shown in Figure 11 is higher than the expected applied K_I from normal plant cooldowns. Therefore, this applied K_i could be sufficient to WPS the flaw tip of internal SSBFs that exist at the time of the hydrostatic test. However, if new internal SSBFs are created after the shop hydro or if pre-service internal SSBFs extend deeper during RPV service, then shop hydro WPS may not be effective in preventing shallow flaw crack initiation. WCAP-16168-NP [14] states that "Fatigue crack growth is recognized as the primary degradation mechanism in the carbon and low alloy steel components in PWR Nuclear Steam Supply System (NSSS), that could contribute to any potential growth of existing flaws in the component base materials and weld metals." In response to NRC questions on WCAP-16168-NP, the PWR Owners group provided reference fatigue crack growth curves for carbon and low alloy ferritic steels. The curves show crack growth rates of approximately 10^{-5} to 10^{-3} inches per fatigue cycle depending on the applied stress. As fatigue crack growth of pre-service internal SSBFs occurs during RPV service, shop hydro WPS may no longer apply. Because of potential fatigue crack growth of pre-service internal SSBFs and possible new internal SSBFs that might be created during RPV service, shop hydro WPS may not be effective and shop hydro WPS has not been assumed for the internal SSBF analyses in this report.

4 Loading Path Effects

The maximum cooldown rate (CDR) allowed by the ASME Boiler and Pressure Vessel Code is 100°F per hour. Based on analyses and sensitivity calculations for cooldowns at 100°F per hour, no set of assumptions has been identified that systematically limits CPF to less than the 1.0E-06. Therefore, additional analyses have been performed to define the CPF for actual cooldowns that are assumed to occur approximately once per year to then calculate the expected TWCF.

Four plant models were developed to evaluate plant cooldowns for a range of plant geometries, material properties and embrittlement. The plant models are described in Appendix B.

Because FAVOR limits flaw depth to 1% increments of RPV wall thickness, a minimum flaw depth is chosen for each RPV as the 1% RPV wall thickness increment that just extends through the stainless-steel clad into the ferritic steel vessel wall. The clad thicknesses and flaw depths for the four plants are shown in Table 4-1.

Table 4-1: Vessel Wall Thickness, Clad Thickness and Flaw Depth

Plant	Vessel Wall Thickness (in.)	Clad Thickness (in.)	Clad Thickness (% wall)	Flaw Depth (% of RPV Wall)	Flaw Depth (in.)
PWR A	8.75	0.25	2.86%	3%	0.2625
PWR B	8.988	0.313	3.48%	4%	0.3595
PWR C	8.626	0.188	2.18%	3%	0.2588
PWR D	8.036	0.156	1.94%	2%	0.1607

To provide a consistent evaluation that shows the impact of vessel geometry, clad thickness, and plant embrittlement on CPF, each of these four plants was evaluated for a constant 100°F per hour CDR from 550°F to 70°F. Then the plant with the most limiting CPF was evaluated for 11 actual plant cooldown pressure-temperature profiles selected for this study. These actual plant cooldown profiles were selected from the 42 plant cooldowns discussed in Appendix A.

4.1 PWR Cooldowns

4.1.1 Plant Cooldown at the ASME Maximum 100°F per Hour CDR

The four plants shown in Table 4-1 were evaluated for the cooldown transient shown in Figure 12. This transient is a 100°F per hour cooldown from 550°F to 70°F using the 50th percentile pressure versus temperature profile described in Appendix A and assuming a minimum 0.5 ksi pressure at the end of the cooldown. FAVOR was used to determine the CPF for this transient assuming a single internal SSBF with the flaw depths shown in Table 4-1. The plant embrittlement maps were developed for Plants 1, 2 and 3 based on data from RVID2 and other available sources, which was then extrapolated to 60 EFPY. This extrapolation likely results in embrittlement values that are different from those actually reported by licensees at 60 years of operation, but that are bounding for 60 years of operations. Plant D used a more detailed 60 EFPY embrittlement map that was developed as part of previous Pressurized Thermal Shock (PTS) evaluations. The plant geometry and other FAVOR inputs are summarized in Table 4-1 and shown in detail in Appendix B.

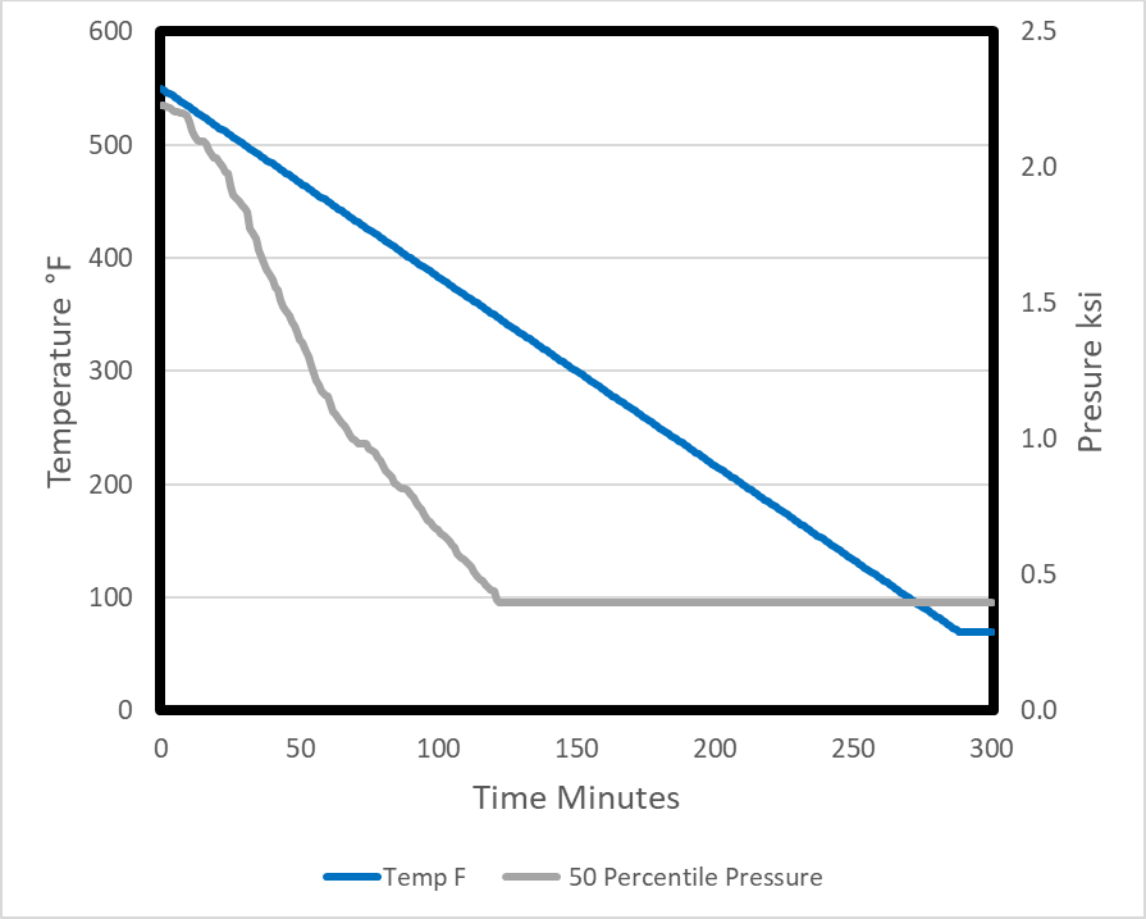

Figure 12 – Cooldown from 550°F to 70°F at 100°F per Hour at 50th Percentile Pressure

The FAVOR calculated mean CPF for these four plant evaluations is shown in Table 4-2.

Table 4-2 CPF for a Cooldown from 550°F to 70°F at 100°F per hour and 50th Percentile Pressure versus Temperature

Plant	RT_{PTS} at vessel ID	Flaw Depth	CPF
PWR A	~ 320°F	3%	3.1E-04
PWR B	~ 300°F	4%	3.1E-05
PWR C	~ 260°F	3%	6.2E-07
PWR D	~ 275°F	2%	1.2E-06

Note: fluence values used for embrittlement calculations came from RVID2 and other available sources and were scaled up to 60 EFPY

The calculated CPF is above 1.0E-06 for Plants PWR A, PWR B and PWR D and slightly less than 1.0E-06 for PWR C. PWR C has relatively thin stainless steel cladding (0.188 in.) and relatively low embrittlement. Because cooldown based on a maximum cooldown rate of 100°F per hour resulted in CPF greater than 1.0E-06 for three of these four plants, additional studies were performed based on several actual plant cooldowns from Appendix A. However, the CPF values in Table 4-2 should be understood in the context of the assumptions and conservatisms discussed in Section 1.4.

4.1.2 Sensitivity Studies on Cooldown Scenarios

Forty-two actual plant cooldowns were obtained from 17 different US PWR plants for internal SSBF evaluations. One profile from 11 of the 17 plants was selected for FAVOR analysis. Ten of these 11 cooldowns were selected because they are representative of normal plant cooldowns prior to a refueling outage. For refueling outage cooldowns, the RCS temperature and pressure are reduced relatively quickly after the plant was shut down to Hot Zero Power (HZP). One outage was selected (Plant 7 – 1997) because the system pressure was held at operating pressure for approximately 100 hours with the plant at HZP. While no explanation was provided for this cooldown profile, the plant may have been kept at HZP for maintenance to allow a quick return to power. Probably because maintenance was not completed after an extended time at HZP, the plant was then apparently cooled down to ambient temperature to complete the required maintenance. This cooldown profile was selected to determine whether remaining at full system pressure for an extended time has a significant impact on FAVOR calculated CPF.

Figure 13 provides a plot of RCS temperature versus time for the 10 cooldowns prior to refueling (the plant remaining at HZP for an extended time was omitted from this figure to show the refueling outages cooldowns on an appropriate time scale). Plots of both RCS temperature and pressure versus time for all 11 transients are provided in Appendix A.

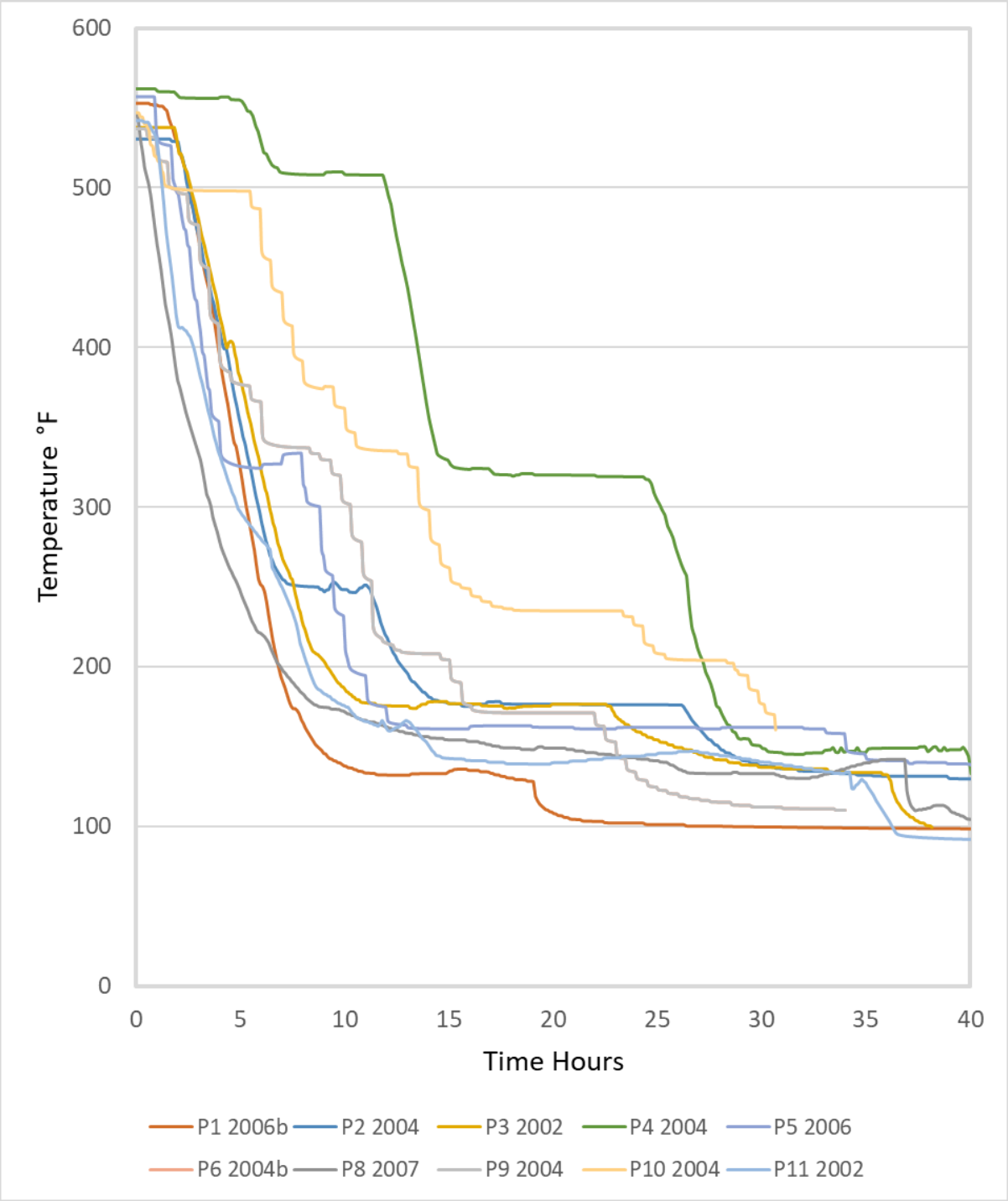

Figure 13 – Plant Cooldown Temperature versus Time

The FAVOR code was used to analyze one 3% surface breaking flaw per vessel for these 11 actual plant P-T transients based on the plant geometry for PWR A with 60 EFPY embrittlement values (extrapolated from RVID2 and other sources of available information) and other plant inputs shown in Appendix B. Table 4-3 shows the results of these actual plant cooldowns along with TWFC calculated assuming one transient per year, which agrees with the frequency for a normal cooldown as reported in the BTP 5-3 closure memo

[5]. As shown in this table, the TWCF for these actual plant transients is substantially less than 1.0E-06 per year for all 11 transients. The TWCF for PWRs B, C, and D (see Table 4-1) are lower than PWR A primarily because the embrittlement is lower for these other plants.

Table 4-3: FAVOR Analysis of PWR A TWCF for 11 Actual Plant Transients

Actual Cooldown	CPF_{mean}	Transients per year	TWCF
Plant 1 2006b	6.80E-16	1.00E+00	6.80E-16/yr.
Plant 2 2004	1.91E-12	1.00E+00	1.91E-12/yr.
Plant 3 2002	2.50E-13	1.00E+00	2.50E-13/yr.
Plant 4 2004	0.00E+00	1.00E+00	0.00E+00/yr.
Plant 5 2004	9.29E-13	1.00E+00	9.29E-13/yr.
Plant 6 2004	0.00E+00	1.00E+00	0.00E+00/yr.
Plant 7 1997	2.69E-10	1.00E+00	2.69E-10/yr.
Plant 8 2007	1.50E-08	1.00E+00	1.50E-08/yr.
Plant 9 2004	1.10E-11	1.00E+00	1.10E-11/yr.
Plant 10 2004	0.00E+00	1.00E+00	0.00E+00/yr.
Plant 11 2002	0.00E+00	1.00E+00	0.00E+00/yr.

The actual plant transients with the highest CPF and TWCF are Plant 7-1997 and Plant 8-2007. The Plant 8-2007 cooldown transient is a cooldown prior to a refueling outage. As shown in Figure 14, during this Plant 8-2007 cooldown, the RCS temperature is reduced from 547°F to about 300°F in 3.6 hours at an average rate of 69°F per hour. The cooldown from 300°F to 150°F occurs over the next 13.8 hours at an average of 11°F per hour. Figure 15 shows the rolling 15-minute average cooldown rate versus temperature for Plant 8-2007. At approximately 36 hours into the cooldown there is a cooldown of 25°F in less than 15 minutes. This fast 25°F cooldown is representative of the RCS temperature change when the last reactor coolant pump is shut down. The initial pressure reduction from operating pressure of 2250 psia to 350 psia occurs over 2.7 hours. The pressure then remains at about 350 psia until about 38 hours when the RCS pressure is reduced to atmospheric.

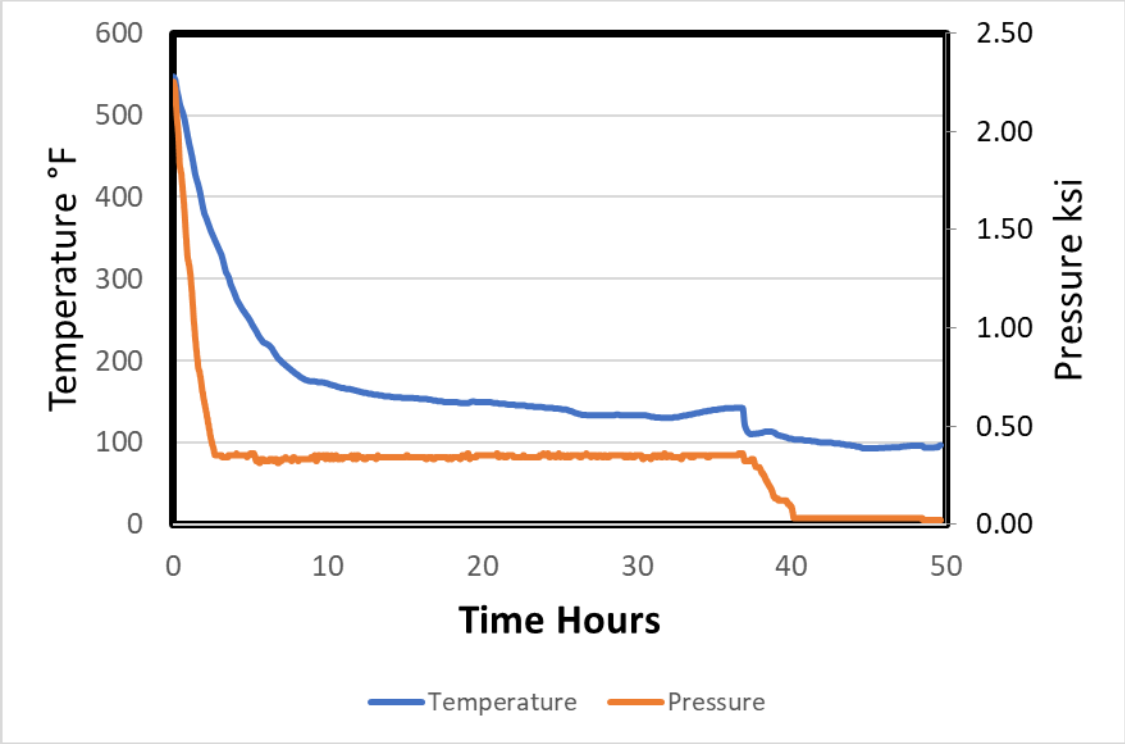

Figure 14: Plant 8 2007 Cooldown Profile

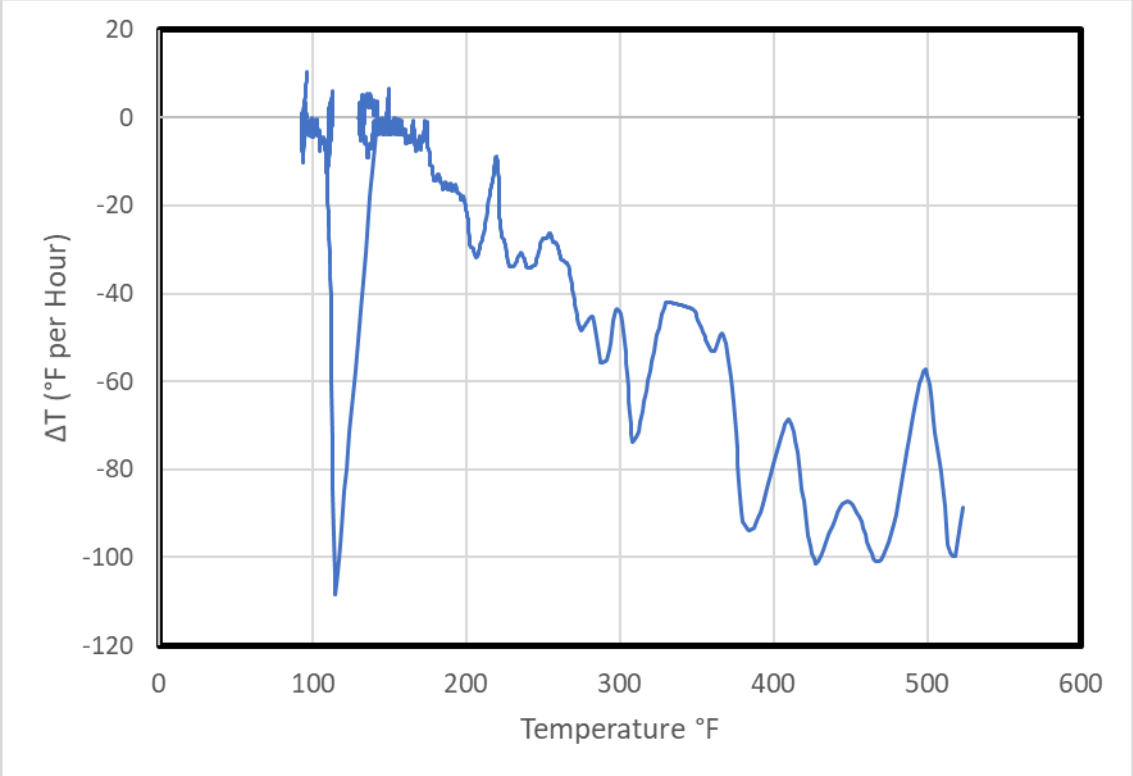

Figure 15: Plant 8 2007 Cooldown Rate Versus Temperature

The FAVOR calculated stress intensity factor for the Plant 8-2007 cooldown based on the PWR A geometry and 60 EFPY embrittlement values (extrapolated from RVID2 and other available sources of information) is shown in Figure 16 and compared to the ASME K_{Ic} and FAVOR $_aK_{IC}$. As shown in Figure 16, the short duration spike in cooldown rate at 36 hours causes a spike in stress intensity factor to values above $_aK_{Ic}$. This spike in stress intensity factor at relatively low temperature above $_aK_{Ic}$ explains why the FCI for this transient is higher than the other refueling outage cooldowns.

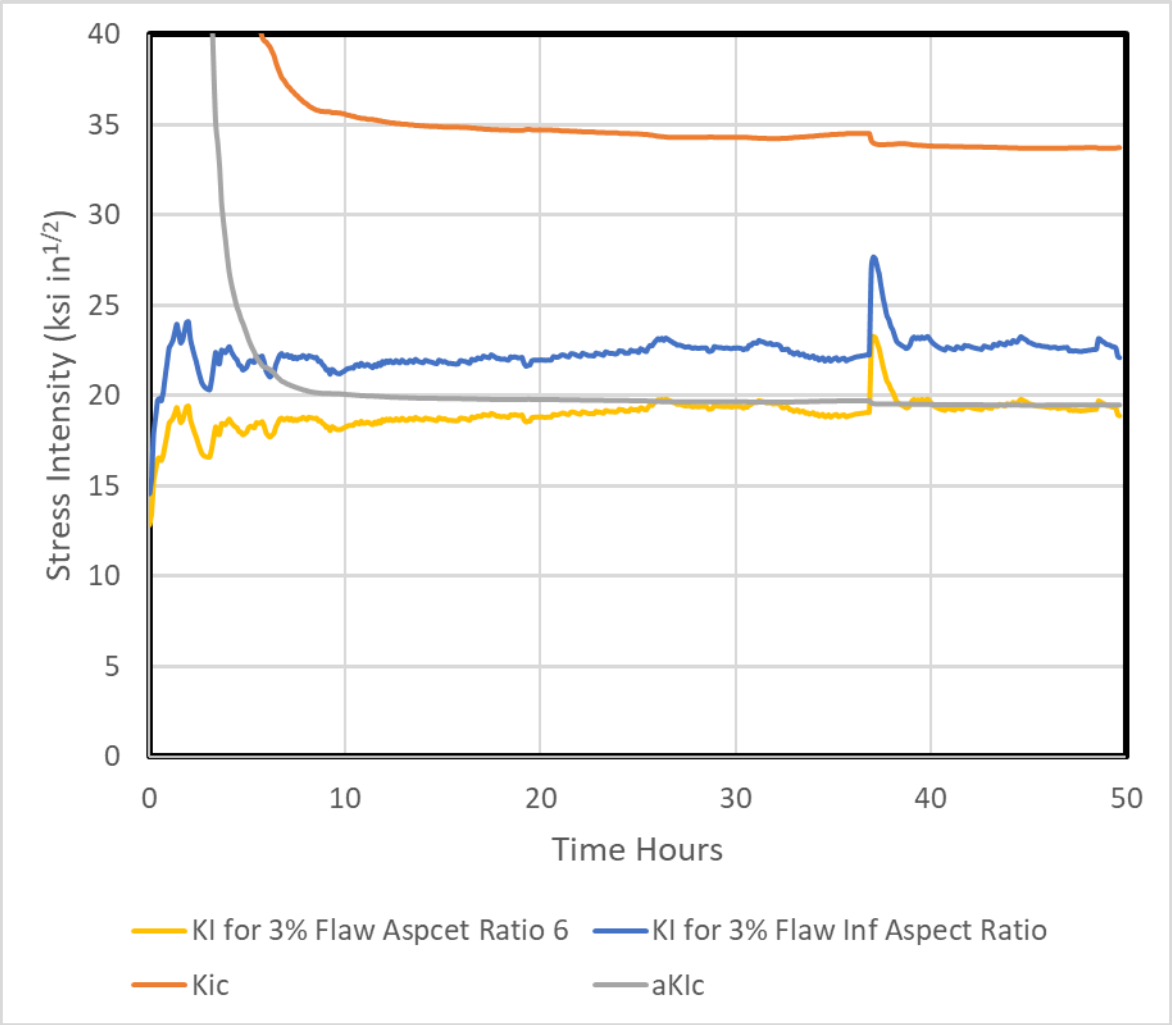

Figure 16: Stress intensity factor for Plant 8-2007 Cooldown Based on PWR A Embrittlement

The Plant 7-1997 cooldown transient is not a typical cooldown prior to a refueling outage. As shown in Figure 17, during this Plant 7-1997 cooldown, the RCS temperature is slowly reduced from 535°F to about 280°F over 150 hours at an average rate of 1.8°F per hour. The cooldown from 300°F to 120°F occurs over the next 50 hours at an average of 3.2°F per hour with a final cooldown to 72°F. Figure 18 shows the rolling 1-hour average cooldown rate versus temperature for Plant 7-1997. RCS pressure for the Plant 7-1997 is held at 2250 psia for about 100 hours. The pressure is then reduced to about 400 psia and remains at this pressure for at least the 250 hours of data provided.

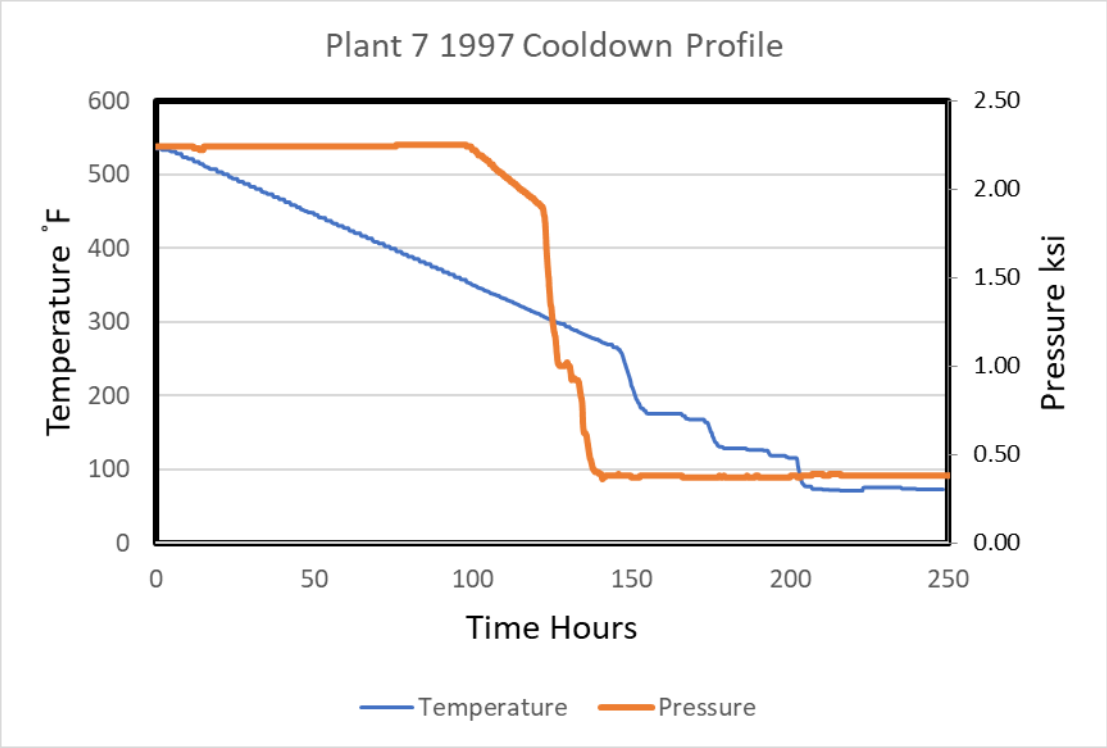

Figure 17: Plant 7-1997 Cooldown Profile

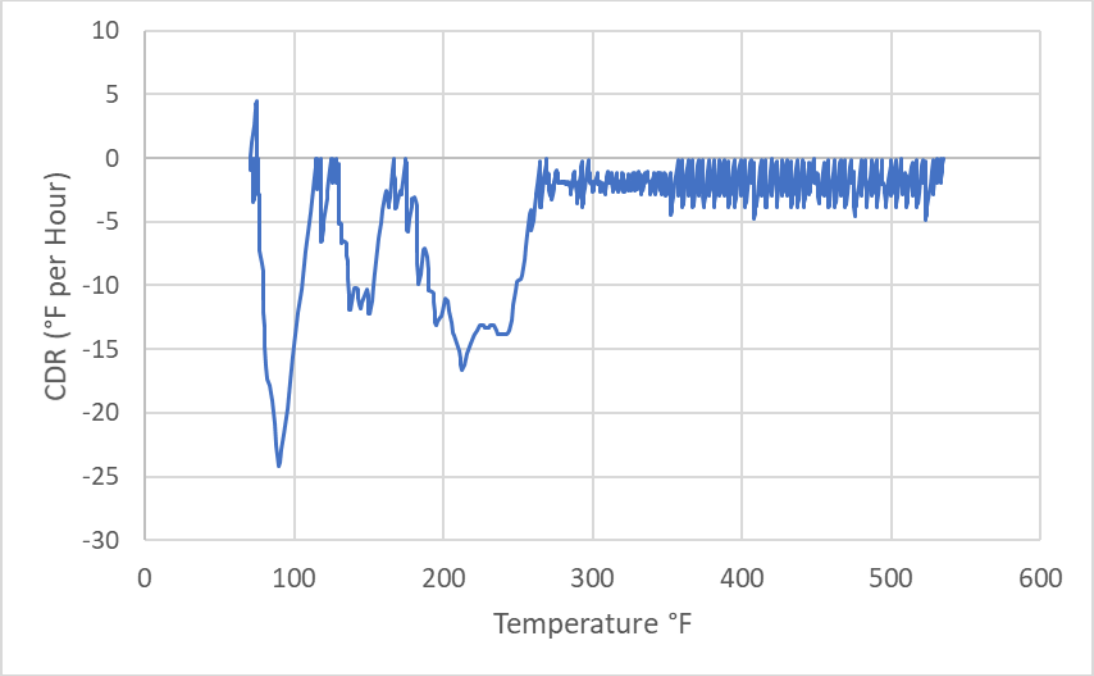

Figure 18: Plant 7-1997 Cooldown Rate versus Temperature

The FAVOR calculated stress intensity factor for the Plant 7-1997 cooldown based on the PWR A geometry and 60 EFPY embrittlement (from RVID2 and other sources of information) is shown in Figure 19 and compared to the ASME K_{Ic} and FAVOR ${}_aK_{IC}$. As shown in Figure 19, the cooldown at CDR of 25°F/hr. near

ambient temperature causes an increase in stress intensity factor to values above $_aK_{Ic}$. This increase in stress intensity factor at relatively low temperature above $_aK_{Ic}$ explains why the CPI for this transient is higher than the other cooldowns. In addition, the cooldown to ambient temperature increases the total stress intensity factor above the values earlier in the transient when the pressure was held near 2250 psia. Thus, warm pre-stress does not prevent crack growth initiation for this combination of flaw depth and cooldown transient.

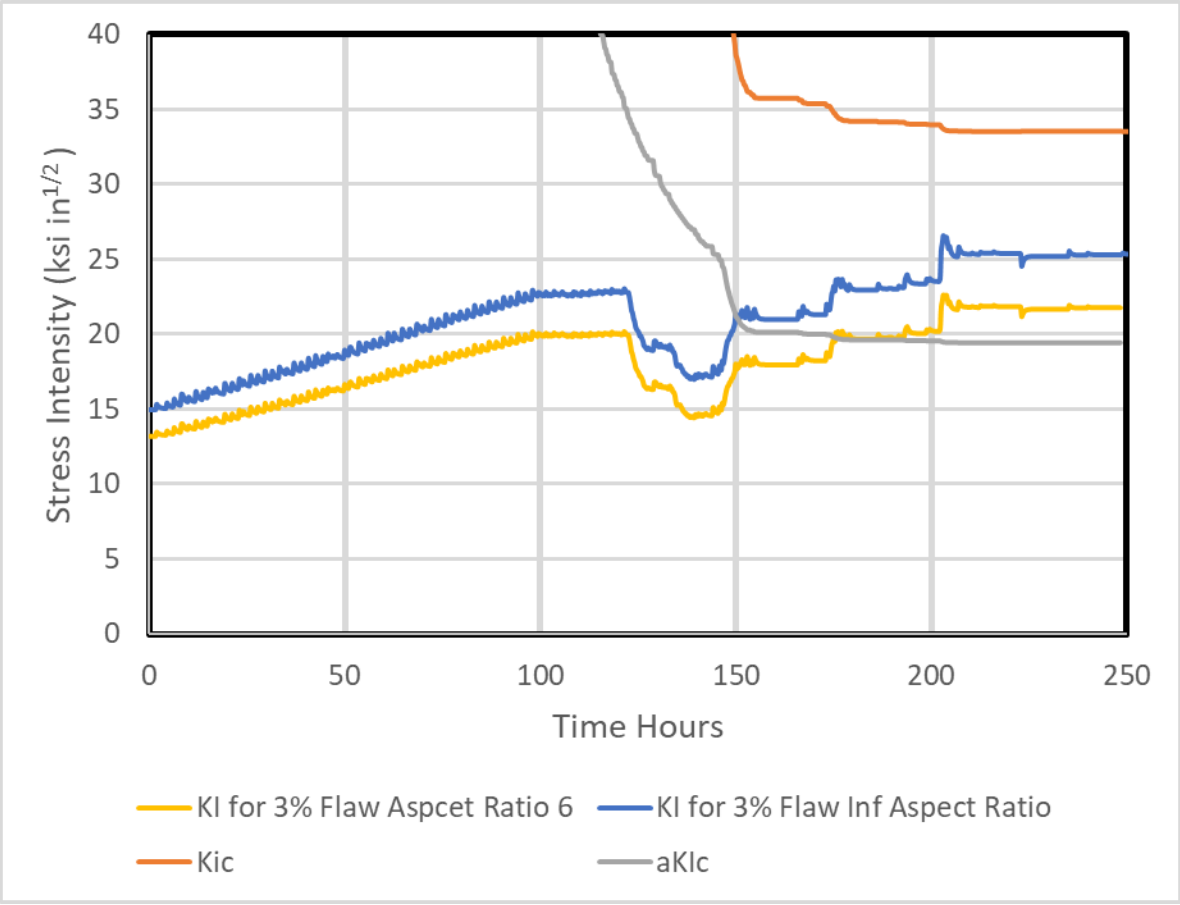

Figure 19: Stress intensity factor for Plant 7-1997 Cooldown Based on PWR A Embrittlement

From this analysis of a limited set of actual transients, actual plants initially tend to cooldown at rates close to the maximum 100°F per hour with the plant secondary system heat sink. Except for a case like the Plant 7-1997 cooldown that was probably not for a refueling, the RCS pressure is reduced as soon as the cooldown begins. Maintaining full system pressure during a normal cooldown for refueling would require addition of water to offset level shrinkage as the RCS water density increases with decreasing temperature. If the plant is being cooled down for refueling, pressure is maintained above saturation but not at full system pressure. As discussed in Section 3.1, this simultaneous pressure and temperature reduction means that flaws up to approximately 6% of the vessel wall thickness are not prevented from crack initiation by WPS.

For refueling outage cooldowns, the CDR is normally substantially lower after the plant switches over to the Residual Heat Removal (RHR) system at approximately 300°F. The heat removal capacity of RHR heat exchangers is significantly less than heat removal by the plant secondary system, which can remove the

full operating plant heat output. Especially where the plant has only been shut down from full power and still has a significant decay heat output, cooldown on RHR tends proceed at or below a CDR of 50°F per hour. This CDR is further decreased as the difference between the RCS and the heat sink for RHR is reduced. The final temperature at the end of most plant cooldowns for refueling is also generally about 100°F or higher and not the 70°F ambient temperature usually assumed for FAVOR analysis.

The Plant 7-1997 cooldown is not a typical cooldown. For this cooldown, the initial CDR was at a rate of less than 2°F per hour and the plant pressure was maintained at plant operating pressure for over 100 hours. This would be expected if a plant trip occurred and the plant operators decided to maintain the plant close to HZP conditions to allow a return to power. Then the plant pressure was reduced relatively quickly from about 2250 psia to just below 500 psia once the plant had cooled to 300°F and switched over to RHR. This is the only transient (among those studied) where the final RCS temperature was close to 70°F. Because this cooldown was not for refueling, the RCS pressure was only reduced to approximately 500 psia. As shown in Figure 19, this type of cooldown can result in an applied K_I near the end of the cooldown above all previous K_I values and above ${}_aK_{Ic}$.

While the actual PWR cooldowns evaluated in this section are a small sample of both plant models and cooldown transients, the FAVOR calculated CPF for all these actual transients is less than 1.0E-06.

4.1.3 P-T Limit Cooldowns

As discussed in Section 4.1.2, actual PWR plant cooldowns tend to occur at cooldown rates much less than 100°F per hour after the cooldown switches over to RHR. As power plants continue to operate and accumulate additional neutron embrittlement of the RPV, plant licensees evaluate the RPV material properties, vessel fracture toughness, and temperature for transition from brittle to ductile behavior. "Arkansas Nuclear One (ANO) Unit 1 Pressure-Temperature Limits at 54 EFPY," [15] provides revised Pressure -Temperature (P-T) limits for continued plant operation to 54 EFPY. As stated in this report,

> "Pressure-temperature limits for the ANO-1 reactor vessel are developed in accordance with the requirements of 10 CFR Part 50, Appendix G [1], utilizing the analytical methods and flaw acceptance criteria of topical report BAW-10046A, Revision 2 [4] and ASME Code Section XI, Appendix G."

Table 4-5 provides ANO Unit 1 Technical Specifications pressure versus temperature limits for normal plant cooldowns at selected temperatures from Table 7-3 of the ANO report [15]. The ANO maximum pressure versus temperature is plotted in Figure 20 along with the 50th percentile pressure versus temperature for actual cooldowns in Appendix A. ANO Technical Specifications limit the maximum CDR to 50°F in any ½ hour period (100°F per hour) from plant operating temperature to 280°F. After that, the maximum CDR limited to 25°F in any ½ hour period (50°F per hour) from 280°F to 150°. There is a special provision in the ANO P-T limits for the short-term cooldown that is expected to occur when the last RCP trips. As noted on page 8 of the ANO P-T limits [15], there is a rapid cooldown of about 25°F within 20 seconds after the final RCP is tripped. While the final RCP trip may occur at a temperature as high as 255°F, the final RCP is allowed to operate down to a temperature of 175°F to circulate RCS water for chemistry control. After this RCP trip, the RCS temperature drops from 175°F to 150°F and is held at 150°F for two hours. The plant cooldown below 150°F is limited to 25°F per hour.

Table 4-4: ANO P-T Limits

ANO Unit 1 - Tech Specification P-T Limits for Normal Cooldown														
°F	70	130	150	170	190	208	228	248	340	390	430	470	500	560
psia	535	619	717	904	1103	1364	1788	2422	2532	2544	2602	2697	2787	3022

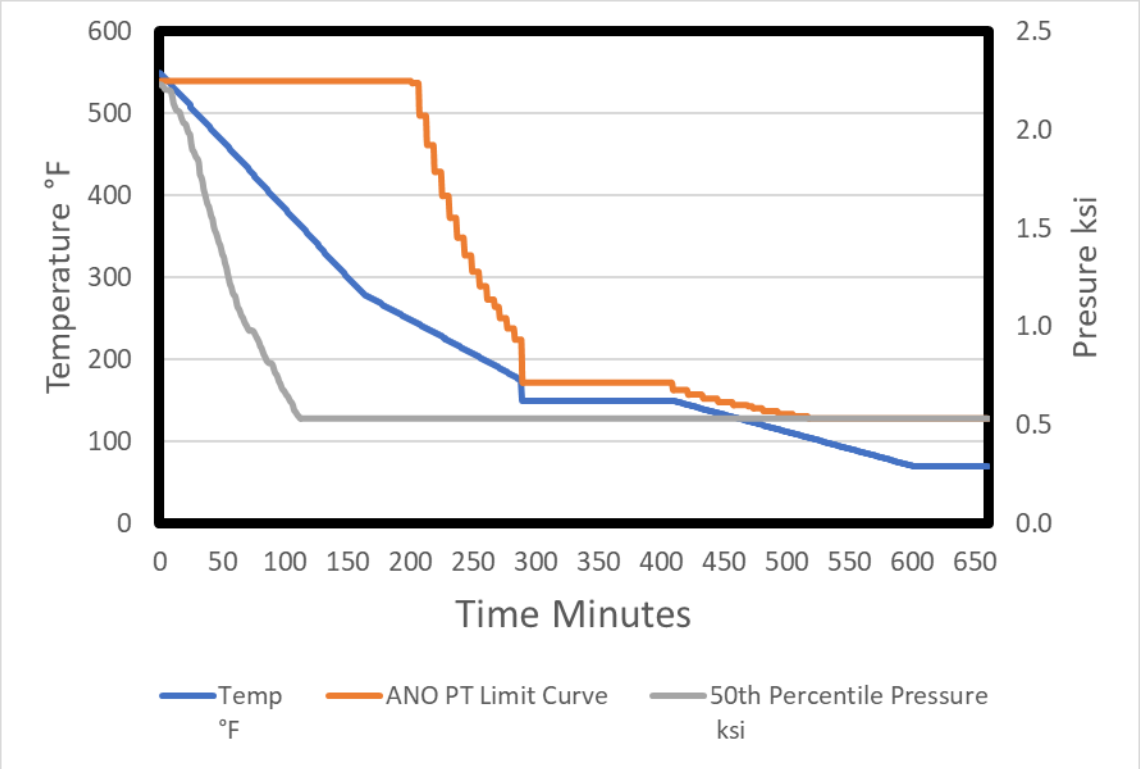

Figure 20: Cooldown based on P-T Limits for ANO Unit 1

FAVOR analyses were performed for PWRs A through D based on the RCS transient described in Figure 20. The cooldown simulated used the maximum CDR versus temperature allowed by the ANO Unit 1 Technical Specifications P-T limits in combination with the 50th percentile pressure in Figure 20. This pressure versus temperature is based on the 50th percentile pressure versus temperature determined from the actual plant cooldown transients discussed in Appendix A. A minimum pressure of 535 psi was used based on the P-T limit curve allowed pressure at 70°F. Figure 21 shows the applied the crack tip stress intensity factor for PWR A with this cooldown. The 25°F temperature decrease from 175°F to 150°F produces a spike in K_I at 288 minutes into the cooldown. The FAVOR calculated CPF for PWRs A through D subjected to the Figure 20 cooldown is provided in Table 4-5.

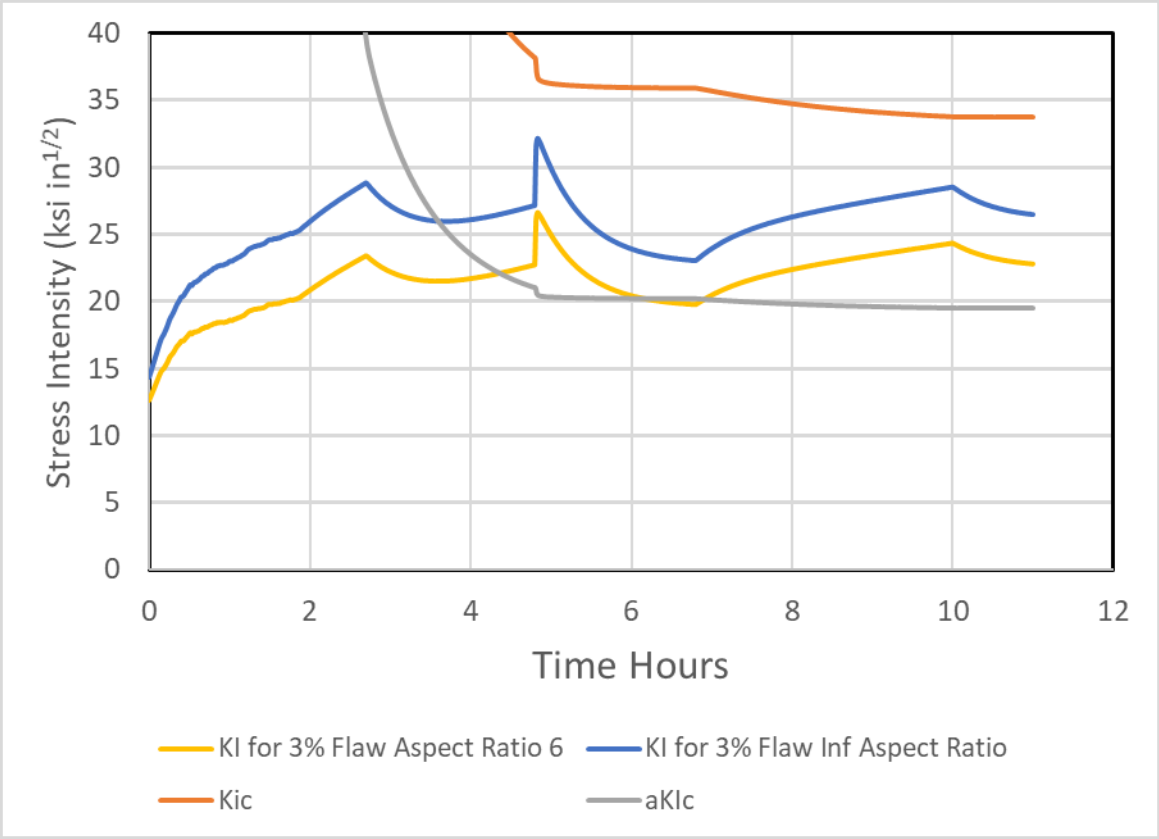

Figure 21: K_I for PWR A with the ANO Unit 1 P-T Limit Cooldown at 50th Percentile of Actual Cooldown Pressure

Table 4-5 CPF for a Cooldown from 550°F to 70°F at the ANO P-T Cooldown Rate Limits and 50 Percentile Pressure versus Temperature

Plant	RT_{PTS} at vessel ID	Flaw Depth	CPF
PWR A	~ 320°F	3%	2.22E-06
PWR B	~ 300°F	4%	1.30E-08
Plant C	~ 260°F	3%	0.00E+00
Plant D	~ 275°F	2%	1.64E-10

As compared to a cooldown CPF for a constant CDR of 100°F per hour shown in Table 4-2, the CPF for the Figure 20 cooldown (compare with Figure 12 cooldown) is approximately two orders of magnitude lower. The only CPF in Table 4-5 that is above 1.0E-06 is for PWR A that is modelled with high embrittlement. The cooldown at the maximum cooldown rate allowed by the ANO T [15] limits is higher than the typical actual plant cooldowns discussed in Section 4.2.1. Actual cooldowns tend to proceed at cooldown rate and pressure less than the maximum allowed values.

Another PWR A analysis with the P-T limit cooldown was performed with the assumption that the final RCP was tripped at 250°F instead of 175°F. Figure 21 shows the applied the crack tip stress intensity factor for PWR A with this cooldown. The 25°F temperature decrease from 250°F to 225°F produces a spike in

K_I at 198 minutes into the cooldown. Because the K_I spike occurs at a higher temperature when $_aK_{Ic}$ is higher, the FAVOR calculated CPF is 2.75E-9 – almost three orders of magnitude lower than for a final RCP trip at 175°F.

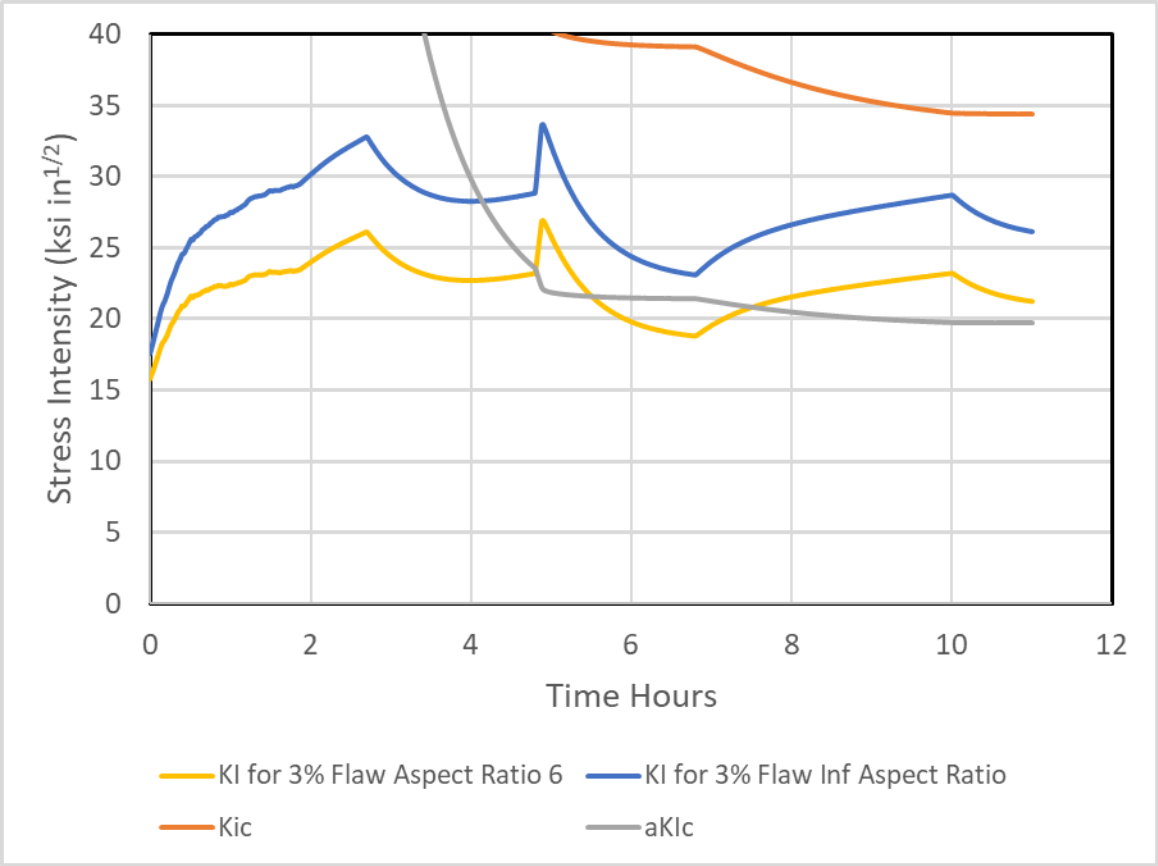

Figure 22: K_I for PWR A with ANO P-T Limit Cooldown – Last RCP Trip at 250°F

This analysis illustrates the potential importance of the RCS temperature at which the last RCP is tripped. As shown in Figure 21 and Figure 22, the rapid 25°F RCS temperature drop associated with tripping the last RCP produces a spike in crack tip K_I even if the RCS temperature is maintained constant for 2 hours after this temperature drop.

The normal plant cooldowns shown in Appendix A were surveyed to determine whether actual plant cooldowns exhibit a rapid 25°F cooldown when the final RCP is tripped as discussed in the ANO P-T limits [15]. While most actual cooldowns do not show this 25°F rapid temperature drop, there are six actual cooldowns that do have a fast 25°F ΔT near the end of the cooldown. One cooldown transient (Plant 8, Cooldown 5) that shows a rapid 25°F ΔT (Figure 23) was selected for evaluation with FAVOR.

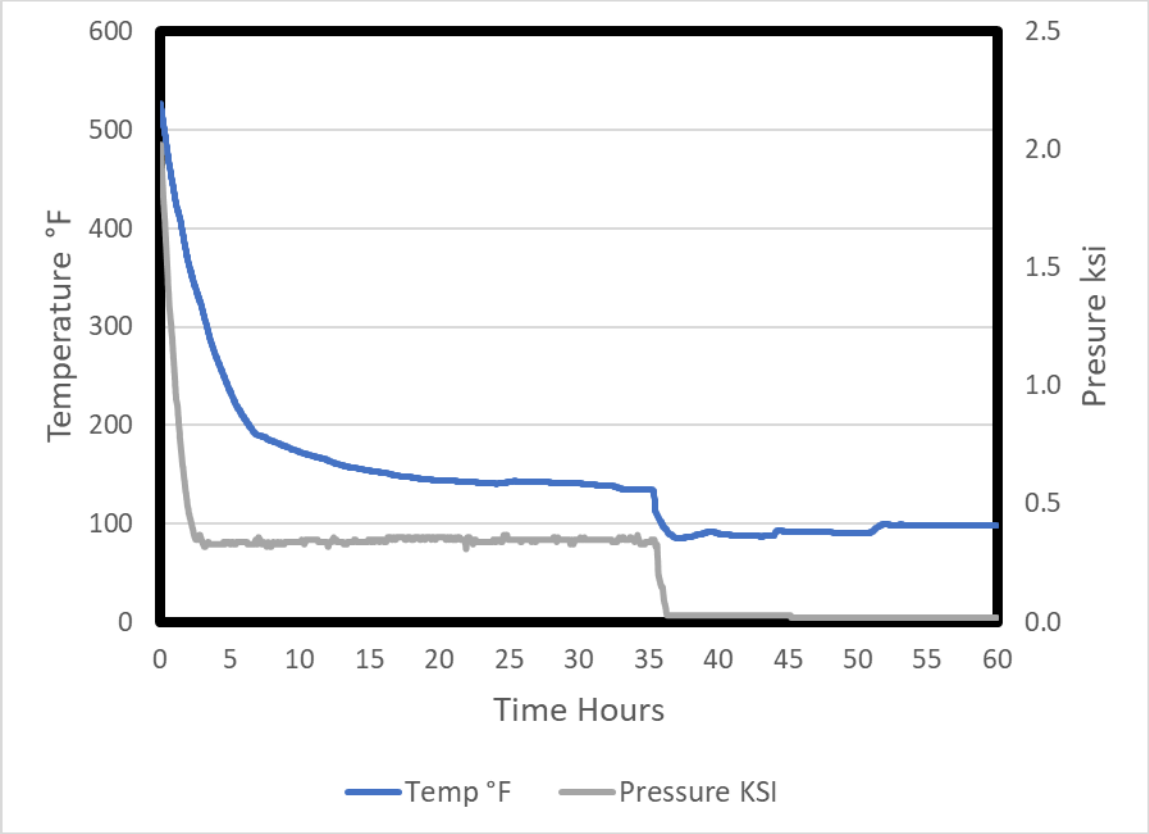

Figure 23 – Plant 8 Cooldown 5 Measured Pressure and Temperature

During the Plant 8 Cooldown 5, the RCS temperature dropped from 133°F to 107°F within less than 6 minutes at 35.4 hours the cooldown. As shown in Figure 23, this temperature drop occurs just before the RCS pressure is reduced to atmospheric. Therefore, the rapid ΔT discussed in the ANO P-T limits does occur in some normal plant cooldowns.

A FAVOR analysis of this cooldown using the PWR A geometry and embrittlement model resulted in a CPI of 3.5E-06 and a CPF of 3.8E-08, resulting in TWCF well below 1.0E-06 per year. These values are within the values of the other transients shown in Table 4-3.

4.1.4 Summary on PWR Cooldowns

As shown in Table 4-2, cooldowns at the ASME maximum allowed 100°F per hour CDR from plant operating temperature to 70°F may result in FAVOR calculated CPF values for internal SSBFs above 1.0E-06 depending on the level of plant embrittlement and the cladding and vessel wall thickness. However, as shown in Section 4.1.2, the expected CPF (and TWCF) for actual plant cooldowns is significantly less than 1.0E-06 (per year for TWCF). Furthermore, the CPF values in Table 4-2 should be understood in the context of the assumptions and conservatisms discussed in Section 1.4, and it should be noted that when considering realistic transient frequencies, the TWCF values are expected to be far below 1E-06 per year.

As discussed in Section 4.1.3, normal PWR plant cooldowns do not typically occur at the maximum allowed CDR of 100°F per hour because of both plant design and plant specific P-T limits. The initial plant cooldown to approximately 300°F may occur at a CDR close to 100°F per hour because the plant is being cooled

down by the plant secondary system, which is capable of rapid cooldown. However, at approximately 300°F, the plant cooldown switches over to the residual heat removal (RHR) system. The CDR on the RHR system tends to be lower because this system has less heat removal capacity than the plant secondary system. In addition, as shown in [15], plants may also have specific limits on CDR in P-T limits.

EPRI report MRP-437 [6] provides an assessment of internal SSBFs based on both ASME Section XI Appendix G P-T limits. MRP-437 provides a maximum CDR at temperatures below 250°F for maintaining CPF less than 1.0E-06 per year and a set of relationships to define this limiting CDR as a function of vessel wall thickness and adjusted vessel reference temperature. EPRI MRP-437 and this report are consistent in showing that, depending on vessel geometry and embrittlement, the CDR needs to be less than the maximum 100°F per hour to keep CPF less than 1.0E-06 per year.

As shown in this report and in MRP-437, CPF for actual plant cooldowns is generally significantly less than 1.0E-06 per year. Both design considerations, including switch over to RHR at temperatures below approximately 300°F and P-T limitations, tend to limit CDR as the vessel wall temperature drops below the vessel ART. Based on these FAVOR analyses, CPF values for realistic plant cooldowns are substantially less limiting than those for cooldowns at the maximum CDR and pressure allowed by ASME Section XI, Appendix G.

4.2 BWR Transients

ONRL 2016 [1] provides an analysis of RPVs subjected to plant cooldown from operating temperature and pressure to cold shutdown. Most of the analyses presented in ORNL 2016 focus on PWRs. The operating pressure for PWR reactors is approximately 2.25 ksi and is maintained well above saturation pressure. The operating pressure for BWR reactors is determined by the saturation pressure at the core exit and is typically approximately 1.05 ksi. BWR reactor vessels typically have larger diameters and thinner vessel walls than PWR RPVs. The typical RPV radius/diameter ratio for PWR reactors is approximately 10 and this ratio is approximately 15 to 20 for BWR RPVs.

BWR Technical Specifications Pressure-Temperature (P-T) limits for reactor cooldown generally allow cooldown at a maximum rate of 100°F per hour from operating temperature to cold shutdown. The maximum pressure allowed by the BWR P-T curve is set based on ASME criteria and operational considerations. BWRs do not have a pressurizer to maintain pressure significantly above saturation pressure based on the core exit coolant temperature. A BWR plant must be either water solid or establish a pressurized air/nitrogen bubble to establish a system pressure significantly above atmospheric. BWR plant Technical Specifications typically allow cooldown at pressure significantly above saturation and the FAVOR analyses in Section 4.2.1 consider cooldowns at the maximum Technical Specifications allowed pressure. More realistic BWR cooldowns are evaluated in Section 4.2.2.

BWR plants are pressurized at relatively low temperature for leak tests before plant startup from a refueling outage. These leak test conditions are evaluated in Section 4.2.3.

Two BWR plants were selected for the analyses below. One of these plants (BWR A) has an RPV radius/thickness ratio of 15 and the other plant (BWR B) has a radius/thickness ratio of 20. The FAVOR models for these two plants are described in Appendix C.

4.2.1 P-T Limit Cooldowns

BWR plants cooldowns from full power to cold shutdown must be within P-T limits for RCS pressure and temperature, provided in either Plant Technical Specifications (Section 3.4.9) or the Plant Pressure Temperature Limits Report. Technical Specifications P-T limits for Hatch Unit 1 [16] and Quad Cities Unit 1 [17] were selected for evaluating BWR plant cooldowns at the maximum allowed cooldown rate and operating pressure. These plant P-T limits, shown in Figure 24 and Figure 25 were taken from the plant technical specifications and used to create inputs for FAVOR analyses.

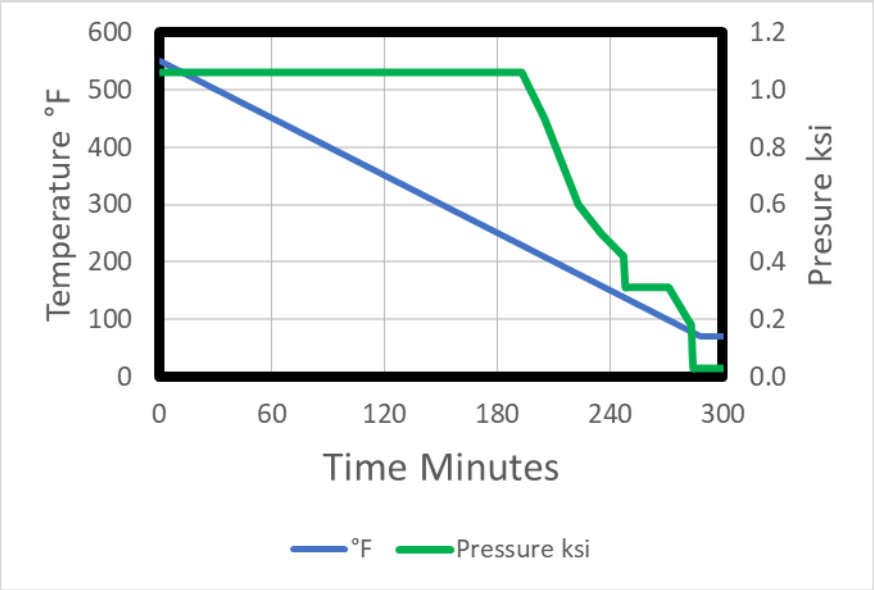

Figure 24 – Hatch Unit 1 Technical Specifications P-T Limits for 54 EFPY

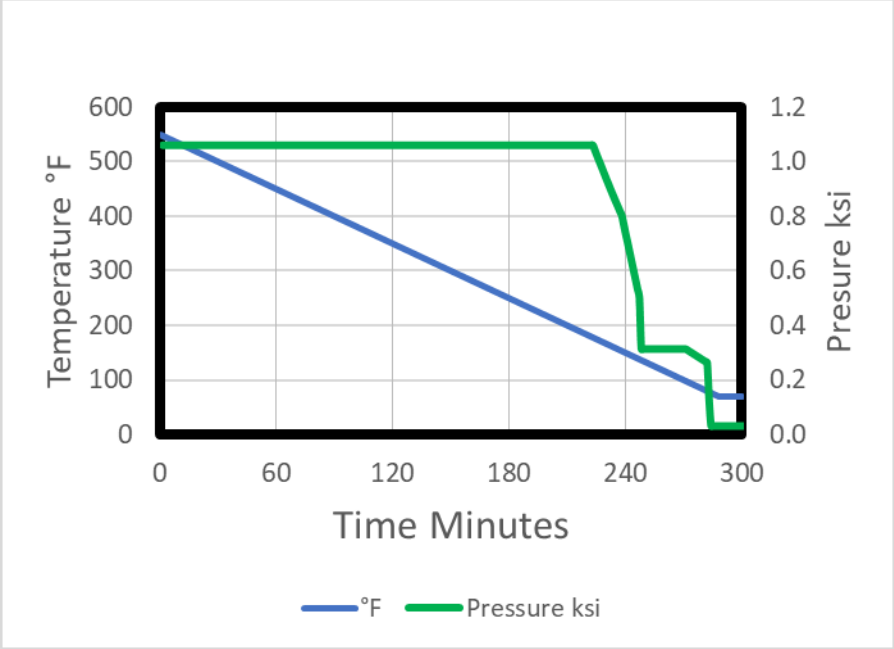

Figure 25 – Quad Cities Unit 1 Technical Specifications P-T Limits for 54 EFPY

FAVOR was used to analyze plants BWR A and BWR B for each of these two cooldown transients shown in Figure 24 and Figure 25. For the cooldown shown in Figure 24, the applied stress intensity factor (K_I) calculated at the tip of a 4% internal SSBF as a function of time is shown in Figure 26 and Figure 27 for BWR A and BWR B, respectively. As a result of the thinner RPC vessel wall for BWR A (5.38 in) compared with BWR B (7.12 in), the K_I for BWR A is less than the K_I for BWR B, because of lower thermal stress at the crack tip.

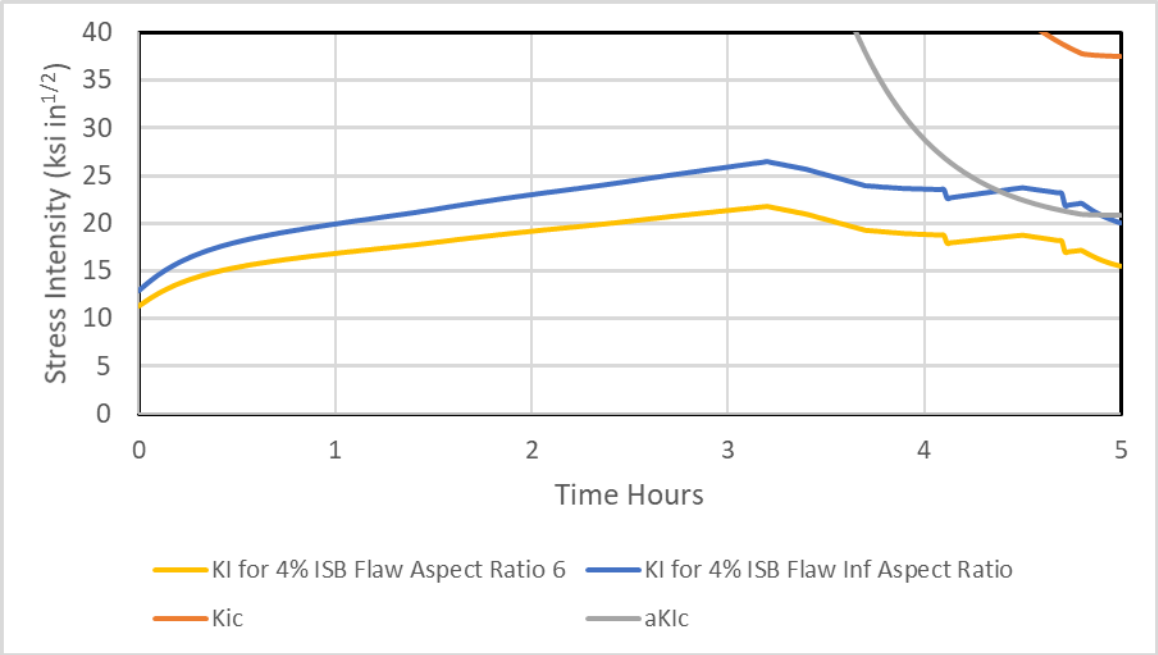

Figure 26 – BWR A K_I for 4% internal SSBF with Figure 24 TS Limit Cooldown

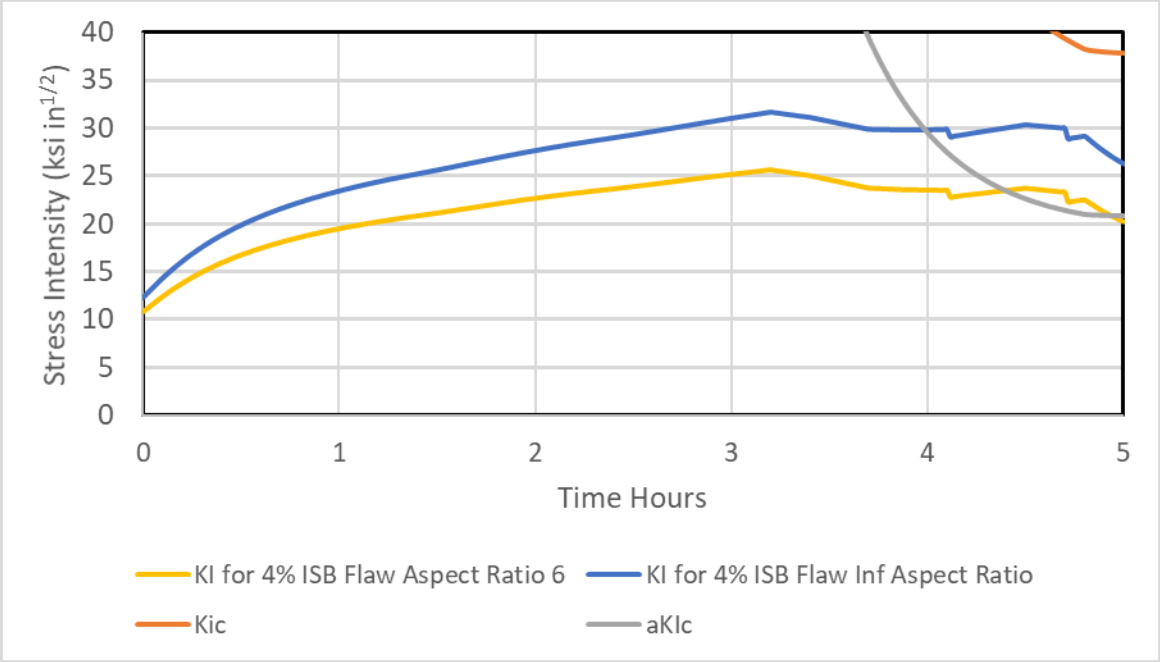

Figure 27 – BWR B K_I for 4% internal SSBF with Figure 24 TS Limit Cooldown

For the cooldown shown in Figure 25, the applied stress intensity factor (K_I) calculated at the tip of a 4% internal SSBF as a function of time is shown in Figure 28 and Figure 29 for BWR A and BWR B, respectively. Because the Figure 25 (Quad Cities) Technical Specifications cooldown allows full system pressure at a lower temperature, the peak K_I for this cooldown occurs later and at lower RCS temperature.

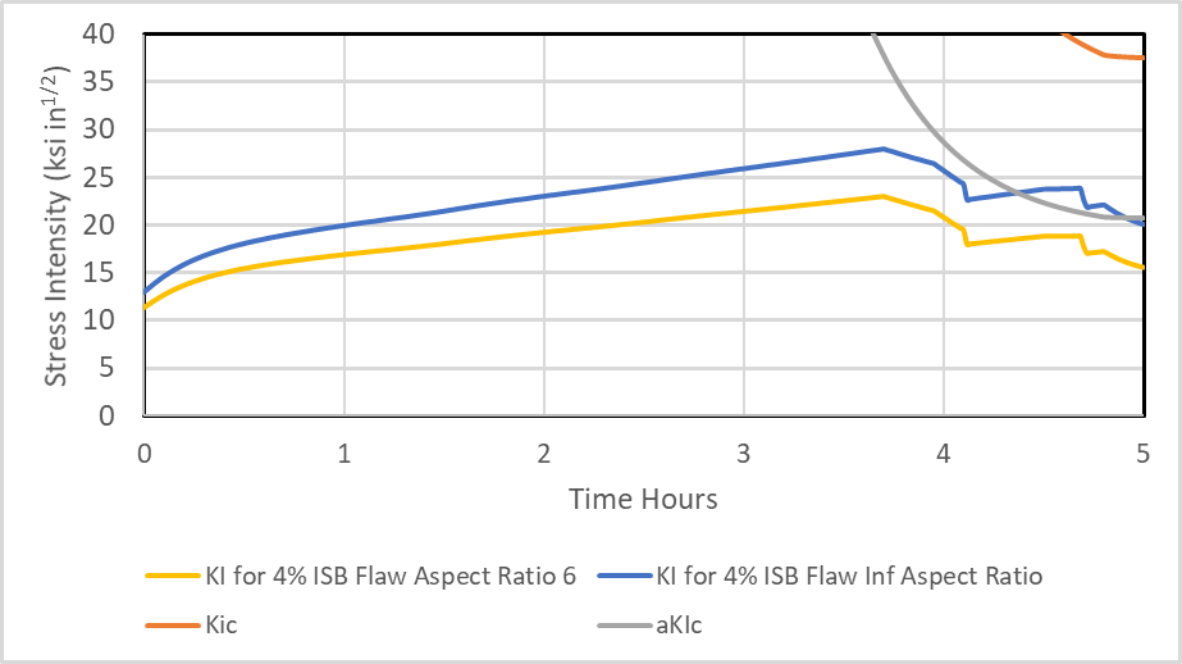

Figure 28 – BWR A K_I for 4% internal SSBF with Figure 25 TS Limit Cooldown

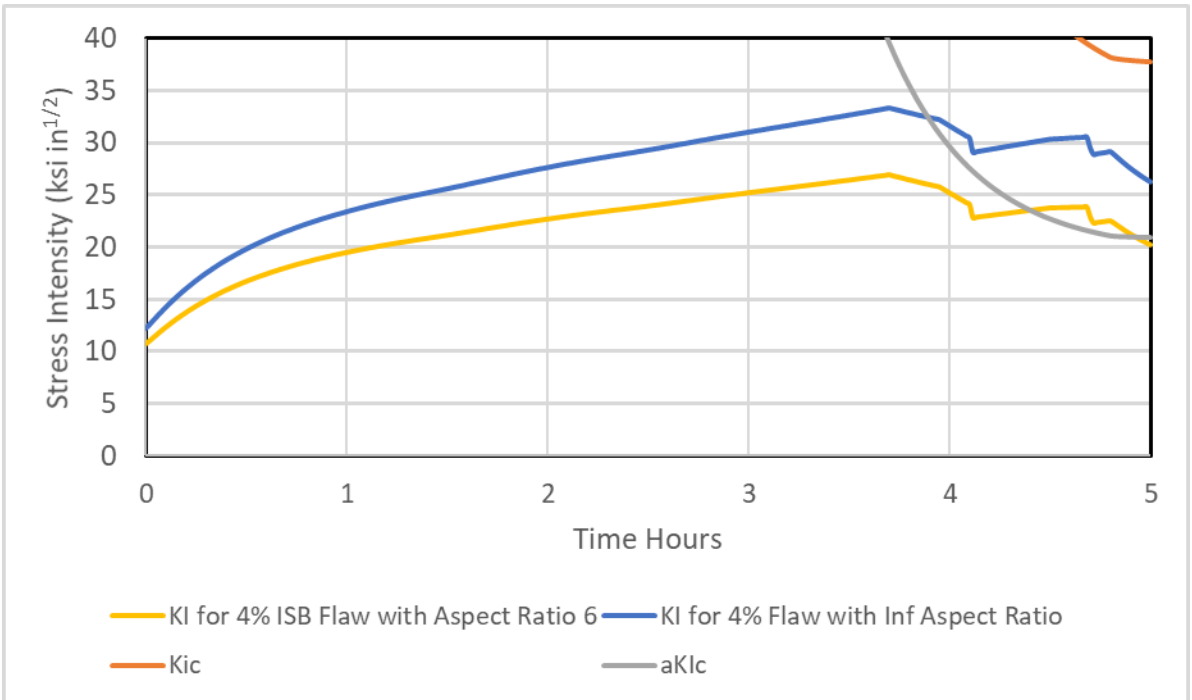

Figure 29 – BWR B K_I for 4% internal SSBF with Figure 25 TS Limit Cooldown

The four cooldown transients in Figure 26 to Figure 29 were evaluated with FAVOR to determine the CPF with the BWR A and BWR B model assumptions described in Appendix C. Because K_I versus time for these P-T limit cooldowns reaches a peak value before K_I exceeds ${}_aK_{Ic}$, crack initiation would be prevented if warm pre-stress is assumed. Because actual plant cooldowns would occur at close to saturation pressure and would not provide warm pre-stress, the FAVOR PFM analyses shown in Table 4-6 does not assume WPS. Even with these very conservative assumptions of cooldown at the maximum CDR of 100°F per hour and maximum pressure, the highest calculated mean CPF is below 1.0E-06

Table 4-6 – BWR CPF for Cooldown at Technical Specifications Limits for CDR and Pressure

Embrittlement	RPV Wall (in)	Flaw Depth (in)	Flaw Type	Transient	CPF mean
BWR A 72 EFPY	5.38	0.215	4% internal SSBF with NUREG/CR-6817 Aspect Ratios	Hatch P-T Tech Specs for 54 EFPY	0.0E+00
BWR A 72 EFPY	5.38	0.215	4% internal SSBF with NUREG/CR-6817 Aspect Ratios	Quad Cities P-T Tech Specs for 54 EFPY	1.8E-11
BWR B 72 EFPY	7.12	0.285	4% internal SSBF with NUREG/CR-6817 Aspect Ratios	Hatch P-T Tech Specs for 54 EFPY	2.3E-07
BWR B 72 EFPY	7.12	0.285	4% internal SSBF with NUREG/CR-6817 Aspect Ratios	Quad Cities P-T Tech Specs for 54 EFPY	4.4E-07

One reason that the CPF for internal SSBFs is lower for BWR plants than for PWR plants is that BWR reactors generally have thinner RPV walls, resulting in lower thermal stresses. BWR plants also have larger pressure vessels and with a greater thickness of shielding between the reactor core and the vessel wall. Therefore, neutron fluence and embrittlement tends to be lower for BWR vessels compared with PWR vessels.

Plants BWR A and BWR B have RPV wall thickness values that are typical for most US BWR plants. However, as discussed in BWRVIP-328 [6], there are a few US BWRs with RPV wall thicknesses of 9.5 inches. For these 9.5-inch-thick BWR vessels, BWRVIP-328 states that the maximum CDR may need to be lower than for the other BWRs. An additional analysis was performed for the BWR A plant model where the wall thickness was increased to 9.5 inches and the clad thickness was increased to 0.25 inches. This analysis assumed a 3% internal SSBF that just extends past the clad into the ferritic steel vessel wall. The calculated CPF for this case increased from 1.8E-11 shown in Table 4-6 to 7.3E-07. This confirms the observation that CPF increases with greater wall thickness. However, the CPF remains below 1.0E-06 even for a very conservative assumption of cooldown at Technical Specifications maximum CDR and pressure.

4.2.2 Realistic Cooldowns

BWR plants normally operate at a system pressure close to the saturation pressure for temperature at the core exit. Therefore, a realistic cooldown would follow the saturation pressure curve as the plant cools down as shown in Figure 30 for the maximum CDR of 100°F per hour.

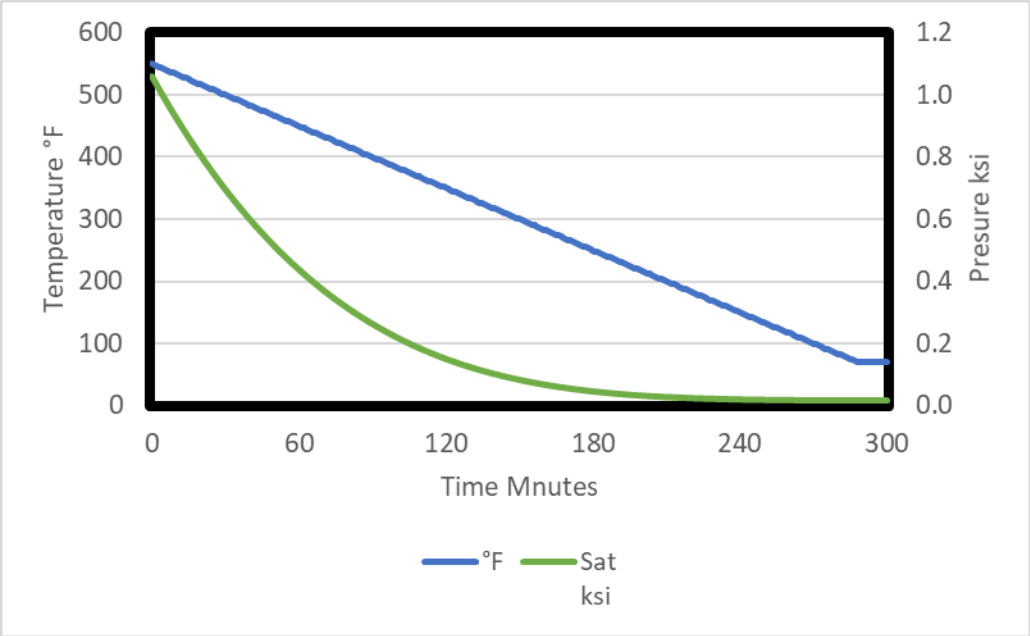

Figure 30 – Saturation Pressure Cooldown at 100°F CDR

FAVOR analyses were performed for BWR A and BWR B for cooldown at the maximum allowed CDR of 100°F per hour and for a more realistic CDR of 50°F per hour with a 4% internal SSBF. As discussed in Section 4.2.1, the thermal stress and CPF are higher for thicker walled vessels. Additional analyses were performed for a 9.5-inch vessel wall by modifying the BWR A model to increase the vessel wall to 9.5 inches and the clad thickness to 0.25 inches. This thicker wall BWR was analyzed for a 3% internal SSBF that that extends just into the ferritic steel vessel base metal for CDRs of 100°F and 50°F per hour. Figure 31 shows that the applied stress intensity factor (K_I) for this 9.5-inch thick BWR has a single peak at the end of the cooldown that exceeds ${}_aK_{IC}$. Figure 32 shows that the applied stress intensity factor (K_I) for this 9.5-inch BWR is lower for a 50°F per hour CDR but still exceeds ${}_aK_{IC}$ at the end of this cooldown. Figure 33 shows that the applied stress intensity factor (K_I) peak at the end of the cooldown for a more typical 5.38-inch BWR vessel (BWR A) with a 50°F per hours CDR remains below ${}_aK_{IC}$ at the peak thermal stress at the end of this cooldown.

The CPF for BWR A, BWR B and BWR A modified to increase RPV wall thickness to 9.5 inches are provided in Table 4-7 for CDRs of 100°F and 50°F per hour at saturation pressure. The highest CPF is 6.1E-08 for the 9.5-inch thick RPV at a CDR of 100°F per hour. Based on these analyses the CPF for BWR vessels would be much less than 1.0E-06 per year for all realistic cooldowns, which would also result in TWCF below 1E-06 per year.

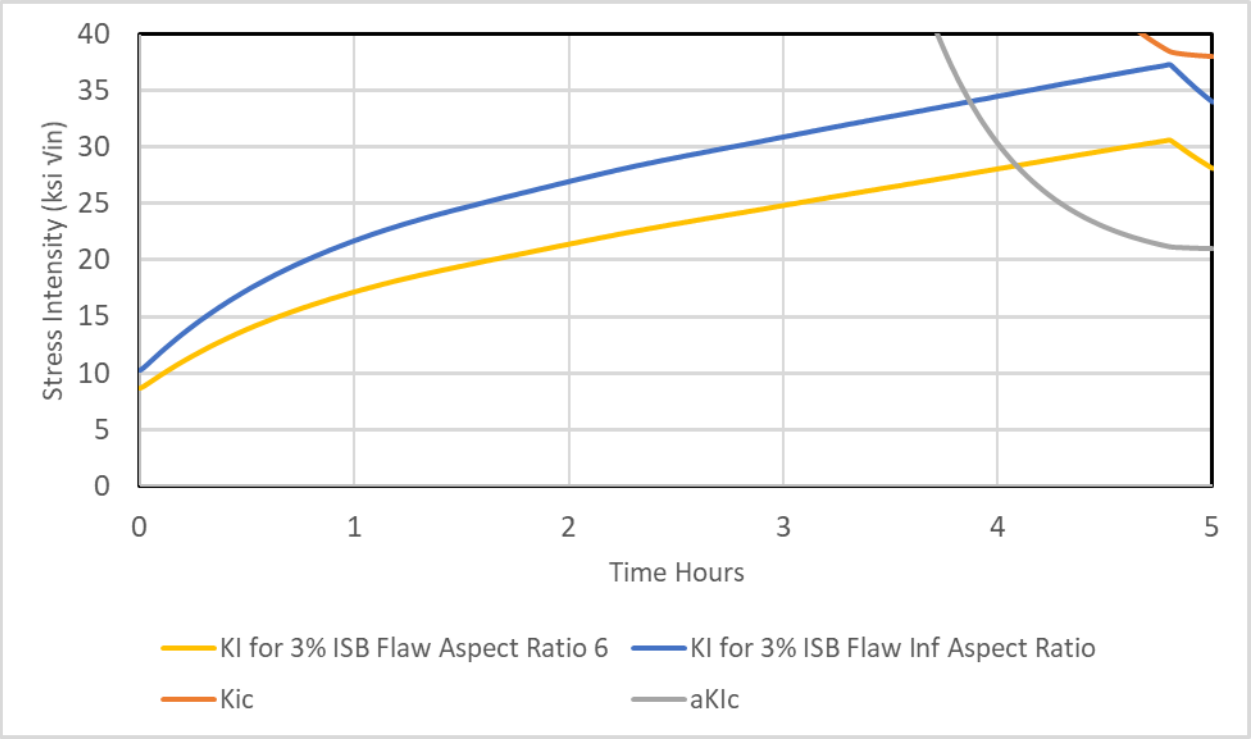

Figure 31 – K_I for a 9.5-inch BWR Vessel Wall with Saturation Pressure 100°F per Hour CDR

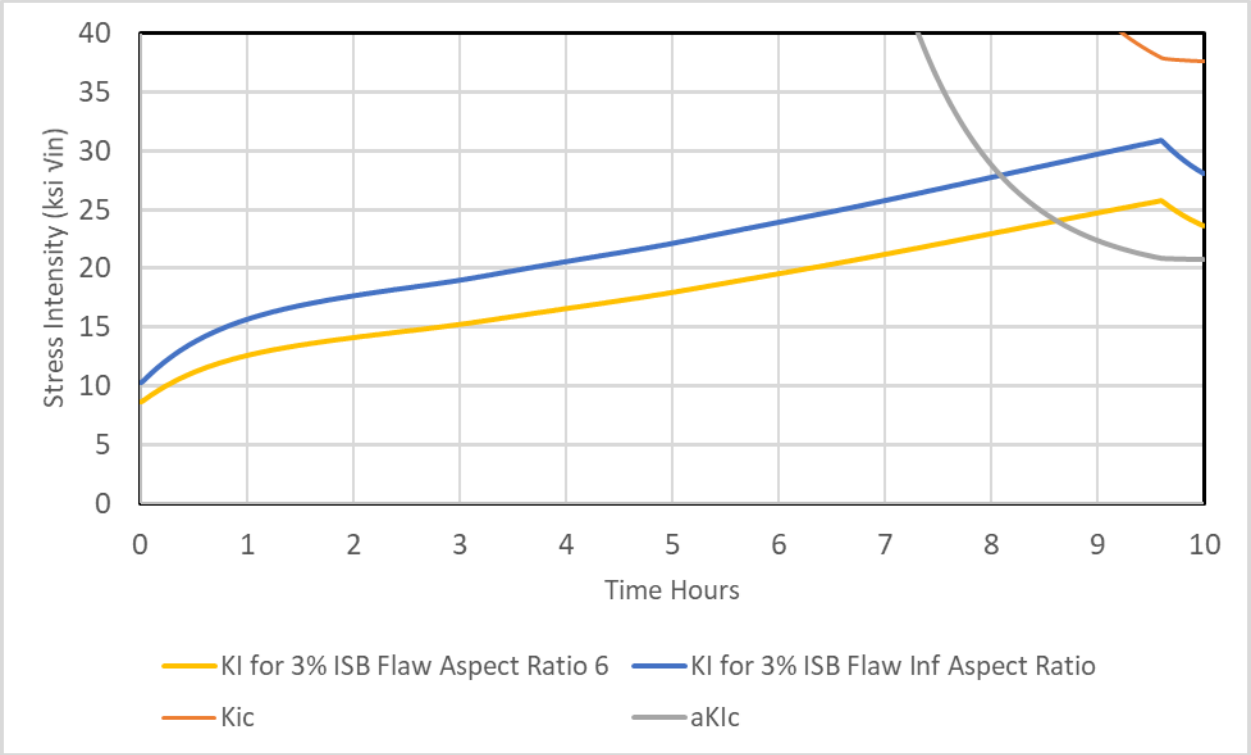

Figure 32 – K_I for a 9.5-inch BWR Vessel Wall with Saturation Pressure 50°F per Hour CDR

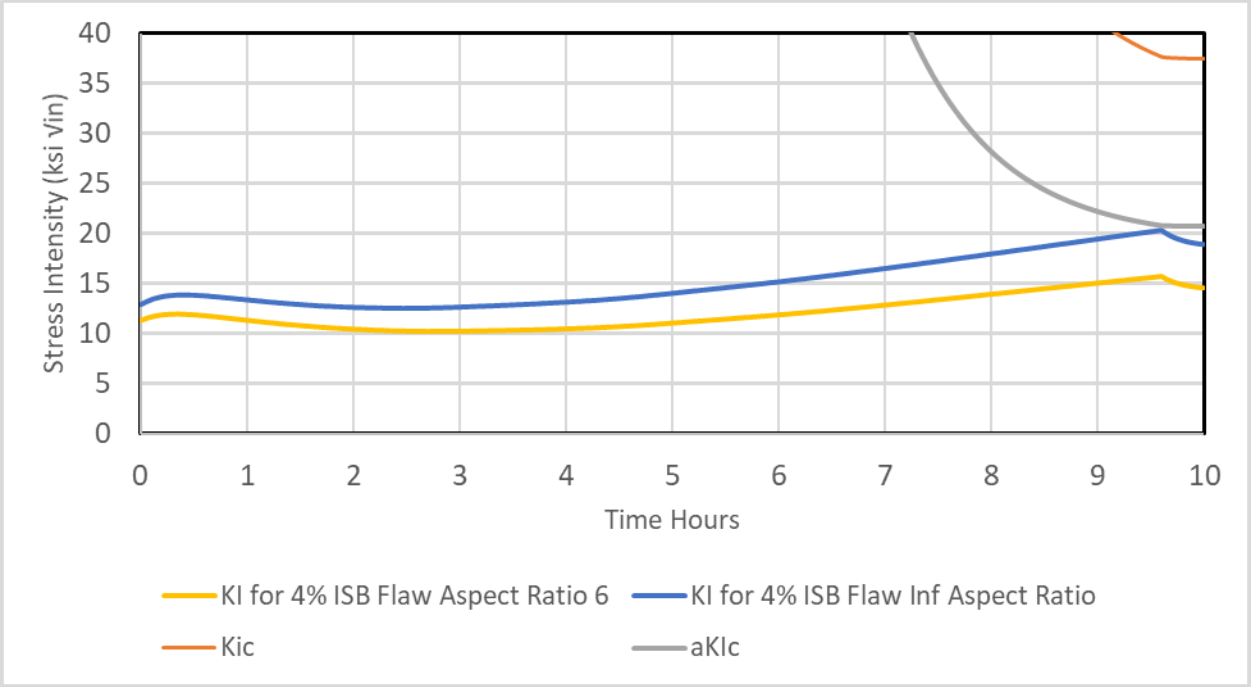

Figure 33 – K_I for a 5.38-inch BWR Vessel Wall with Saturation Pressure 50°F per Hour CDR

Table 4-7 – CPF for 100°F and 50°F per Hour CDR at Saturation Pressure

Embrittlement	RPV Wall (in)	Flaw Depth (in)	Flaw Type	Transient	CPF $_{mean}$
BWR A 72 EFPY	5.38	0.215	4% internal SSBF with NUREG/CR-6817 Aspect Ratios	100°F CDR Saturated Pressure Cooldown	0.0E+00
BWR A 72 EFPY	5.38	0.215	4% internal SSBF with NUREG/CR-6817 Aspect Ratios	50°F CDR Saturated Pressure Cooldown	0.0E+00
BWR B 72 EFPY	7.12	0.285	4% internal SSBF with NUREG/CR-6817 Aspect Ratios	100°F CDR Saturated Pressure Cooldown	1.3E-08
BWR B 72 EFPY	7.12	0.285	4% internal SSBF with NUREG/CR-6817 Aspect Ratios	50°F CDR Saturated Pressure Cooldown	0.0E+00
BWR 9.5-inch RPV 72 EFPY	9.5	0.285	3% internal SSBF with NUREG/CR-6817 Aspect Ratios	100°F CDR Saturated Pressure Cooldown	6.1E-08
BWR 9.5-inch RPV 72 EFPY	9.5	0.285	3% internal SSBF with NUREG/CR-6817 Aspect Ratios	50°F CDR Saturated Pressure Cooldown	1.1E-10

4.2.3 Leak Test Transients

Three leak test transients were studied:

- Leak test along the P-T limit with heatup and cooldown rates of 40°F/hour, labelled LT40-40
- leak test along the P-T limit with heatup rate of 40°F/hour and cooldown rate of 100°F/hour, labelled LT40-100
- actual leak test transient for which pressure and temperature histories were known, labelled LTA

Figure 34 shows the pressure and temperature histories used for a BWR leak test transient with a 40°F/hour heatup rate and a 40°F/hour cooldown rate. The allowable pressure and temperature were derived from the ASME Section XI Appendix G, Paragraph G-2215 rules, as was done for the P-T limit cooldowns. For this transient, the leak test pressure and temperature were 1.1 ksi and 167°F, respectively. This transient is referred to as the 'LT40-40' transient in this document.

Figure 35 shows the pressure and temperature histories used for a BWR leak test transient with a 40°F/hour heatup rate and a 100°F/hour cooldown rate. The allowable pressure and temperature were derived from the ASME Section XI Appendix G, Paragraph G-2215 rules [6], as was done for the P-T limit cooldowns. For this transient, the test pressure and temperature were 1.1 ksi and 167°F, respectively. This transient is referred to as the 'LT40-100' transient in this document.

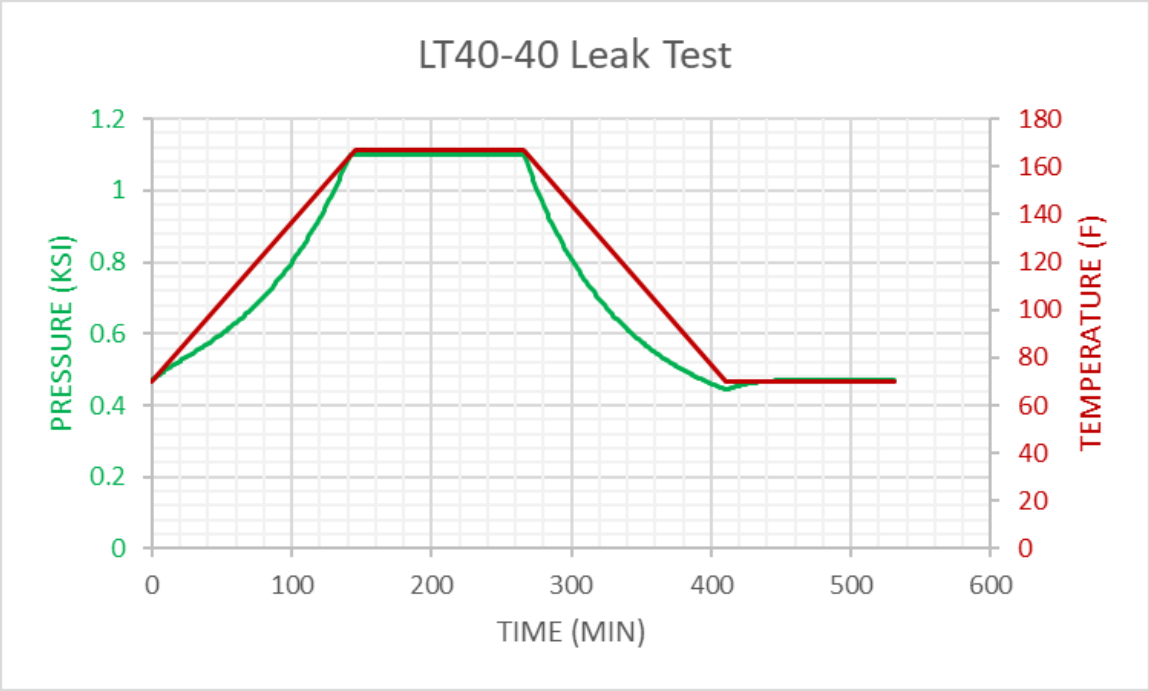

Figure 34: BWR LT40-40 Leak Test Transient Characteristics

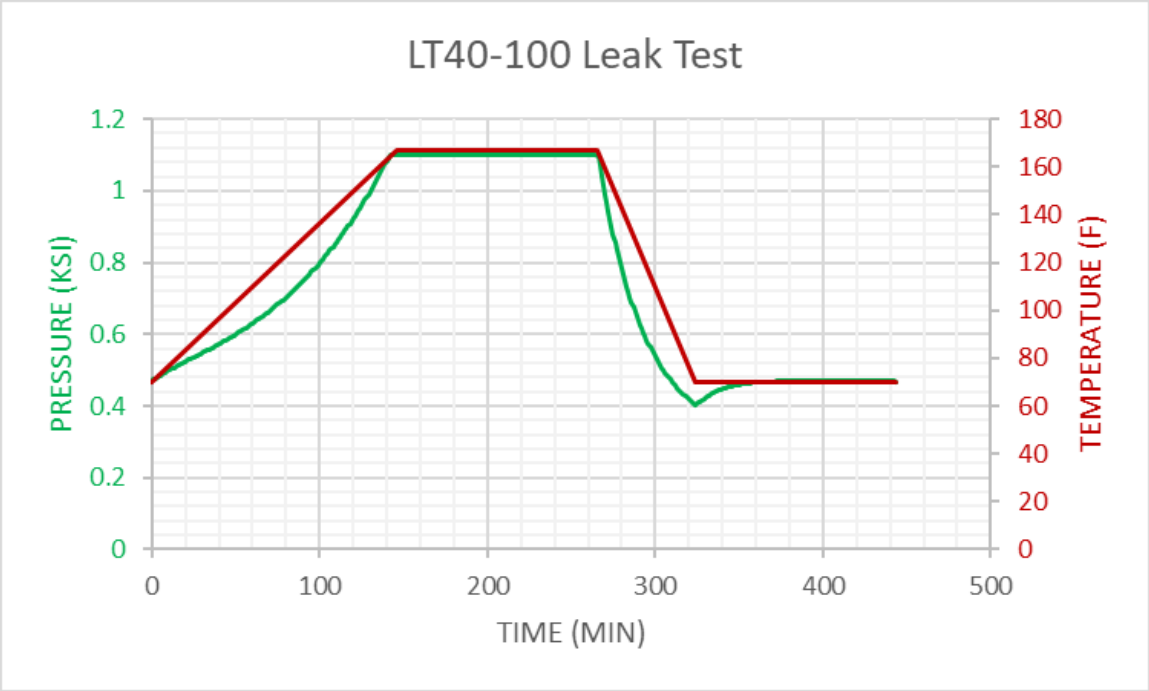

Figure 35: BWR LT40-100 Leak Test Transient Characteristics

Figure 36 shows the pressure and temperature histories used for the actual leak test transient obtained from EPRI. For this transient, the leak test pressure and temperature were 1.0 ksi and 208.5°F, respectively. This transient is referred to as the 'LTA' transient in this document.

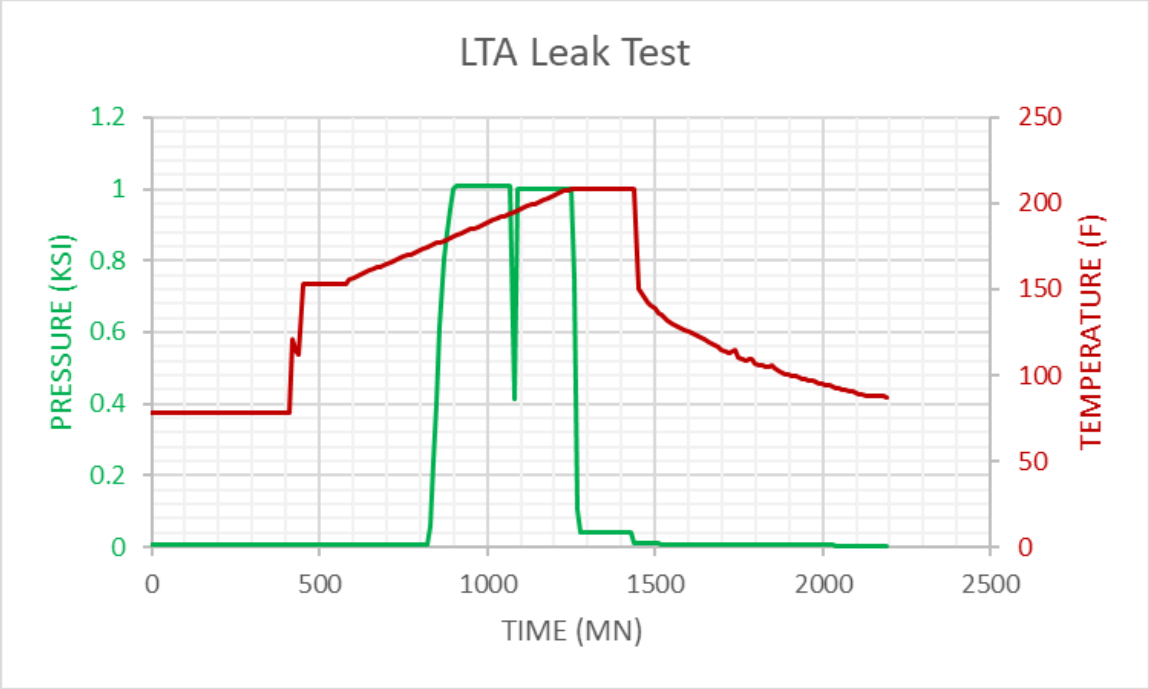

Figure 36: BWR LTA Leak Test Transient Characteristics

FAVOR analyses were performed for BWR A assuming a 4% internal SSBF. Figure 37, Figure 38, and Figure 39 show the stress intensity factor history for the 4% internal SSBF for transients LT40-40, LT40-100, and LTA, respectively.

The stress intensity factor histories are identical for LT40-40 and LT40-100 until the cooldown starts after the pressure and temperature plateau. Once the temperature and pressure are decreasing, the stress intensity factor is slightly higher for the LT40-100 transient because of the higher cooldown rate that results in higher thermal stresses. However, the applied stress intensity factor does not exceed the lower bound Kia arrest toughness, thus no crack growth initiation would be expected for these P-T limit leak test transients with a 4% internal SSBF. It should nonetheless be noted that for a cooldown rate of 100°F/hour along the P-T limit, the applied stress intensity factor is very close to crossing the Kia threshold for an infinite flaw aspect ratio, thus it is recommended that the cooldown rates be kept below 100°F/hour for cooldowns along the P-T limit.

The actual leak test transient produces overall much lower applied stress intensity factors that remain far below Kia despite some very rapid heatup and cooldown periods (125°F/hour maximum heatup rate and 183°F/hour maximum cooldown rate). The lower applied stress intensity factor is because of the fact that the pressure is low during the high heatup and cooldown rate periods, resulting in a low-pressure stress during the periods of high thermal stress.

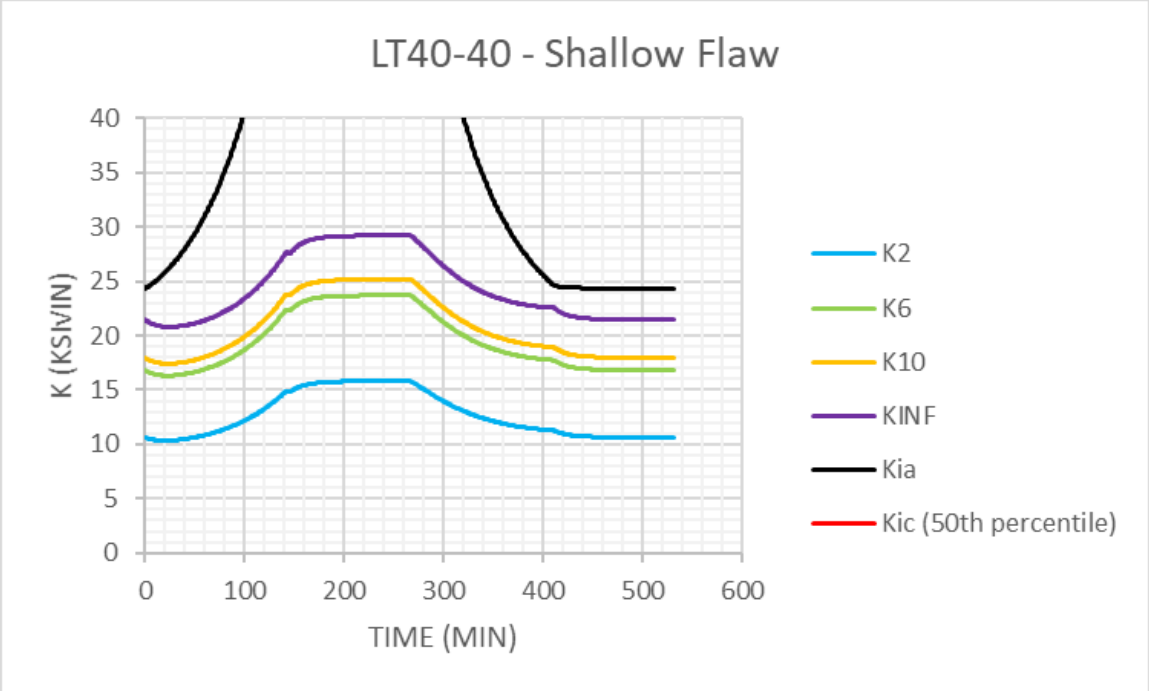

Figure 37: Stress Intensity Factor for the BWR LT40-40 Leak Test for a 0.04 T Flaw for Flaw Aspect Ratios of 2, 6, 10 and Infinity

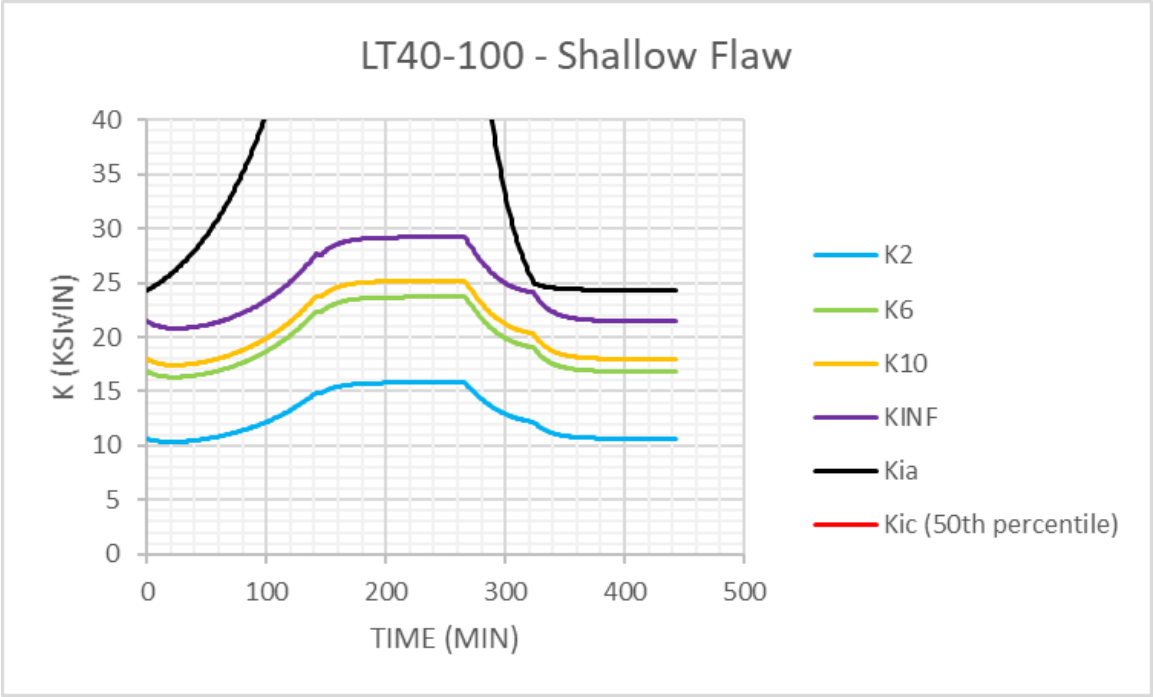

Figure 38: Stress Intensity Factor for the BWR LT40-100 Leak Test for a 0.04 T Flaw for Flaw Aspect Ratios of 2, 6, 10 and Infinity

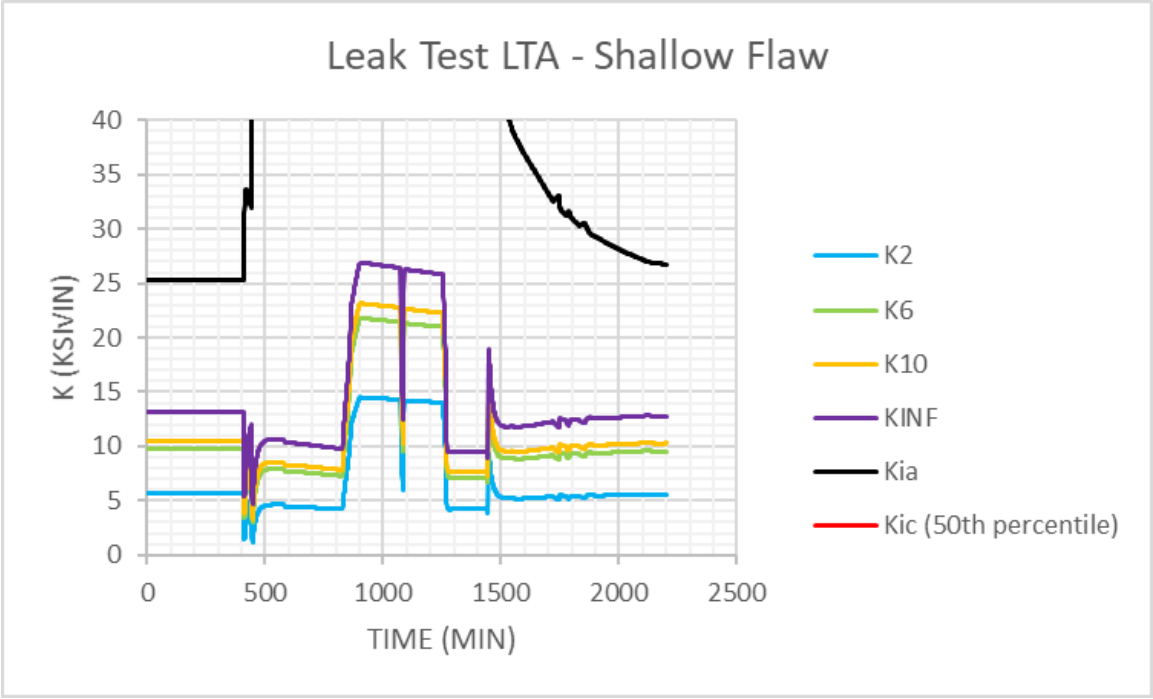

Figure 39: Stress Intensity Factor for the BWR LTA Leak Test for a 0.04 T Flaw for Flaw Aspect Ratios of 2, 6, 10 and Infinity

Probabilistic FAVOR analyses were performed for these 3 transients with a 4% internal SSBF of aspect ratio equal to 6 to confirm that the shallow flaw did not result in CPF values above the threshold for further

investigation (i.e., above 1.0E-06). In all cases, the values of CPF were equal to zero, thus the leak test transients do not appear to be an issue for shallow flaws.

4.2.4 Summary on BWR Transients

Based on the analyses in Section 4.2.1, the highest FAVOR calculated CPF for a BWR plant cooldown is 7.3E-07 per year for a 9.5 inch wall RPV assuming that the cooldown from operating temperature and pressure to ambient is at the maximum allowed CDR of 100°F per hour at the maximum pressure allowed by typical BWR plant Technical Specification P-T limit curves. Because BWRs do not normally cooldown at the maximum allowed Technical Specification P-T limits all the way to ambient temperature, there is low annual probability that this P-T limit cooldown will occur.

Realistic BWR cooldowns were evaluated in Section 4.2.2 based on a pressure during cooldown set to the saturation pressure as a function of temperature. With this realistic assumption for pressure, the maximum CPF for the 9.5-inch RPV was 6.1E-08 compared with the 7.3E-07 CPF estimated at the maximum allowed pressure by typical BWR Technical Specifications P-T limit curves. With a realistic assumed CDR of 50°F per hour, the calculated CPF for the 9.5 in RPV is further reduced to 1.1E-10. Based on these analyses, the calculated CPF for BWRs with internal SSBFs is well below 1.0E-06 for realistic cooldowns, resulting in TWCF also well below 1E-06 per year.

In BWRVIP-328 [6], EPRI evaluated BWR cooldowns based on ASME Appendix G P-T limit curves that allow higher pressure compared with BWR plant Technical Specifications P-T limits. Based on this more conservative ASME Appendix G P-T analysis, EPRI recommends limiting BWR CDR to less than 100°F per hour at temperatures below 250°F and provides a graph in Figure 5-1 of BWRVIP-328 showing maximum recommended CDR as a function of Adjusted Reference Temperature and vessel wall thickness. Based on the analyses in this report, these reduced CDRs below 250°F do not seem to be necessary for realistic BWR cooldowns at saturated pressure.

Regarding leak tests, based on the analyses described in 4.2.3, shallow flaws do not represent a safety issue for cooldown rates at least up to 100°F/hour if the leak test is performed along the P-T limit. Higher cooldown rates than 100°F/hour may be acceptable for BWR leak tests along the P-T limit, but were not considered as part of these studies.

Based on the estimated TWCF for realistic BWRs cooldowns, no further evaluation of internal SSBFs is recommended for BWRs.

5 Conclusions

Sensitivity studies were performed with FAVOR to explore potential solutions to the SSBF issue. As summarized below, some of the sensitivity parameters that were studied did not significantly change the CPF calculated by FAVOR. Importantly, the conclusions should be understood with the discussion of assumptions and conservatisms explained in Section 1.4. Section 1.4 describes conditions or circumstances not accounted for in the current study because of modeling limitations in the FAVOR code, and discusses potential conservatisms associated with the modeling limitations. With conservatisms and actual transient frequencies taken into account, resulting TWCF values are expected to be far below 1E-06 per year.

- Cladding thermo-mechanical modeling:
  - Cladding stress-free temperature (SFT): the recommended SFT of 488°F is within the range of values reported in the literature for RPV analyses. Although reducing the SFT does result in lowering the CPF for a given analysis, the variability in cladding residual stress measurements and calculated SFT do not support a reduction in SFT below 488°F. **In conclusion, SFT is not a viable path to decrease the high CPF values resulting from the assumed internal SSBFs in RPVs analyzed in this study, and 488°F is the recommended value for SFT in FAVOR analyses. Considering realistic transient frequencies, the TWCF is far below 1E-06 per year.**
  - Cladding coefficient of thermal expansion (CTE): the temperature-dependent CTE from the 1998 ASME code has historically been used in FAVOR analyses, and sensitivity studies show that this CTE model results in the lowest calculated CPI and CPF, when compared to other CTE data sources. **The 1998 ASME CTE model results in the lowest calculated CPF, but these values still result in CPF larger than 1.0E-06. As a result, changing the CTE is not a viable path for decreasing the high CPF values resulting from the assumed internal SSBFs in RPVs analyzed in this study. Considering realistic transient frequencies, the TWCF is far below 1E-06 per year.**
- Warm pre-stress effects:
  - Choice of warm pre-stress (WPS) models: the existence of WPS has been well established and accepted for RPV integrity analysis. **Past and current studies in support of the shallow flaw issue already use the WPS model that provides the most WPS benefit, but some calculated CPF values still exceeded 1.0E-06, thus WPS is not a viable path for decreasing the high CPF values resulting from the assumed internal SSBFs in RPVs analyzed in this study. Considering realistic transient frequencies, the TWCF is far below 1E-06 per year.**
  - Shop hydro testing: the applied shop hydro K_I is likely much higher than the expected applied K_I from normal plant cooldowns, and thus could be sufficient to WPS the flaw tip of internal SSBFs that exist at the time of the hydrostatic test. However, because of potential fatigue crack growth and possible new flaws that might be created during RPV service, shop hydro WPS may not be effective throughout the life of the vessel. **Shop hydro WPS is not deemed a viable path for decreasing the high CPF values resulting from the assumed internal SSBFs in RPVs analyzed in this study, largely because of**

unknowns about the shop hydro test itself, as well as the potential evolution of cracks in the vessel during service (potentially because of fatigue crack growth).

- Loading path effects
  - PWR cooldowns: cooldowns at the ASME maximum allowed 100°F per hour CDR from plant operating temperature to 70°F may result in FAVOR calculated CPF values for internal SSBFs above 1.0E-06 depending on the level of plant embrittlement and the cladding and vessel wall thickness. Assuming 1 cooldown per year, this would imply TWCF larger than 1.0E-06 per year. However, normal PWR plant cooldowns do not occur at the maximum allowed CDR of 100°F per hour nor at the maximum allowed pressure, because of both plant design and plant specific P-T limits. **Consequently, although a 100°F per hour P-T limit PWR cooldown can result in CPF higher than 1.0E-06, the calculated CPF for actual plant cooldowns is significantly less than 1.0E-06. Even for 100°F per hour P-T limit PWR cooldown, the TWCF remains far below 1E-06 per year when considering realistic transient frequencies.**
  - BWR cooldowns: the highest FAVOR calculated CPF for a BWR cooldown is 7.3E-07 for cooldown of a 9.5-inch wall thickness RPV at the maximum allowed CDR of 100°F per hour along the P-T limit curve. With a realistic cooldown at the saturation pressure, the maximum CPF for the 9.5-inch RPV was 6.1E-08 for a CDR of 100°F per hour and 1.1E-10 for a CDR of 50°F per hour. Based on these analyses, **the calculated TWCF for BWRs with internal SSBFs is well below 1.0E-06 per year for both the 100°F per hour P-T limit cooldown and for realistic cooldowns, and thus shallow flaws are not an issue for BWR cooldowns.**
  - BWR leak tests: **shallow flaws do not represent a safety issue for BWRs for cooldown rates at least up to 100°F/hour if the leak test is performed along the P-T limit. Higher cooldown rates than 100°F/hour may be acceptable for BWR leak tests along the P-T limit, but were not considered as part of these studies.**
- EPRI studies: as documented in MRP-437/BWRVIP-328, EPRI performed extensive studies to address the shallow flaw issue. A significant portion of EPRI's work focused on determining cooldown rates such that TWCF would not exceed 1.0E-06 per year.
  - **For PWRs, MRP-437/BWRVIP-328 and this report are consistent in showing that, depending on vessel geometry and embrittlement, the CDR needs to be less than the maximum 100°F per hour below 250°F to keep CPF less than 1.0E-06 for the assumed internal SSBFs in RPVs analyzed in the EPRI study. Considering realistic transient frequencies, the TWCF is far below 1E-06 per year.**
  - Based on the conservative ASME Appendix G P-T analysis using FAVOR without accounting for WPS, EPRI recommends limiting BWR CDR to less than 100°F per hour at temperatures below 250°F. **Based on the analyses in this report which account for WPS, reduced CDRs below 250°F do not seem to be necessary for BWRs, especially when considering that realistic BWR cooldowns occur at or near saturated pressure.**

6 References

[1] B. R. Bass, T. L. Dickson, P. T. Williams and H. B. Klasky, "The Effect of Shallow Inside Surface-Breakng Flaws on the Probability of Brittle Fracture of Reactors Subjected to Postulated and Actual Operational Cool-Down Transients, A Status Report, ORNL/TM-2015/59531/REV-01, ADAMS ML16043A170," ORNL, Oak Ridge, TN, February 2016.

[2] P. T. Williams, T. L. Dickson, B. R. Bass and H. B. Klasky, "Fracture Analysis of Vessels - Oak Ridge FAVOR, v16.1, Computer Code: Theory and Impementation of Algorithms, Methods, and Correlations, ORNL/TLR-2016/309, ADAMS ML16273A033," ORNL, Oak Ridge TN, August 2016.

[3] T. L. Dickson, P. T. Williams, B. R. Bass and H. B. Klasky, "Fracture Analysis of Vessels - Oak Ridge FAVOR v16.1, Computer Code User's Guide, ORNL/TM/2016/310, ADAMS ML16273A034," ORNL, Oak Ridge TN, August 2016.

[4] American Society of Mechanical Engineers, "Boiler and Pressure Vessel Code, Section XI, Rules for Inservice Inspection of Nuclear Plant Components, Nonmandatory Apendix G, Fracture Toughness Criteria for Peotection Against Failure," ASME, New York, 2015.

[5] D. Rudland, S. Sheng and S. Lyons, "Closure Memorandum Supporting the Limited Revision of NUREG-0800 Branch technical Position 5-3, "Fracture Toughness Requirements", ADAMS ML16364A285," U.S. Nuclear Regulatory Commission, Washington, DC, USA, 11 April 2017.

[6] N. Palm and T. Hardin, "Assessment of the Effect of Small Inner Surface Flaws on ASME Section XI Appendix G Pressure-Temperature Limits (MRP 437 and BWRVIP-328)," EPRI, Palo Alto, CA, May 2020.

[7] L. M. Smith, T. L. Dickson and A. Dyszel, "TLR-RES/DE/REB-2021-13, Enclosure 1: Assessment of Reactor Pressure Vessel Inside Diameter Shallow Surface Breaking Flaws, ADAMS ML21260A246," NUMARK Associates, INC., Washington, D.C., 2018.

[8] M. L. Smith, T. L. Dickson and A. Dyszel, "TLR-RES/DE/REB-2021-13, Enclosure 2: Assessment of Reactor Pressure Vessel Inside Diameter Surface Breaking Flaws Based on Actual Plan Transients, ADAMS ML21260A247," NUMARK Associates, INC., Washington, D.C., 2019.

[9] PWR Owner's Group (PWROG), "PWROG-15109-NP-A, Revision 0: PWR Pressure Vessel Nozzle Appendix G Evaluation, ADAMS ML20024E573," Westinghouse Electnc Company LLC, Cranberry Township, PA, January 2020.

[10] S.-F. Iradj and M. Anderson, "Cladding Effects on Structural Integrity of Nuclear Components," Swedish Nuclear Power Inspectorate (SKI), June 2016.

[11] X. Ruan, T. Nakasuji and K. Moris, "3D CFD and FEM Evaluations of RPV Stress Intensity Factor during PTS Loading," Vols. 9-2, April 2017.

[12] M. Jhung, S. Klim, Y. Choi, Y. Chang, X. Xu, J. M. Kim, J. W. Kim and C. Jang, "Probabilistic Fracture Mechanics Round Robin Analysis of Reactor Pressure Vessels during Pressurized Thermal Shock," *Journal of Nuclear Science and Technology,* January 2012.

[13] M. Abendroth and E. Altstadt, "FZD-474: Fracture Mechanical Analysis of a Thermal Shock Scenario fo a VVER-440 RPV," Forschungszentrum Dresden Rossendorf, Dresen, Germany, June 2007.

[14] B. A. Bishop, C. L. Boggess and N. Palm, "Risk-Informed Extension of the Reactor Vessel In-Service Inspection Interval, WCAP-16168-NP-A, Rev. 3, ADAMS ML11306A084," Westinghouse, Cranberry Township, PA, October 2011.

[15] S. J. Killian and D. E. Noronha , "Arkansas Nuclear One (ANO) Unit 1 Pressure-Temperature Limits at 54 EFPY, AREVA 43-330-000, ADAMS ML14241A241," Areva, June 2014.

[16] Southern Nuclear Operating Company, "Edwin I. Hatch Renewed Facility Operating License DPR-57, ADAMS ML052930172," Nuclear Regulatory Commission, Washington, D.C., January 2002.

[17] Exelon Generation Company, LLC, "Quad Cities Nuclear Power Station, Unit 1 Renewed Facility Operating License No. DPR-29, ADAMS ML042960543," Nuclear Regulatory Commision, Washington, D.C., October 2004.

[18] F. A. Simonen, S. R. Doctor, G. J. Schuster and P. G. Heasler, "A Generalized Procedure for Generating Flaw-Related Inputs for the FAVOR Code, NUREG/CR-6817, Rev. 1, ADAMS ML13240A258," Nuclear Regulatory Commision, Washington, D.C., March 2013.

Appendix A Actual Plant Transients

A combined 42 actual normal operation plant cooldown histories were obtained from 17 different PWRs. These cooldown histories were analyzed to determine the pressure and temperature histories corresponding to various percentiles of the pressure and temperature history distributions based on the population considered.

It is important to note that no information was available regarding how representative these transients are of actual PWR fleet operations. These transients were simply those that were made available to NRC by Westinghouse in 2013 through an informal exchange of data, and they may or may not be statistically representative of normal PWR cooldowns. Nonetheless, they all appeared to represent successfully terminated cooldowns, and were treated as such.

Figure 40 and Figure 42 respectively show the actual 42 temperature and pressure histories obtained for a total of 17 different PWRs. Figure 41 and Figure 43 respectively show the temperature and pressure histories corresponding to various percentiles of the distribution of the temperature and pressure histories. Figure 44 and Figure 45 show the P-T curves for the actual plant cooldowns as well as the P-T histories corresponding to various percentiles of the population studied. The values of pressure and temperature corresponding to the various percentiles were calculated at each time step based on the distribution of the data for the 42 transients analyzed. The 50^{th} percentile (median) histories are highlighted in bold red lines. Importantly, the time is given here in hours instead of minutes.

When comparing the actual cooldowns with P-T limit cooldowns, the actual cooldown transients generally occur over a much longer period of time. Looking at the median histories (50^{th} percentile), the cooldown rate is roughly ~50°F/hour from 550°F to 350°F, then ~20°F/hour from 350°F to 200°F, then ~2.5°F/hour from 200°F to 100°F. The corresponding pressure reduction rate is roughly 400psig/hour to 500psig/hour for the first 4 hours, such that in 4 to 5 hours, the pressure is reduced to about 350psig, then the pressure is maintained at about 350psig until the temperature reaches about 100°F, then the pressure is rapidly dropped to atmospheric pressure (0psig).

The analysis results for the 50^{th} and 95^{th} percentile of actual cooldown transients are presented in Section 1.3. These transients are referred to as the '50^{th} percentile' and '95^{th} percentile' cooldown transients in this document, and the frequency of occurrence of the 50^{th} percentile transient is estimated at 1.0 events per year.

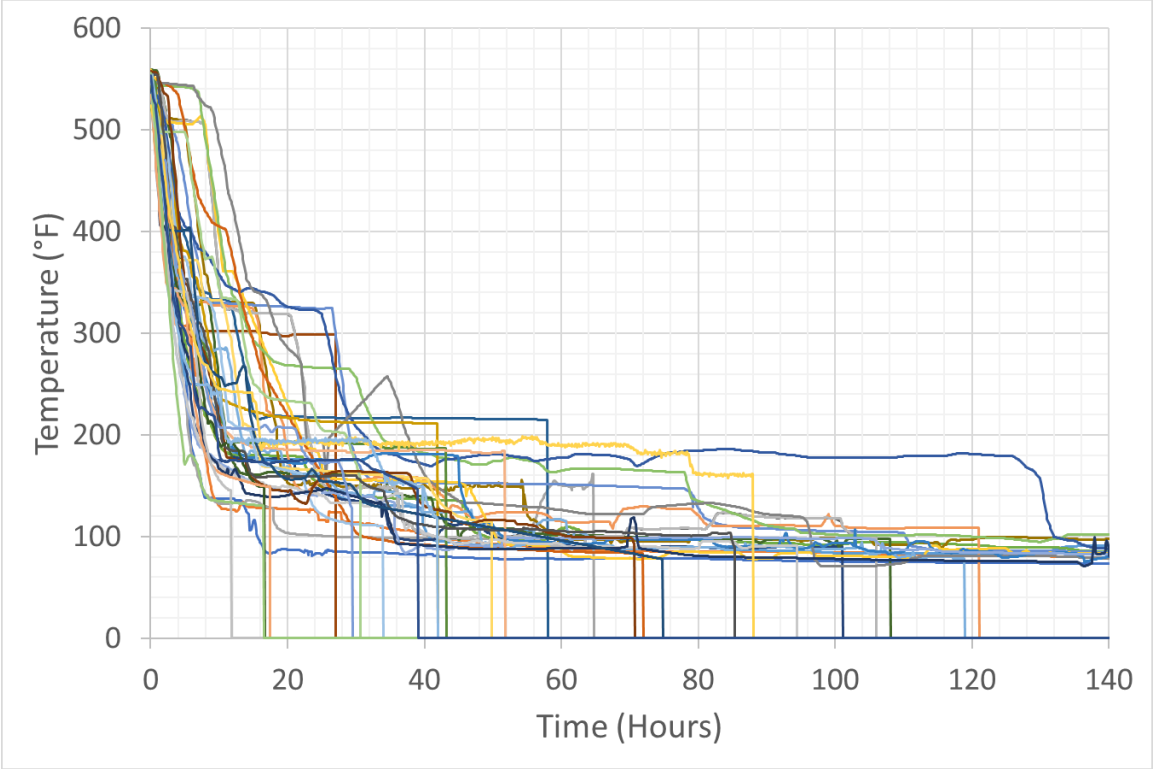

Figure 40: Temperature histories for 42 PWR cooldown transients

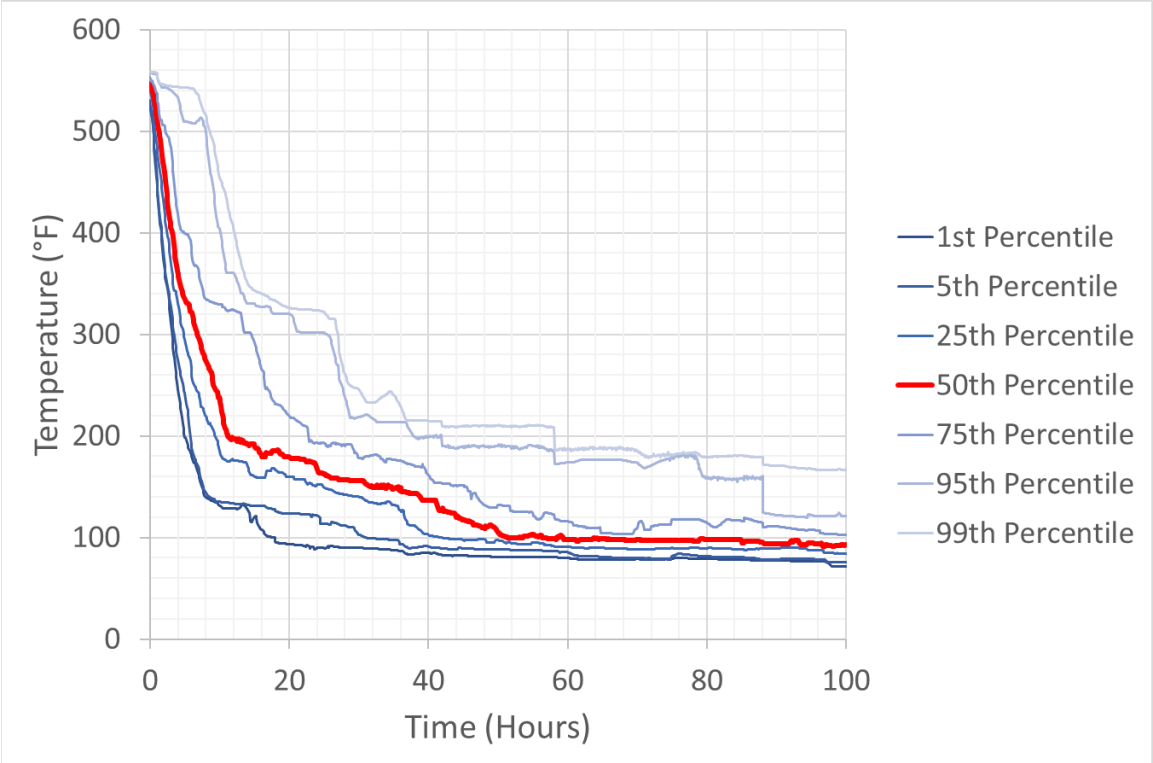

Figure 41: Temperature histories corresponding to various percentiles of the population of PWR cooldowns considered

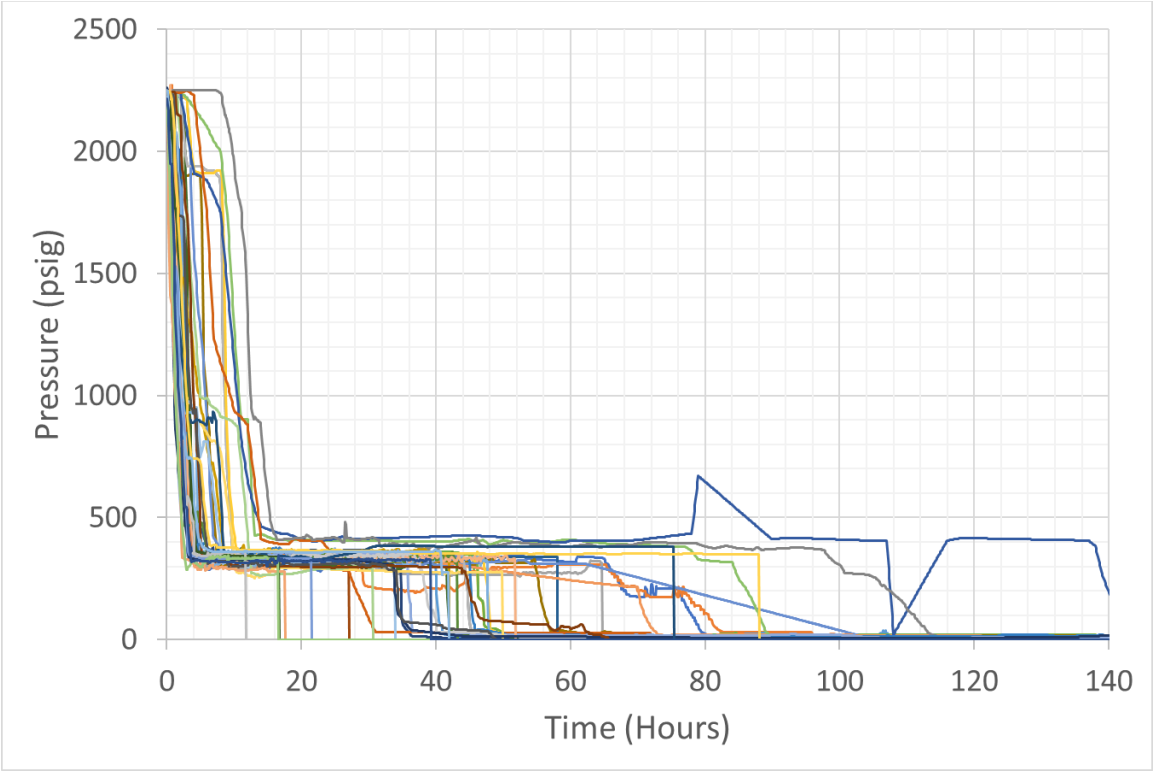

Figure 42: Pressure histories for 42 PWR cooldown transients

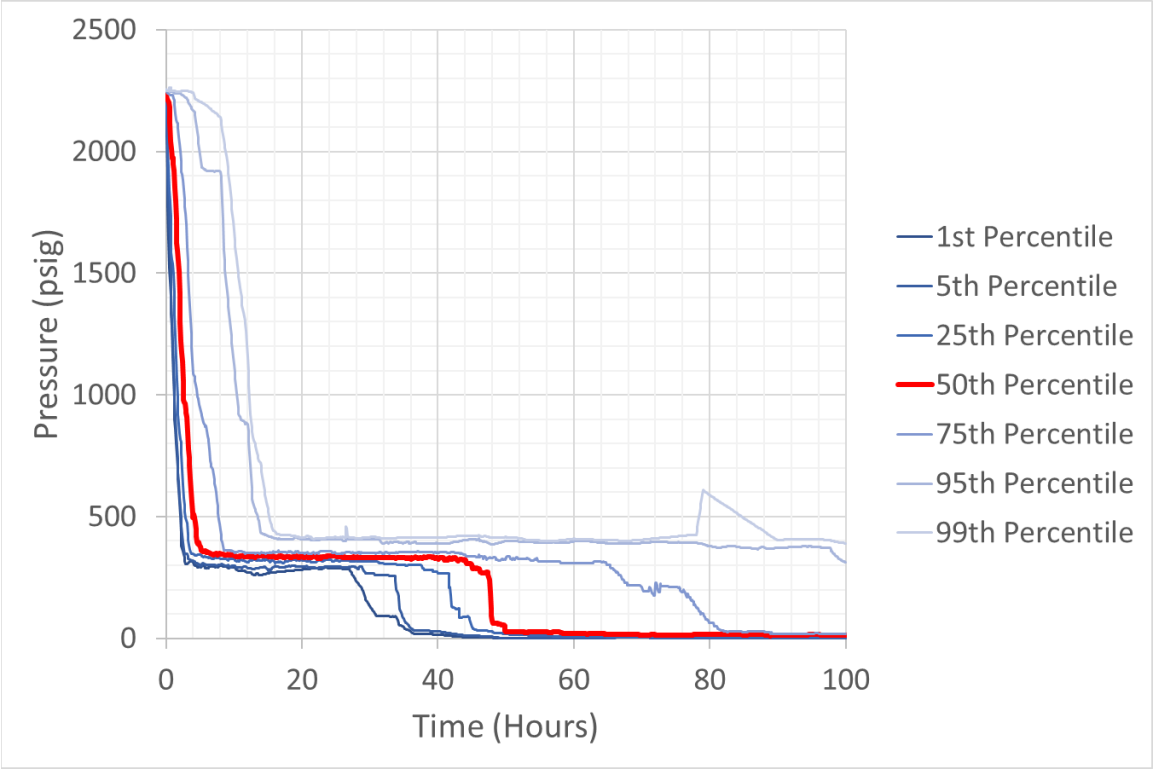

Figure 43: Pressure histories corresponding to various percentiles of the population of PWR cooldowns considered

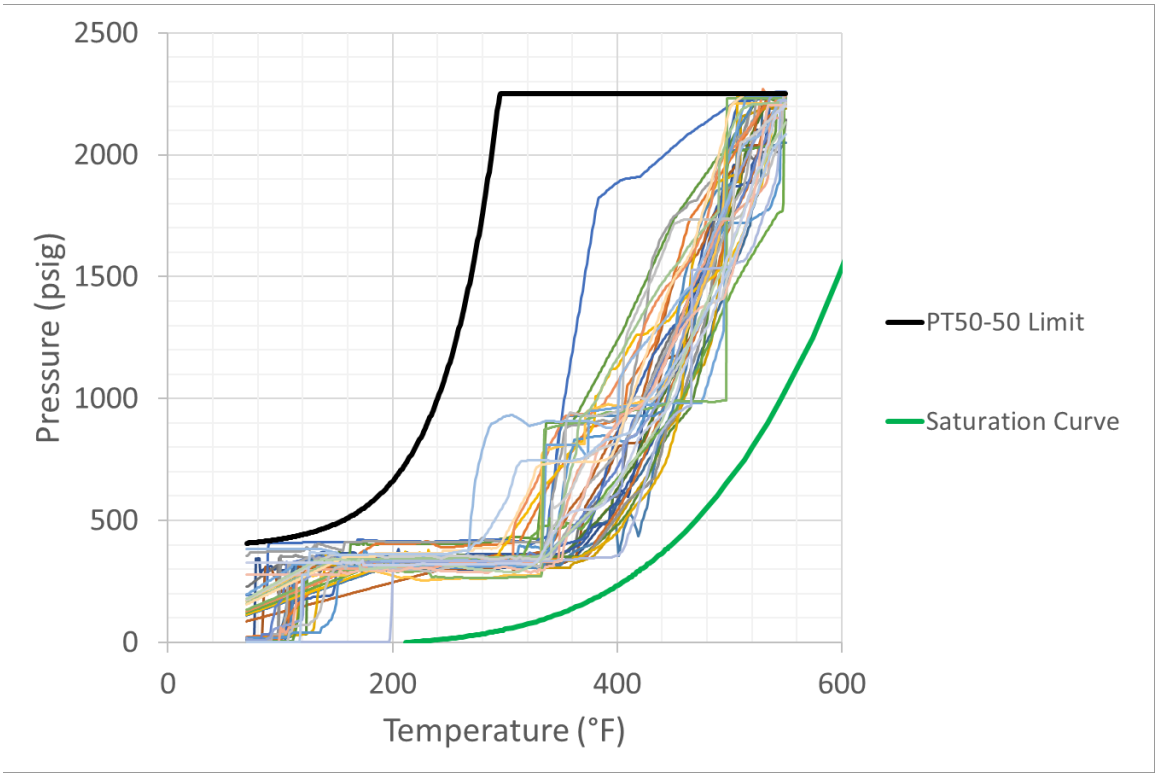

Figure 44: P-T histories for 42 PWR cooldown transients

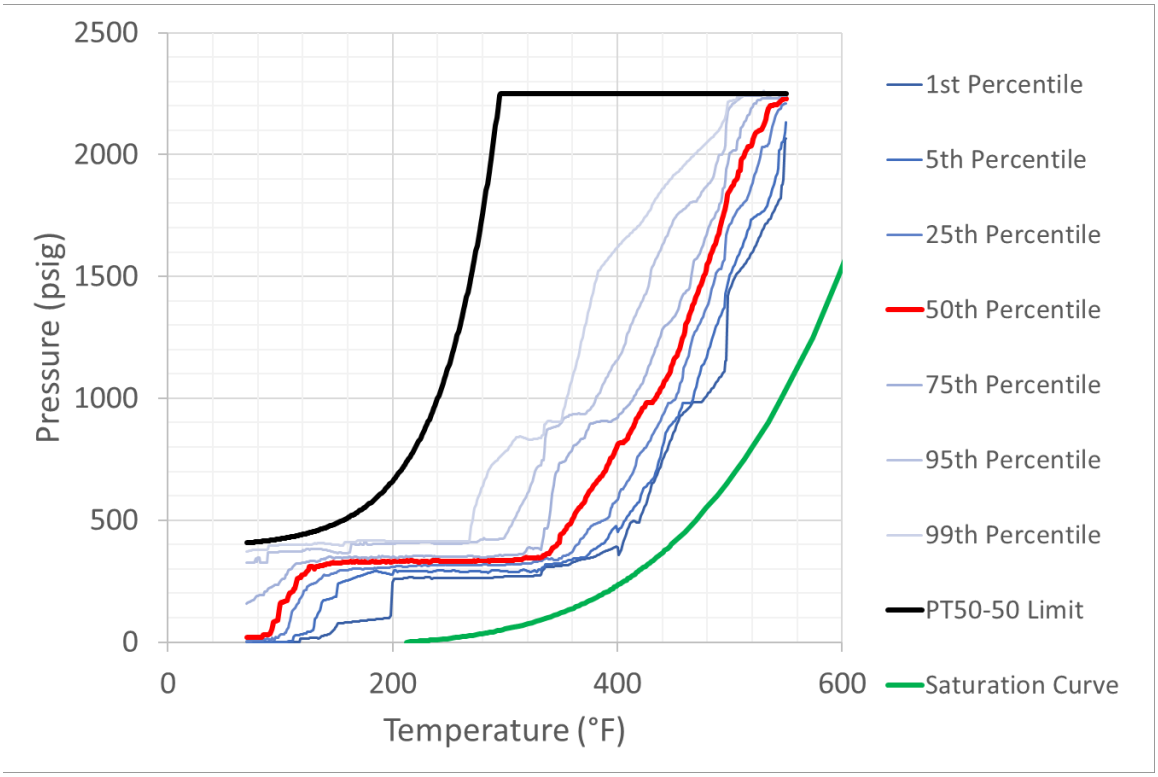

Figure 45: P-T histories corresponding to various percentiles of the population of PWR cooldowns

As discussed above and in Section 4.1.2, 42 actual cooldown profiles for 11 PWR power plants were collected for internal SSBF evaluations. One profile for each of the eleven plants was selected for FAVOR analysis of internal SSBFs. Ten of these eleven were selected because they are representative of normal plant cooldowns prior to a refueling outage – the most frequent type of cooldown. For these refueling outage cooldowns, the RCS temperature and pressure were reduced relatively quickly after the plant power was shutdown to Hot Zero Power (HZP). One outage was selected (Plant 7 – 1997) because the system pressure was held at operating pressure for approximately 100 hours with the plant at HZP. While no explanation was provided for this cooldown profile, the plant may have been kept at HZP for maintenance to allow a quick return to power. After approximately 120 hours at HZP, the plant maintenance may not have been completed and therefore the plant was cooled down to ambient temperature. While this type of plant cooldown is less frequent than a typical plant cooldown for refueling, it was selected for detailed evaluation to determine whether remaining at full system pressure for an extended time in the cooldown outage has a significant impact on FAVOR calculated CPF. Plots of RCS temperature and pressure versus time for these eleven transients is provided below to show typical cooldown rate and plant pressure during normal plant cooldowns.

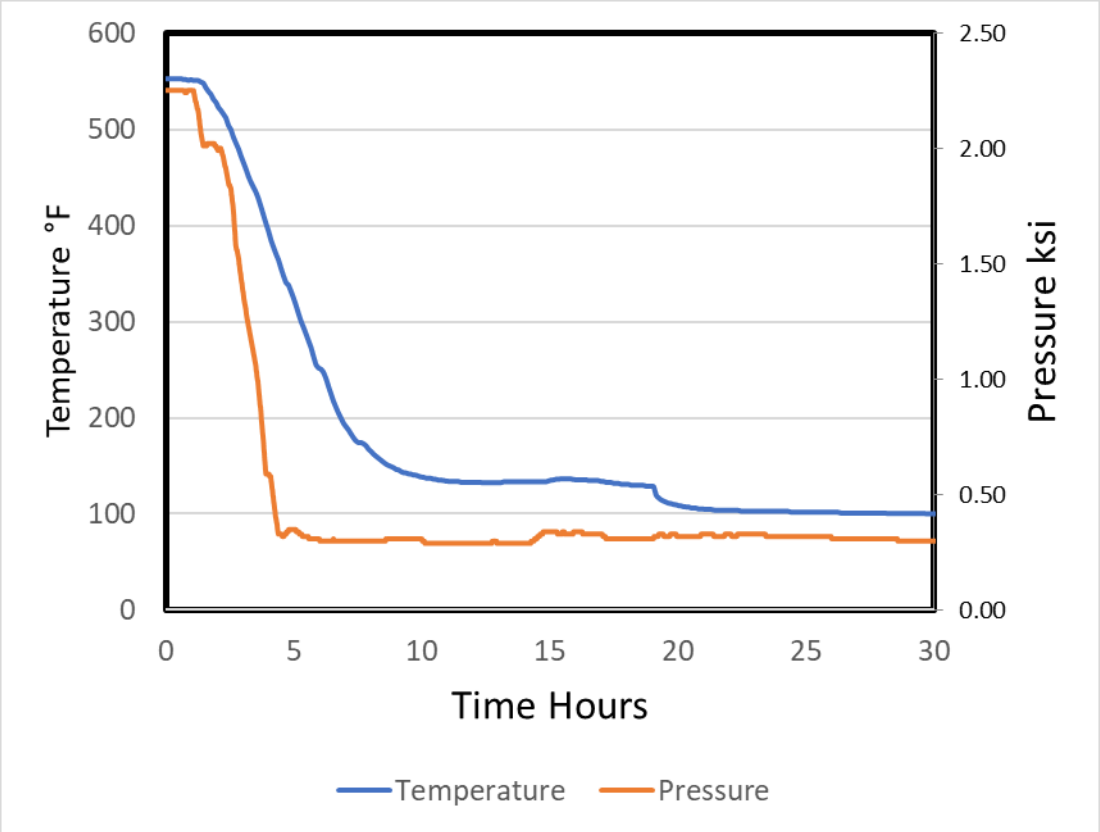

Figure 46 – Plant 1 2006b Cooldown Profile

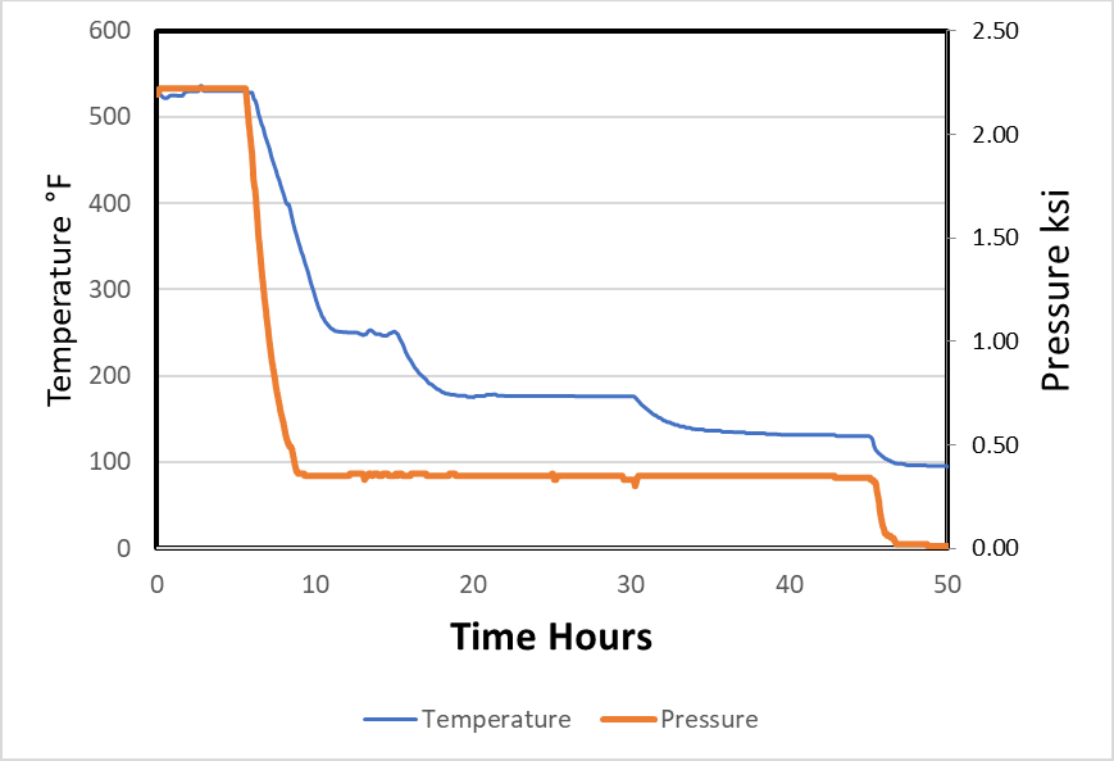

Figure 47 - Plant 2 2004 Cooldown Profile

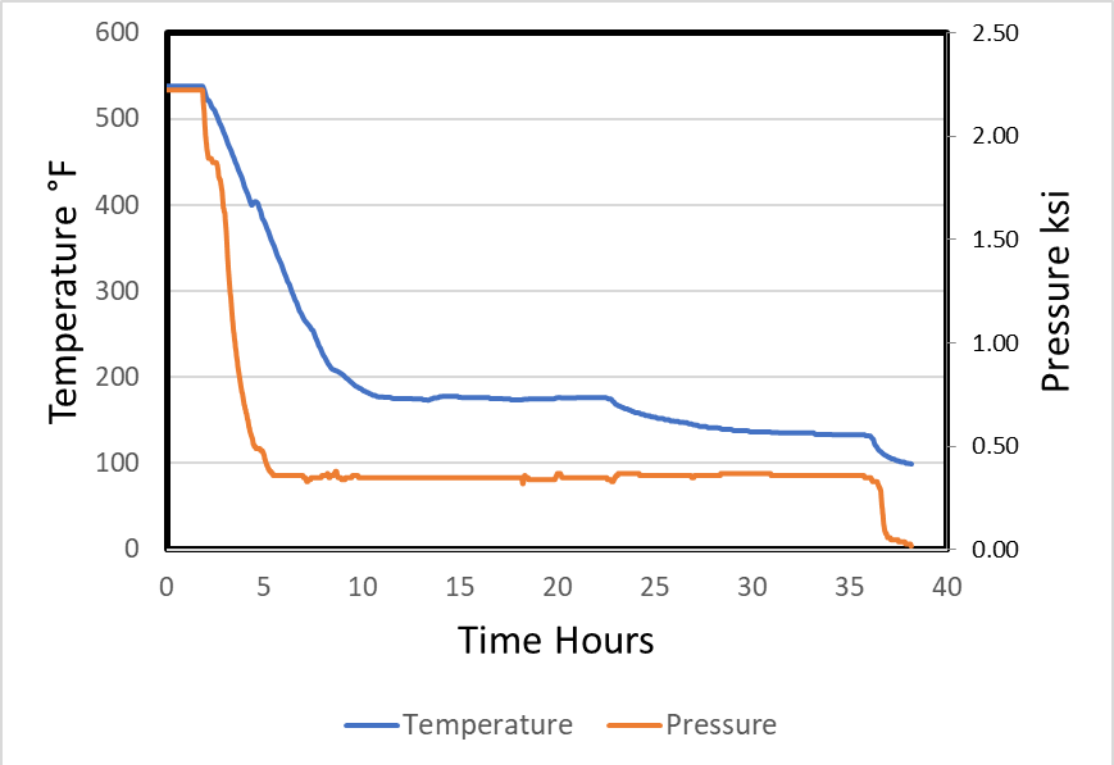

Figure 48 - Plant 3 2002 Cooldown Profile

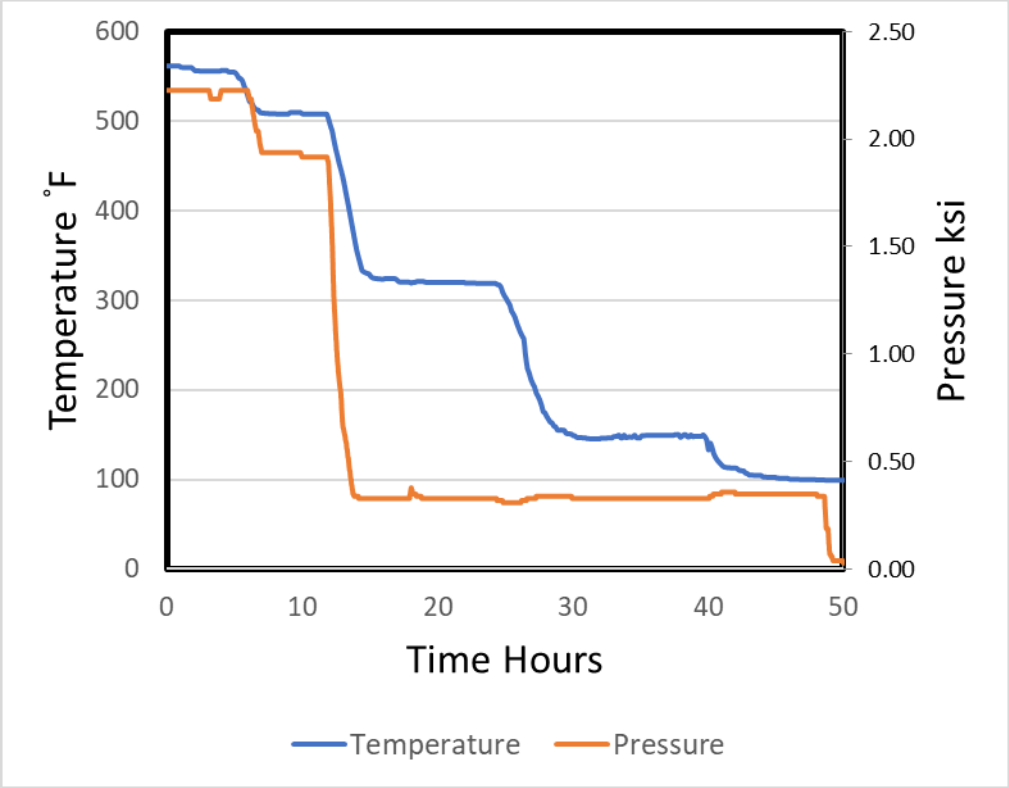

Figure 49 - Plant 4 2004 Cooldown Profile

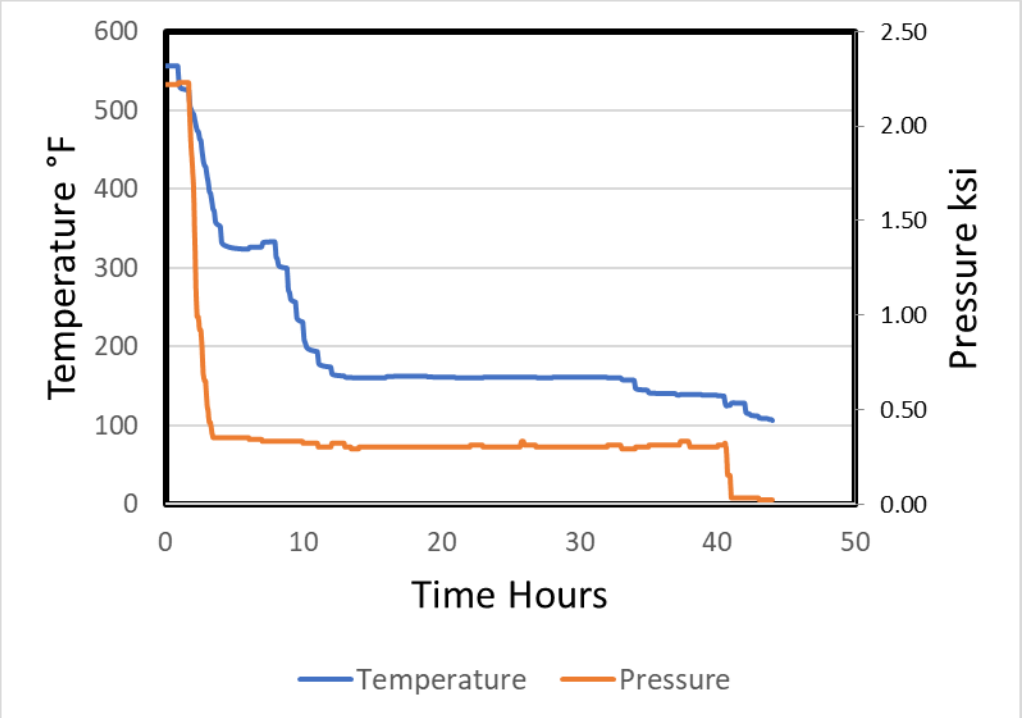

Figure 50 - Plant 5 2006 Cooldown Profile

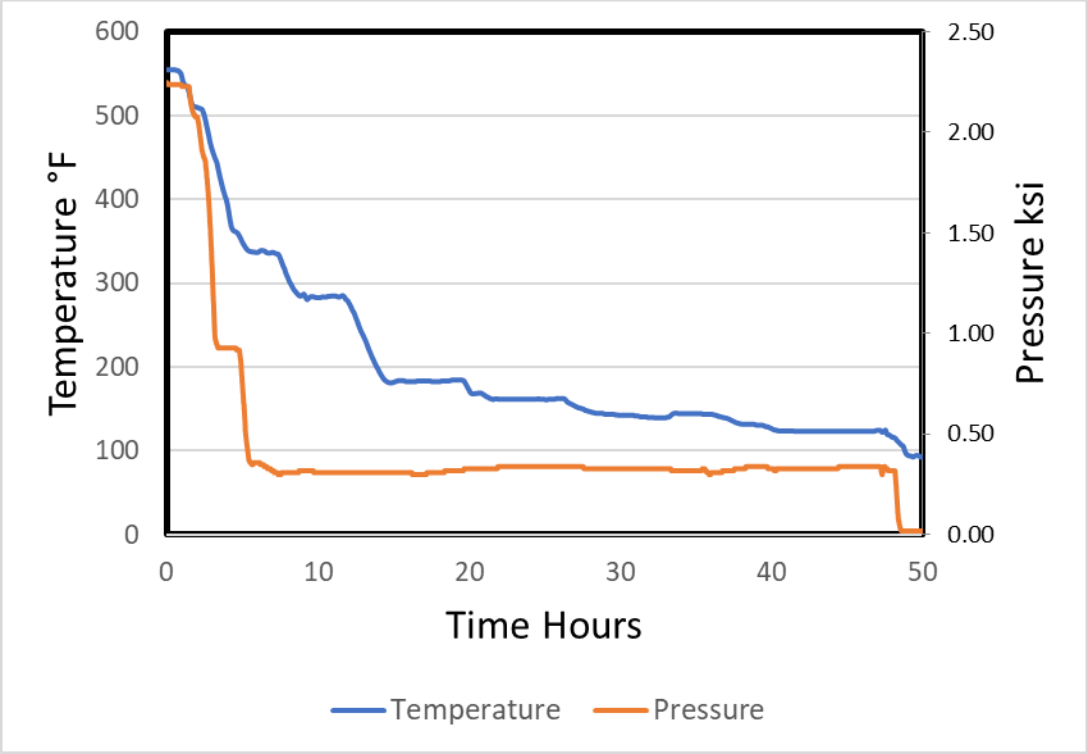

Figure 51 - Plant 6 2004b Cooldown Profile

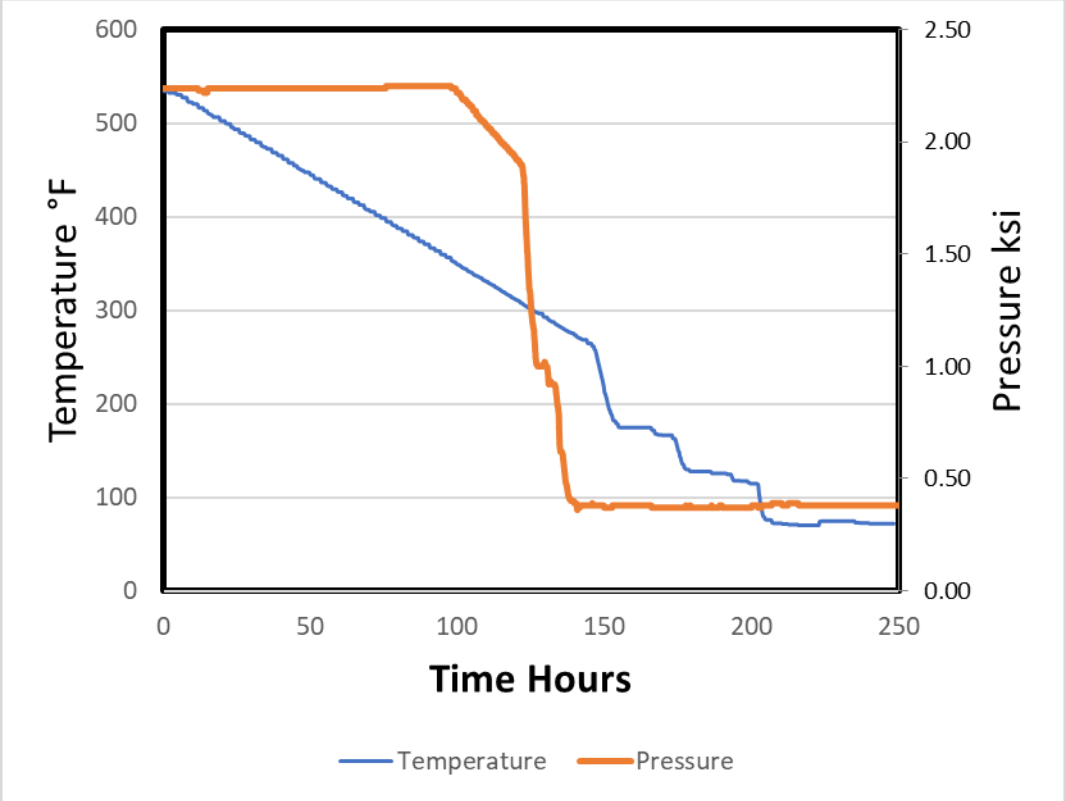

Figure 52 - Plant 7 1997 Cooldown Profile

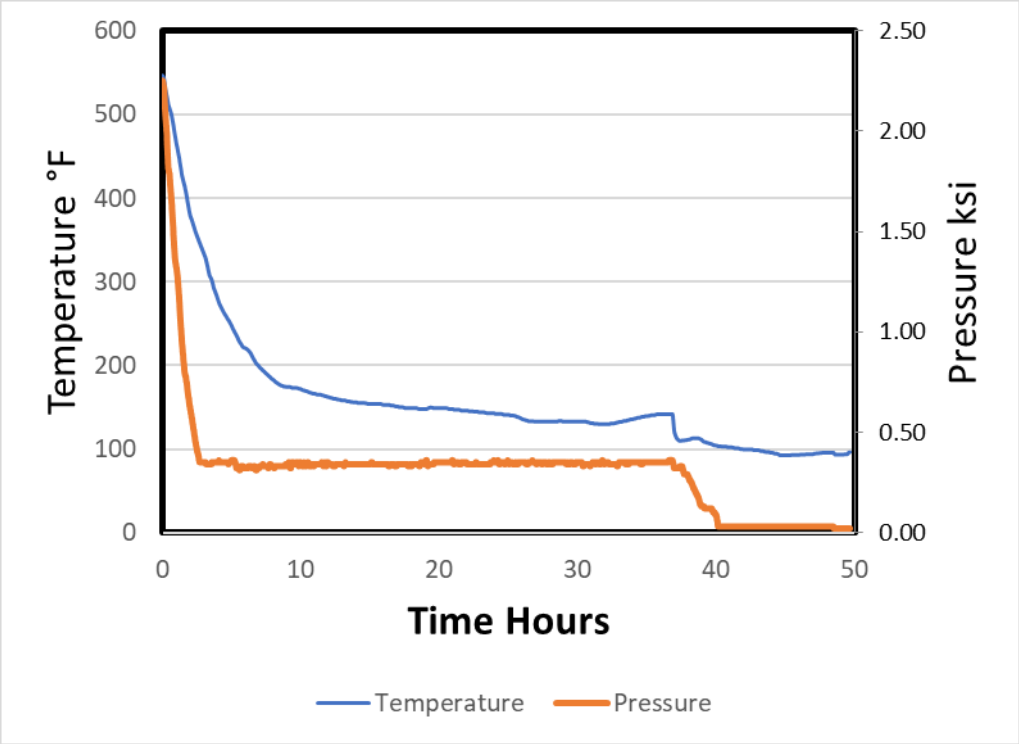

Figure 53 - Plant 8 2007 Cooldown Profile

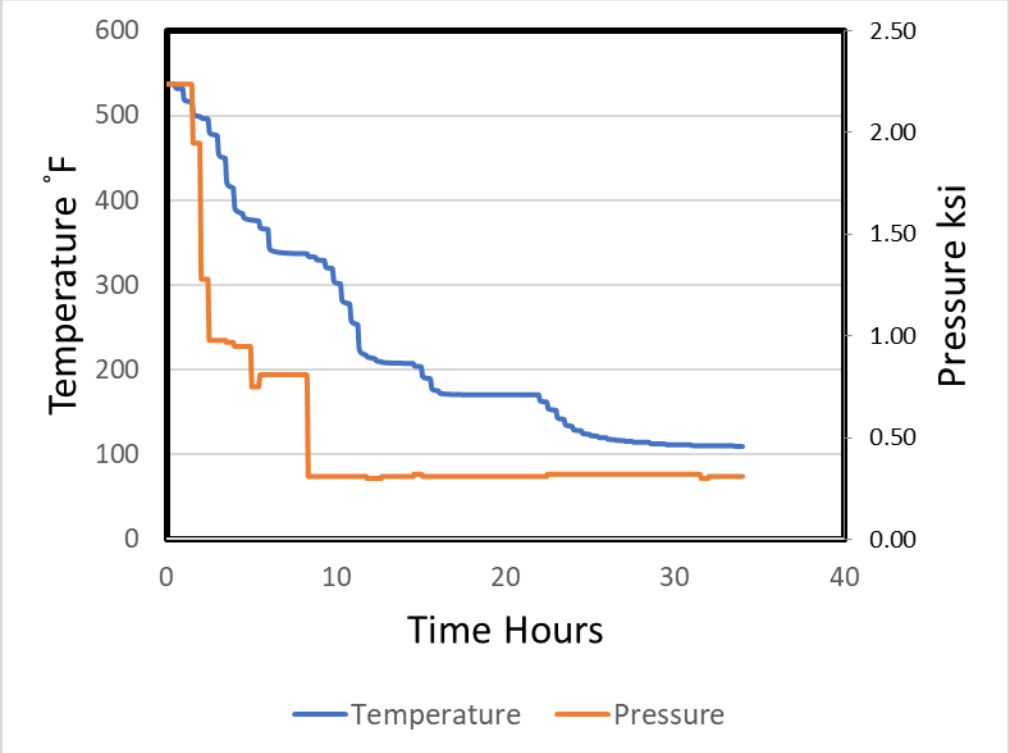

Figure 54 - Plant 9 2004 Cooldown Profile

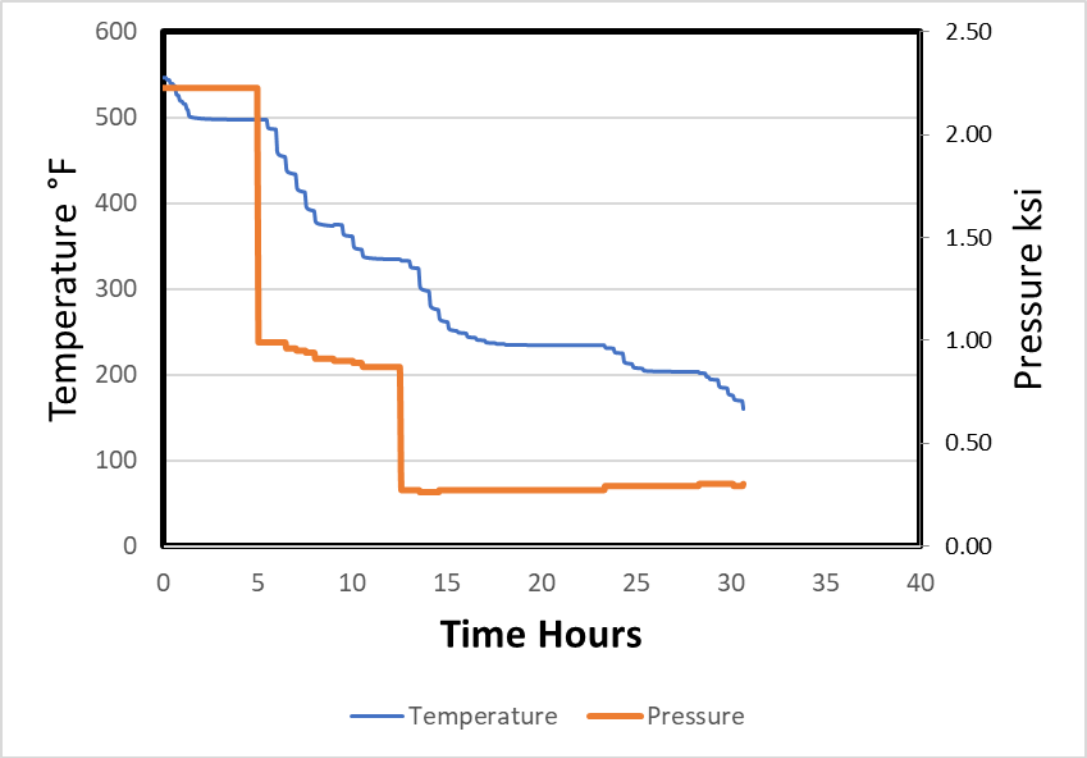

Figure 55 - Plant 10 2004 Cooldown Profile

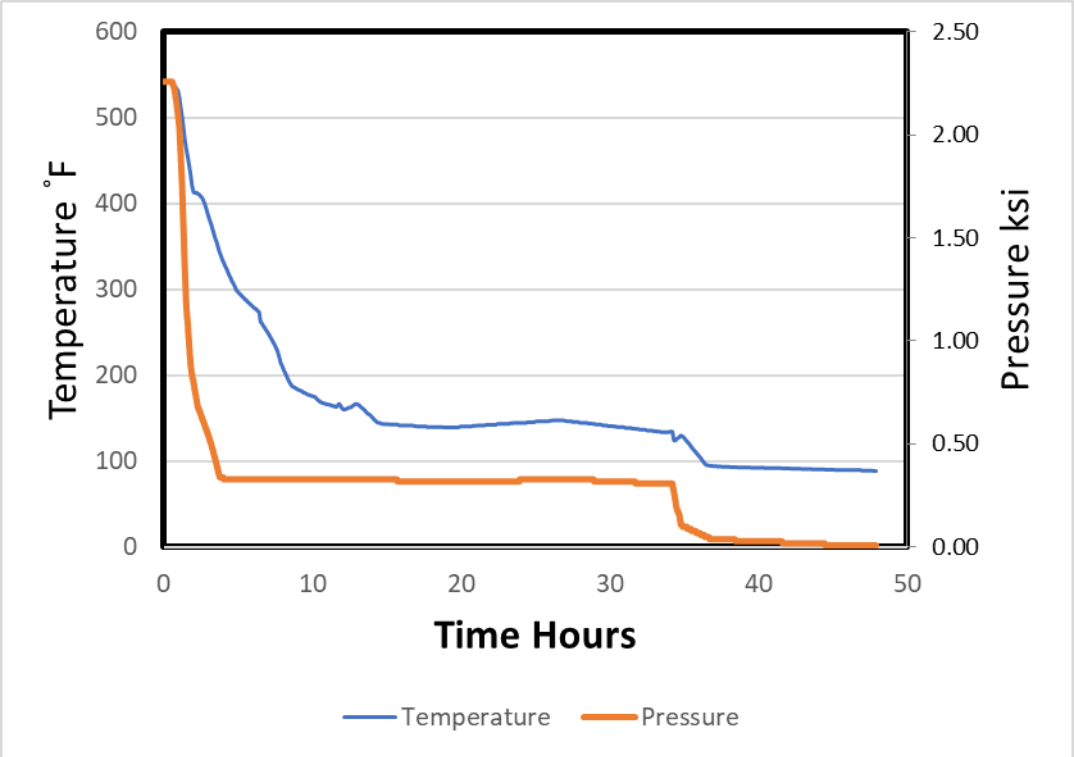

Figure 56 - Plant 11 2002 Cooldown Profile

Appendix B FAVOR Model Inputs for PWR Shallow Flaw Analyses

FAVOR Models for PWR Plants

Except as otherwise discussed in this report, the following FAVOR model and input assumptions are used.

Four PWR RPV geometry and embrittlement maps (designated as Plants 1 through 4) are evaluated. PWR A uses a detailed embrittlement map calculated for 60 Effective Full Power Years (EFPY) of operation. Plants 2 through 4 use thirteen region embrittlement maps based on data from RVID2 and other available sources of information, extrapolated to 60 EFPY.

RPV geometry:

PWR A

- Internal RPV radius 86.0 in
- Thickness of RPV wall (including cladding) 8.75 in
- Cladding Thickness 0.25 in

PWR B

- Internal RPV radius 86.0 in
- Thickness of RPV wall (including cladding) 8.998 in
- Cladding Thickness 0.313 in

PWR C

- Internal RPV radius 85.5 in
- Thickness of RPV wall (including cladding) 8.626 in
- Cladding Thickness 0.188 in

PWR D

- Internal RPV radius 78.5 in
- Thickness of RPV wall (including cladding) 8.036 in
- Cladding Thickness 0.156 in

All four PWR plants used the material property assumptions below:

Temperature independent standard thermo-elastic material properties for the ferritic steel RPV and stainless steel clad:

- Ferritic and Stainless-Steel Density 489 lb_m per ft^3
- Ferritic and Stainless-Steel Poison's Ratio 0.3

The following Tables provide the standard temperature dependent thermo-elastic material properties for the ferritic steel RPV and stainless steel clad. If other values are used, they are listed in the appropriate report sections.

Table B-1: Thermal Conductivity

[BTU/HR-FT-°F}		
Temperature °F	Ferritic Steel Vessel Wall	Stainless Steel Clad
70	24.8	8.1
100	25.0	8.4
150	25.1	8.6
200	25.2	8.8
250	25.2	9.1
300	25.1	9.4
350	25.0	9.6
400	25.1	9.9
450	24.6	10.1
500	24.3	10.4
550	24.0	10.6
600	23.7	10.9
650	23.4	11.1
700	23.0	11.4
750	22.6	11.6
800	22.2	11.9

Table B-2: Specific Heat

[BTU/LB_M-°F]		
Temperature °F	Ferritic Steel Vessel Wall	Stainless Steel Clad
70	0.1052	0.1158
100	0.1072	0.1185
150	0.1101	0.1196
200	0.1135	0.1208
250	0.1166	0.1232
300	0.1194	0.1256
350	0.1223	0.1258
400	0.1267	0.1281
450	0.1277	0.1291
500	0.1304	0.1305
550	0.1326	0.1306
600	0.1350	0.1327
650	0.1375	0.1335
700	0.1404	0.1348
750	0.1435	0.1356
800	0.1474	0.1367

Table B-3: Young's Elastic Modulus

[KSI]	
Temperature °F	Ferritic Steel Vessel Wall
70	29200
200	28500
300	28000
400	27400
500	27000
600	26400
700	25300
800	23900
	Stainless Steel Clad
68	22046
302	20160
482	18420

Table B-4: Coefficient of Thermal Expansion

1.0E-06 /°F		
Temperature °F	Ferritic Steel Vessel Wall	Stainless Steel Clad
100	7.06	8.55
150	7.16	8.67
200	7.25	8.79
250	7.34	8.90
300	7.43	9.00
350	7.50	9.10
400	7.58	9.19
450	7.63	9.28
500	7.70	9.37
550	7.77	9.45
600	7.83	9.53
650	7.90	9.61
700	7.94	9.69
750	8.00	9.76
800	8.05	9.82

Other standard FAVOR analysis assumptions include:

- Stress Free Temperature 488°F
- Crack Face pressure loading applied
- Axial Weld Residual Stress on
- Circumferential Weld Residual Stress on
- Time step for loading calculations 1 minute
- Convective heat transfer coefficient 10,000 BTU/hr-ft^2-°F

FAVPFM Standard FAVOR Model

Except as otherwise discussed in this report, the following FAVOR model and input assumptions are used for the analyses in this report as inputs for FAVPFM calculations.

- Number of RPV simulations 20,000
- Number of IGA trials per flaw 100
- Warm Pre-Stress included Option 1
- RT_{NDT} Irradiation shift model RG 1.99, Revision 2
- RPV Operating Temperature 532°F
- Irradiation Time 60 EFPY
- Apply RT_{NDT}-based ductile tearing Option 1
- Check for ductile tearing as initiating mechanism Option 0
- Irradiated Flow Stress 79 ksi
- K_{1a} Model Option 1
- Layer Option 1
- Wall Thickness Failure Fraction 0.9
- Sigma weld for Cu 0.167
- Sigma weld for Ni 0.162
- Sigma plate for Cu 0.0073
- Sigma plate for Ni 0.0244

PWR A

- Weld Regions 7 major, 1388 subregions
- Plate Regions 6 major, 65688 subregions

PWR B, PWR C, and PWR D

- Weld Regions 7 major, 7 subregions
- Plate Regions 6 major, 6 subregions

The FAVPFM input flaw files assume zero internal flaws and one internal SSBF per reactor vessel. The input flaw assumptions were taken from NUREG/CR-6817, Rev 1, [18]. As discussed in NUREG/CR-6817, clad flaw estimates were developed based on:

1. Data on observed flaws from destructive and nondestructive examinations of the PVRUF vessel (Schuster et al. 1998, 1999, 2000a)

2. Simulations of clad flaws with the PRODIGAL computer code (Chapman and Simonen 1998)

3. Examinations of cladding material performed at Bettis Laboratory (Li and Mabe 1998)

4. An NRC expert judgment elicitation on vessel flaws (Jackson and Abramson 2000).

As discussed in Section 9.6.1 of NUREG/CR-6817, "the numbers and sizes of clad/surface-breaking flaws at the inner surface of a vessel have been estimated from data on flaws that have been detected during examinations of vessel cladding. These flaws can occur randomly in the cladding applied over both weld and base metal." The estimated flaw density in in NUREG/CR-6817 is 0.0036589 flaws per ft^2 of the vessel inner wall. This flaw density is relatively small and is equivalent to approximately 1 to 2 internal SSBFs per vessel. For consistent analysis, a flaw density of 1 flaw per vessel has been assumed for the FAVOR shallow flaw analysis. Figure 9-17 of in NUREG/CR-6817 provides sample FAVOR internal SSBF inputs. Because of restrictions in the FAVOR code for representing flaws, the flaw depth is represented in increments of 1% of the RPV wall thickness. Figure 9-17 provides an estimated distribution of flaw aspect ratios based on the experimental data and exert judgements discussed in this NUREG. The distribution of aspect ratios has been used for the used for FAVOR model of internal SSBFs and shown in Table B-5.

Table B-5: Distribution of IAB Flaw Aspect Ratios

Aspect Ratio	% of Flaws
2	67.450
6	20.769
10	3.964
999	7.817

Appendix C FAVOR Model Inputs for BWR Shallow Flaw Analyses

FAVOR Models for BWR Plants

Except as otherwise discussed in this report, the following FAVOR model and input assumptions are used.

Two BWR RPV geometry and embrittlement maps (designated as Plant BWR A and Plant BWR B) are evaluated. Plants BWR A and BWR B use thirteen region embrittlement maps based on data from RVID2 and other available sources of information, extrapolated to 60 EFPY.

RPV geometry:

Plant BWR A

- Internal RPV radius 100.37 in
- Thickness of RPV wall (including cladding) 5.38 in
- Cladding Thickness 0.21 in

Plant BWR B

- Internal RPV radius 106.5 in
- Thickness of RPV wall (including cladding) 7.12 in
- Cladding Thickness 0.25 in

Both BWR plants used the material property assumptions below:

Temperature independent standard thermo-elastic material properties for the ferritic steel RPV and stainless steel clad:

- Ferritic and Stainless-Steel Density 489 lb_m per ft^3
- Ferritic and Stainless-Steel Poison's Ratio 0.3

The following Tables provide the standard temperature dependent thermo-elastic material properties for the ferritic steel RPV and stainless steel clad. If other values are used, they are listed in the appropriate report sections.

Table C-1: Thermal Conductivity

[BTU/HR-FT-°F}		
Temperature °F	Ferritic Steel Vessel Wall	Stainless Steel Clad
70	24.8	8.1
100	25.0	8.4
150	25.1	8.6
200	25.2	8.8
250	25.2	9.1
300	25.1	9.4
350	25.0	9.6
400	25.1	9.9
450	24.6	10.1
500	24.3	10.4
550	24.0	10.6
600	23.7	10.9
650	23.4	11.1
700	23.0	11.4
750	22.6	11.6
800	22.2	11.9

Table C-2: Specific Heat

[BTU/LB_M-°F]		
Temperature °F	Ferritic Steel Vessel Wall	Stainless Steel Clad
70	0.1052	0.1158
100	0.1072	0.1185
150	0.1101	0.1196
200	0.1135	0.1208
250	0.1166	0.1232
300	0.1194	0.1256
350	0.1223	0.1258
400	0.1267	0.1281
450	0.1277	0.1291
500	0.1304	0.1305
550	0.1326	0.1306
600	0.1350	0.1327
650	0.1375	0.1335
700	0.1404	0.1348
750	0.1435	0.1356
800	0.1474	0.1367

Table C-3: Young's Elastic Modulus

[KSI]	
Temperature °F	Ferritic Steel Vessel Wall
70	29200
200	28500
300	28000
400	27400
500	27000
600	26400
700	25300
800	23900
	Stainless Steel Clad
68	22046
302	20160
482	18420

Table C-4: Coefficient of Thermal Expansion

1.0E-06 /°F		
Temperature °F	Ferritic Steel Vessel Wall	Stainless Steel Clad
100	7.06	8.55
150	7.16	8.67
200	7.25	8.79
250	7.34	8.90
300	7.43	9.00
350	7.50	9.10
400	7.58	9.19
450	7.63	9.28
500	7.70	9.37
550	7.77	9.45
600	7.83	9.53
650	7.90	9.61
700	7.94	9.69
750	8.00	9.76
800	8.05	9.82

Other standard FAVOR analysis assumptions include:

- Stress Free Temperature 488°F
- Crack Face pressure loading applied
- Axial Weld Residual Stress on
- Circumferential Weld Residual Stress on
- Time step for loading calculations 1 minute
- Convective heat transfer coefficient 10,000 BTU/hr-ft^2-°F

FAVPFM Standard FAVOR Model

Except as otherwise discussed in this report, the following FAVOR model and input assumptions are used for the analyses in this report as inputs for FAVPFM calculations.

- Number of RPV simulations 20,000
- Number of IGA trials per flaw 100
- Warm Pre-Stress included Option 1
- RT_{NDT} Irradiation shift model RG 1.99, Revision 2
- RPV Operating Temperature 550°F
- Irradiation Time 72 EFPY
- Apply RT_{NDT}-based ductile tearing Option 1
- Check for ductile tearing as initiating mechanism Option 0
- Irradiated Flow Stress 80 ksi
- K_{1a} Model Option 1
- Layer Option 1
- Wall Thickness Failure Fraction 0.9
- Sigma weld for Cu 0.167
- Sigma weld for Ni 0.0165
- Sigma plate for Cu 0.0073
- Sigma plate for Ni 0.0244
- Weld Regions 7 major, 7 subregions
- Plate Regions 6 major, 6 subregions

The FAVPFM input flaw files assume zero internal flaws and one internal SSBF per reactor vessel. The input flaw assumptions were taken from NUREG/CR-6817, Rev 1, [18]. As discussed in NUREG/CR-6817, clad flaw estimates were developed based on:

1. Data on observed flaws from destructive and nondestructive examinations of the PVRUF vessel (Schuster et al. 1998, 1999, 2000a)

2. Simulations of clad flaws with the PRODIGAL computer code (Chapman and Simonen 1998)

3. Examinations of cladding material performed at Bettis Laboratory (Li and Mabe 1998)

4. An NRC expert judgment elicitation on vessel flaws (Jackson and Abramson 2000).

As discussed in Section 9.6.1 of NUREG/CR-6817, "the numbers and sizes of clad/surface-breaking flaws at the inner surface of a vessel have been estimated from data on flaws that have been detected during examinations of vessel cladding. These flaws can occur randomly in the cladding applied over both weld and base metal." The estimated flaw density in in NUREG/CR-6817 is 0.0036589 flaws per ft^2 of the vessel inner wall. This flaw density is relatively small and is equivalent to approximately 1 to 2 internal SSBFs per vessel. For consistent analysis, a flaw density of 1 flaw per vessel has been assumed for the FAVOR shallow flaw analysis. Figure 9-17 of in NUREG/CR-6817 provides sample FAVOR internal SSBF inputs. Because of restrictions in the FAVOR code for representing flaws, the flaw depth is represented in increments of 1% of the RPV wall thickness. Figure 9-17 provides an estimated distribution of flaw aspect ratios based on the experimental data and exert judgements discussed in this NUREG. The distribution of aspect ratios has been used for the used for FAVOR model of internal SSBFs and shown in Table B-5.

Table C-5: Distribution of IAB Flaw Aspect Ratios

Aspect Ratio	% of Flaws
2	67.450
6	20.769
10	3.964
999	7.817